POLITECNICO
MILANO 1863

SCUOLA DI INGEGNERIA INDUSTRIALE
E DELL'INFORMAZIONE

Underwater CAES for off-shore wind farms: system integration and operating strategy optimization based on techno-economic analysis

TESI DI LAUREA MAGISTRALE IN
ENERGY ENGINEERING - INGEGNERIA ENERGETICA

Author: **Calogero Passanante**

Student ID: 977184
Advisor: Paolo Silva
Co-advisor: Giulio Guandalini

Academic Year: 2022-23

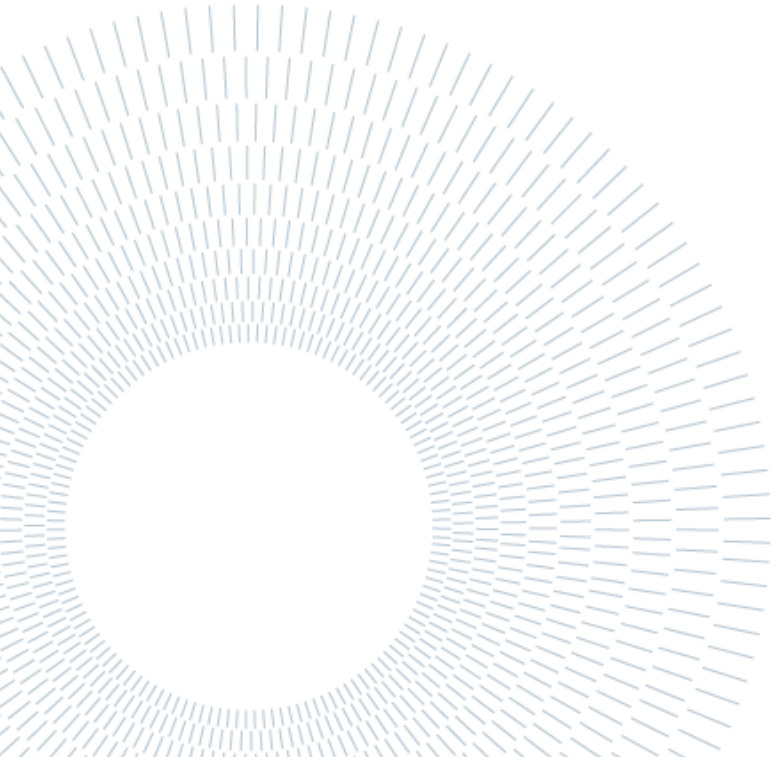

Abstract

The continuous growth of global energy demand is driving humanity to explore increasingly new and efficient methods of energy production. Simultaneously, there is a need to reduce the environmental impact given by human activities by mitigating greenhouse gas emissions. As a result, a growing utilization of renewable energy sources occurs, such as solar and wind, which however pose challenges in energy management due to their non-programmability. Energy storage systems come into play to enhance the management of these renewable sources, maximizing their penetration to reduce dependence on fossil fuels. Among the various large-scale storage systems proposed nowadays, notable examples include Pumped Storage Hydropower (PSH), well established, and chemical storage systems. However, taking advantage of the consolidated knowledge of turbomachines and Thermal Energy Storage (TES) in a Compressed Air Energy Storage (CAES), this other technology becomes an equally attractive possibility. This thesis examines an adiabatic underwater CAES (UW-CAES) coupled with an off-shore wind farm. The objective is to assess its techno-economic feasibility based on a MatLab model developed for plant design and operation evaluation under different constraints. A distinctive feature of an adiabatic UW-CAES system compared to a conventional CAES is the presence of air storage vessels, located on the seafloor to maintain a constant air pressure, and a TES. The developed model is then applied to proposed off-shore wind farms to understand which parameters most influence the plant performance.

Key-words: UW-CAES, non-programmable renewable energy sources, energy storage system, TES, underwater air storage, LCOS.

Abstract in italiano

La continua crescita del fabbisogno energetico a livello globale sta spingendo l'umanità verso la ricerca di sempre nuovi e più efficienti metodi di produzione dell'energia. Allo stesso tempo però c'è la necessità di diminuire l'impatto ambientale dovuto alle attività dell'uomo, contrastando le emissioni di gas serra. Da qui il crescente utilizzo di fonti di energia rinnovabili come il solare e l'eolico, che però comportano problemi di gestione dell'energia prodotta a causa della loro non-programmabilità. Ecco che i sistemi di stoccaggio dell'energia entrano in gioco per cercare di migliorare la gestione di queste fonti rinnovabili, incrementando il più possibile la loro penetrazione per ridurre la dipendenza dai combustibili fossili. Tra i diversi sistemi di stoccaggio su larga scala oggi proposti, è possibile citare i sistemi di pompaggio idroelettrici (PSH), ormai abbastanza consolidati, e i sistemi di stoccaggio chimici. Tuttavia, sfruttando le conoscenze ampiamente consolidate sulle turbomacchine e i sistemi di accumulo termico (TES) in un accumulo energetico ad aria compressa (CAES), si rende quest'altra tecnologia una possibilità altrettanto interessante. In questa tesi si prenderà in esame un CAES adiabatico sottomarino (UW-CAES) accoppiato ad un parco eolico off-shore. L'obiettivo è quello di valutare la sua fattibilità tecno-economica sulla base di un modello sviluppato su MatLab per dimensionare l'impianto e valutarne il suo funzionamento in base a una serie di vincoli. Elemento che caratterizza un sistema UW-CAES adiabatico rispetto ad un CAES convenzionale è proprio la presenza di serbatoi per lo stoccaggio dell'aria, posizionati sul fondale marino per mantenere la pressione dell'aria costante, e del TES. Il modello realizzato viene quindi applicato ad alcuni impianti eolici off-shore proposti, per capire quali sono i parametri che più ne influenzano le sue prestazioni.

Parole chiave: UW-CAES, fonti rinnovabili non programmabili, sistema di accumulo energetico, TES, stoccaggio sottomarino di aria, LCOS.

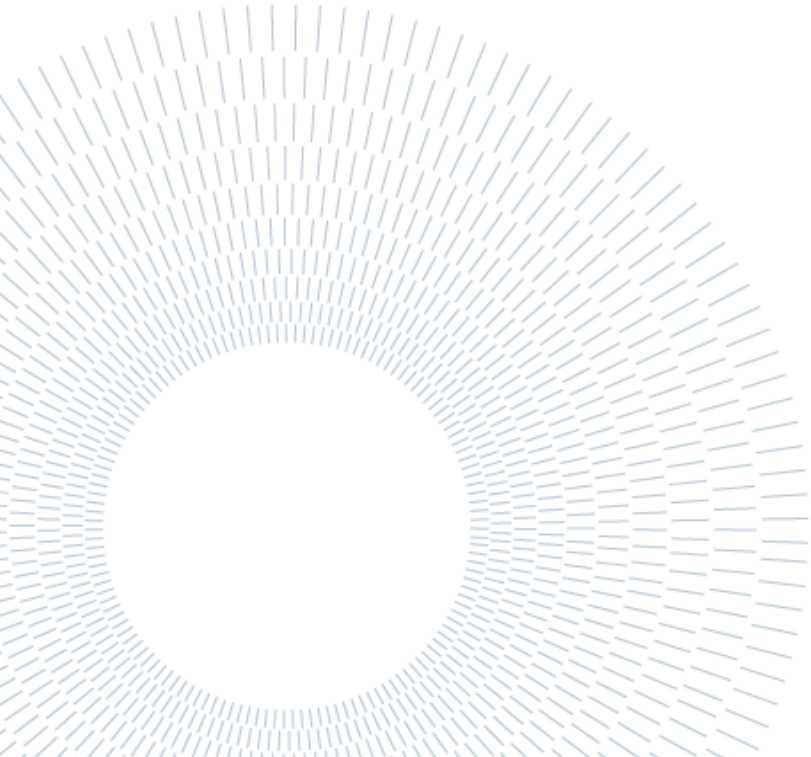

Contents

1 Introduction

1.1. Current Energy Scenario

The amount of energy that humans require has increased continuously in the last years. Fossil fuel consumption increased after the industrial revolution, and today non-renewable sources provide the majority of the primary energy. Developing countries will see an increase in their energy consumption over the coming years, as there is a clear correlation between rising GDP (Gross Domestic Product) and rising energy consumption. The growing demand for electricity, coupled with the need to reduce greenhouse gas emissions, has led to an increase in renewable energy production worldwide in recent years. In fact, many countries are trying to reduce the use of conventional energy production plants, which use fossil fuels, by trying to increase the production of green energy.

In 2021, the total amount of electricity generated in the world from renewables was 7858 TWh, reaching a share of 27.8% of the total electricity generation, with a visible growth in the last years as shown in Figure 1.1, given especially by investment made in Asia. [1]

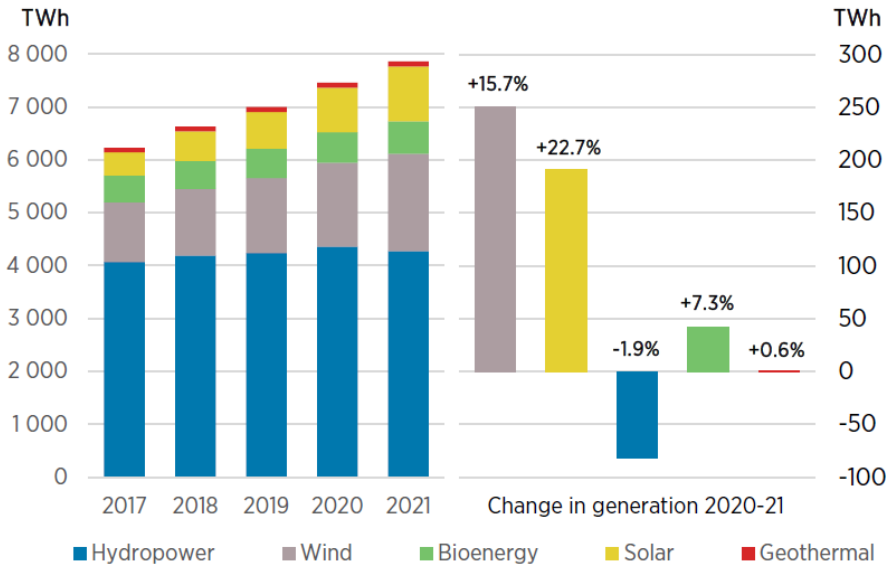

Figure 1.1: Growth in renewable electricity generation in the world (2017-2021). [1]

In Italy, this trend is leading to an increase in the penetration of renewable energy sources, particularly in the last decades by means of wind and solar power plants, as

shown in Figure 1.2 by GSE statistical report. The almost 58 GW of installed renewable power in Italy, in 2021 account for 40.2% of the energy production of the country, of which the main source is represented by hydropower (39%), followed by solar PV (22%), wind (18%), bioenergy (16%) and geothermal (5%) [2].

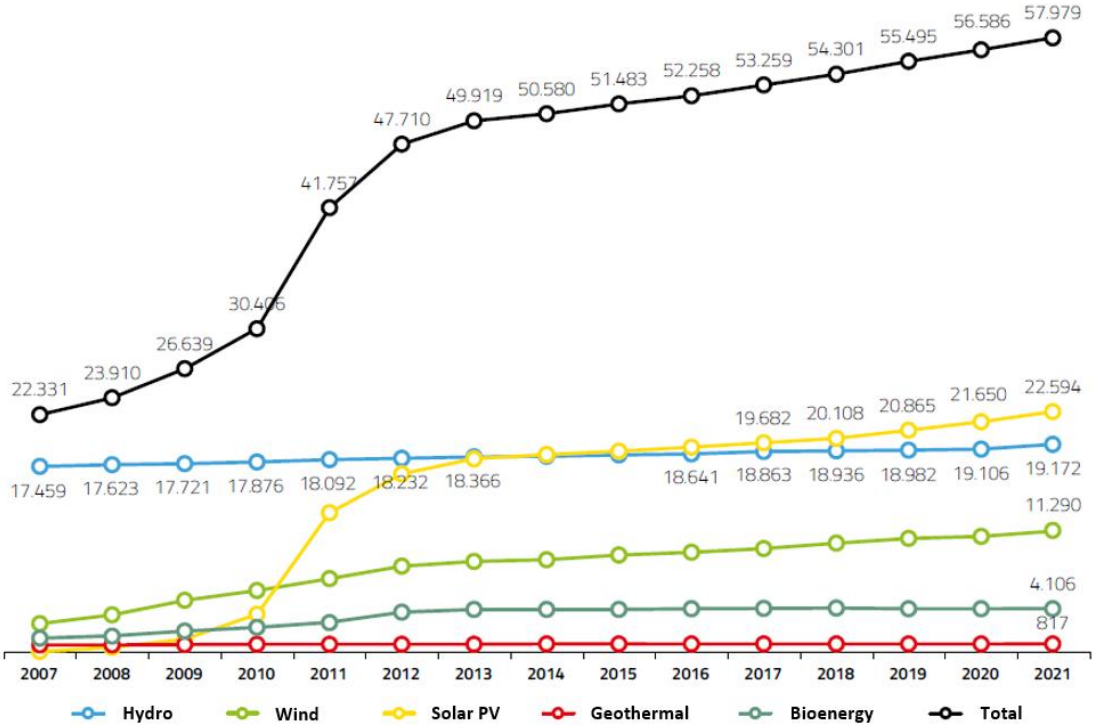

Figure 1.2: Installed capacity in MW of renewable energy production plants in Italy. [2]

However, the non-programmable nature of these resources (NPRES – Non-Programmable Renewable Energy Sources) leads to significant problems in managing the energy they produce, due to unbalance between supply and demand. For this reason, the need arises to introduce energy storage systems into the electric grid, in order to improve its flexibility by storing and releasing energy when it is needed. These technologies therefore have many positive implications, including the possibility of balancing the grid frequency, or avoiding overloading phenomena of lines due to saturation by excess of production, and the possibility of time-shifting the production of green energy, in a peak shaving perspective, with a consequent increase in the penetration of renewable sources and lower CO_2 emissions.

1.2. Storage Systems Overview

There are many energy storage solutions, some of which have already been in use for several years in many fields. A typical application of storage system are UPS (Uninterruptible Power Supply), where technologies such as batteries, flywheel and supercapacitors are widely used to prevent damage of critical loads, for example computer, hospital equipment or communication infrastructures. But the

technological process and new challenges related to the introduction of renewable energy sources are driving research into new technologies.

In general, they are classified according to the storage principle, and to better understand their size and possible applications, their energy capacity can be related to their discharge time as shown in Figure 1.3:

- *Mechanical energy storage*: there are different types, varying from those capable of providing high power for short periods such as flywheels, exploiting the rotational energy of a mass, to those capable of supplying energy for several days, such as pumped hydro storage, which exploits the potential energy of water, or compressed air energy storage, which exploits the volume and pressure work of air;
- *Electrical energy Storage*: there are two types that differ based on the medium in which they store energy. Supercapacitors store it in the electric field, while superconducting coils exploit the magnetic field generated by the coil. They are characterized by low energy capacities but high power, ensuring rapid response times;
- *Electrochemical energy storage*: it concerns classical batteries (Li-Ion, Pb, NiMH), high-temperature batteries (NaS, $NaNiCl_2$), and redox-flow batteries. They are characterized by the type of materials used for the cathode, anode, and electrolyte. Today, they are widely used, ranging from electric mobility to off-grid applications and powering electronic devices;
- *Chemical energy storage*: energy is released during chemical processes and stored in compounds that can be in gaseous, liquid or solid form. Two key characteristics are a wide range of choices for transport and storage and a high energy density. Examples could be hydrogen storage systems and biofuels;
- *Thermal energy storage:* they can be divided into three technology types. Sensible heat storage that involves storing energy in the heat of materials undergoing temperature changes. Latent heat storage that utilizes the energy absorbed or released during phase change of a material, while thermochemical energy storage that relies on the heat released during a chemical reaction.

In this thesis an underwater compressed air energy storage (UW-CAES) will be discussed, which therefore is part of mechanical storage systems.

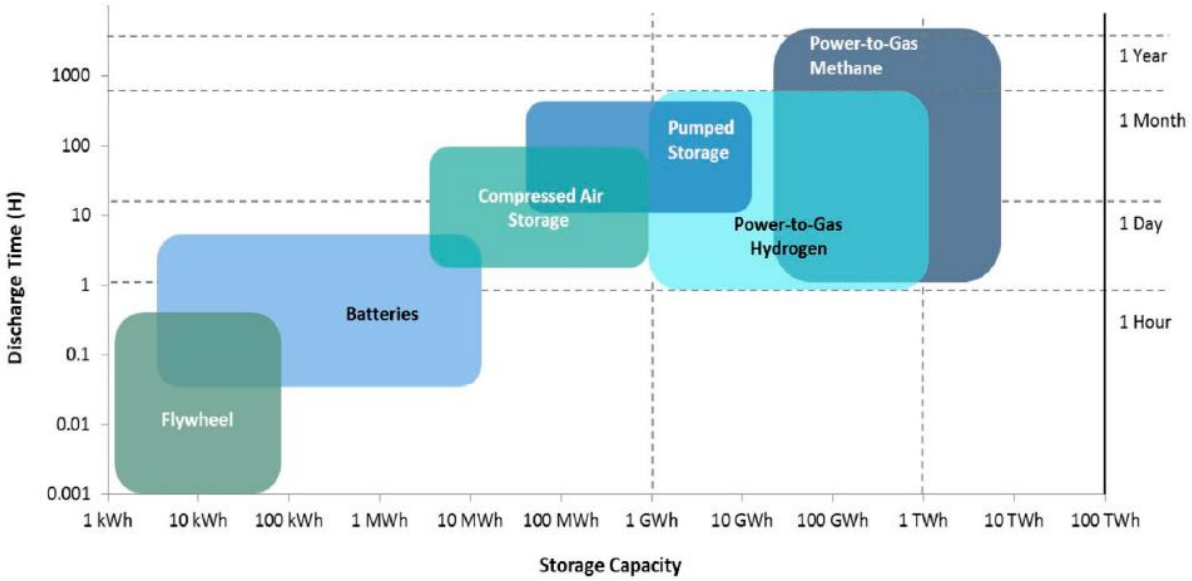

Figure 1.3: Comparison of discharge time vs capacity of energy storage technologies. [3]

1.3. CAES System

CAES (Compressed Air Energy Storage) is an energy storage system that utilizes compressed air to store energy. In a typical CAES system, excess electrical energy is used to compress air and store it in underground tanks or natural cavities. When energy is needed, the compressed air is released and used to generate electricity through a turbine. CAES is considered a large-scale energy storage solution and can help manage the variability of renewable energy sources.

The first plant in the word has been built in 1978 in Huntorf, Germany with a nominal power of 290 MW, even if the concept of CAES system was presented in 1949 by S. Lavale. Then, a second plant was built in 1991 in McIntosh, Alabama, with a nominal power of 110 MW. No other plants have been opened after these two, but in the last decades new interest in them is leading to new research with the increase in the energy produced by NPRES. In fact, a new plant is under investigation in Germany, where the"ADELE" project of 200 MW has been proposed by RWE, General Electric, Zueblin, and the German Aerospace Center. This plant differs for its adiabaticity from the two already existing, that are both diabatic. [4] [5]

There are different solutions to store the compressed air:

- *Salts caverns*: salts are melted to obtain the correct volume using the solution mining techniques. Technology used is well known and adopts water to dissolve salt, and the result is a solid cavern which assure seal also after several cycles;
- *Porous rocks*: in which a layer of impermeable rock seals a region of permeable rocks. The presence of water or natural gas make this solution more dangerous with the respect to the previous case;

- *Caverns*: adequate depth (300 m to 1500 m) avoid the risk of collapse. The use of old mines is the most economic option;
- *Pipes or Tanks*: metal, concrete or composite material can be used to store compressed air, which are placed on the ground or some meters below. Pressure can also reach 300 bar without structural problem also considering rapid charge and discharge [6];
- *Underwater tanks*: uses the hydrostatic pressure of the water to keep constant pressure, during charge and discharge phase. They could be both flexible and rigid. An example of this configuration is made by the group Hydrostor inside Lake Ontario at 80-meter depth [7].

There are various types of CAES systems that has been studied, and their characteristics and configurations are listed below:

- *D-CAES*: it is the traditional one in which the air is stored into a cavern, thus with a diabatic storage (Figure 1.4). The heat of the compression is lost with the use of intercooler and aftercoolers, for increasing the amount of air storable. Therefore, a combustion chamber is necessary before the turbine to increase the enthalpy content of the air flow. This system inevitably includes the use of fuel leading to greenhouse gas emissions;

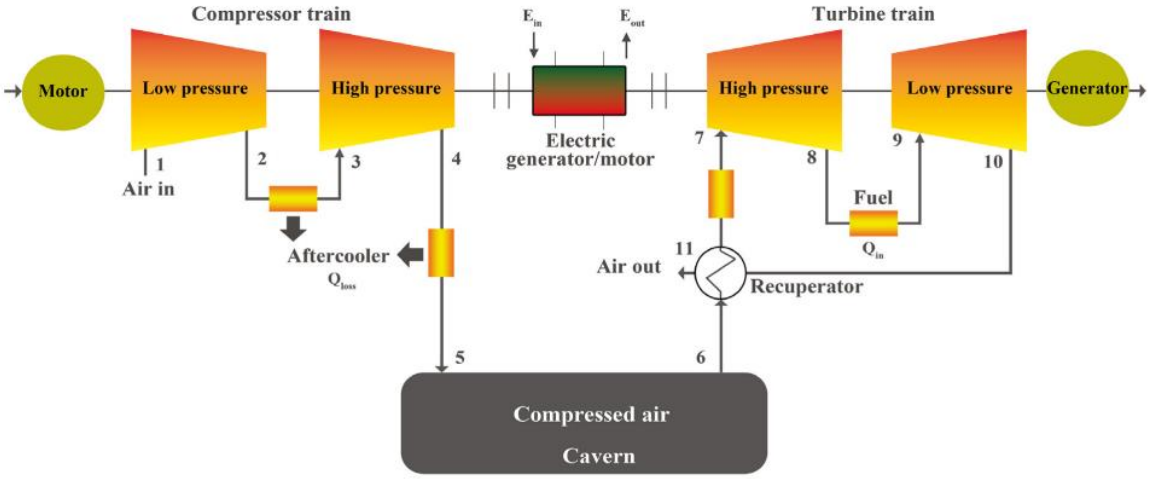

Figure 1.4: Plant layout of a D-CAES system. [8]

- *Steam CAES*: based on D-CAES in which part of the residual heat of the flue gasses is used for a bottom Rankine cycle, or to produce steam to be supplied in the combustion process to enhance the efficiency of the plant;
- *A-CAES*: It is an adiabatic system in which there is no need of fuel and the heat generated during compression is stored and used to heat up air during discharging phase (Figure 1.5). The adiabatic system allows to avoid the production of CO_2 and increase the overall efficiency reachable, because combustion of fuel is not used with all its exergy losses. Lower procedure of authorization of the plant is required, since no pollutant are emitted, and thus

lower territorial constraints limit the use of this type of CAES. The main disadvantage of such configuration is related to the cost of the working fluid used to store the compression heat;

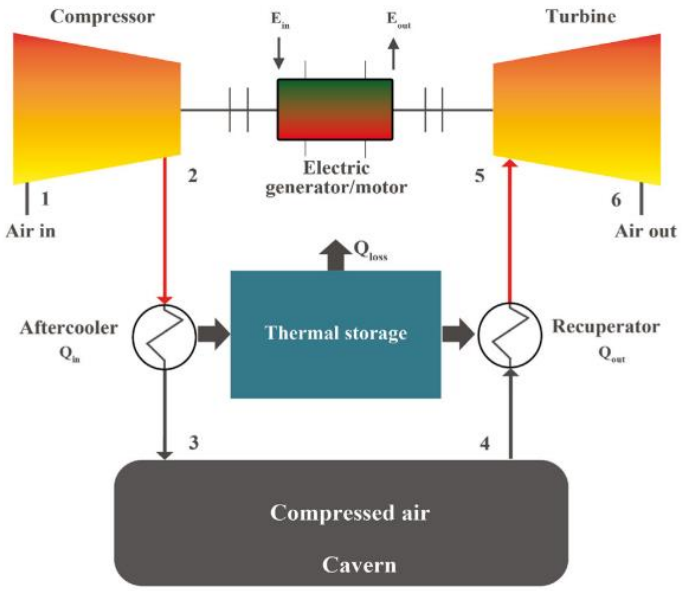

Figure 1.5: Plant layout of a A-CAES system. [8]

- *IsoT-CAES*: which tries to reproduce isothermal transformation with the injection of water to control temperature;
- *Hybrid-CAES*: which couple CAES system with a gas turbine. In this way air from the tank can be preheated with flue gasses, and the use of fuel increases a lot the efficiency of the plant [9].

Obviously, another distinction can be made basing on the kind of air storage system, that can be at constant volume resulting in an isochoric CAES, or with variable volume resulting in an isobaric CAES. The latter is typical of underwater CAES that allows to have better conditions for compressor and turbine, since the outlet pressure of compressor and the inlet pressure of turbine are not affected by the air accumulation and consumption respectively, but at the same time this solution is more expensive.

1.4. Thesis Outline

In this thesis an UW-CAES system is analysed as a possible solution to be integrated with an off-shore wind farm, evaluating its cost-effectiveness. In the following a brief introduction to the next chapters is done:

- Chapter 2: a description is made of the different components that make up an UW-CAES system at the state of the art, defining the main characteristics for their design and highlighting the constraints to be taken into account. Then, possible examples of an integrated system are presented;

- Chapter 3: the equations for the design of each component of the plant are shown, describing how the different parts interact during the entire process;
- Chapter 4: in this chapter, the behaviour of the components of the plant during its annual operation is explained, based on the design. In addiction, the logic used to determine the functioning of the plant is described, explaining all the constraints that must be satisfied;
- Chapter 5: the costs of investment and maintenance of the different components of the plant are analysed, showing then the used parameters to assess the economic feasibility of the CAES system;
- Chapter 6: firstly, the results of the design, operation and economic analysis of the case study are discussed, compering three different years (2019, 2020, 2022), to analyse how different energy prices affect plant operation. Then, the results of two other plants are shown, underling how site location influences the cost-effectiveness of a plant;
- Chapter 7: a sensitivity analysis is conducted from both a technical and economical point of view, mainly on the case study;
- Chapter 8: the conclusions of this work are drawn.

2 UW-CAES layout

An UW-CAES system is composed by different components. In the following, they and their roles are shortly presented [4]:

- Air filter: to clean air from dust and dirt, that can damage the compressor train and other components of the air circuit;
- Compressor: driven by an electric motor, it is used to increase the air pressure from the ambient one to the underwater vessels;
- Intercooler (IC): to cool down air during the compression phase between consecutive compressors, in order to decrease the absorbed work and control the temperature at the compressor outlet;
- Heat exchangers (HX): used to transfer heat between air and thermal fluids;
- Thermal Energy Storage (TES) system: used to store thermal energy, it is the component that, coupled with the HXs, enables an adiabatic system, storing the energy released during air cooling and returning it during the heating process;
- Air tanks: underwater storage units in which air is stored, allowing it to be kept at constant pressure;
- Pipeline: it links the air tanks with the rest of the system, allowing the air to flow through;
- Turbine: to expand the stored air and generate electric power by driving an electric generator.

To better understand the functioning and interaction of these components, it is possible to distinguish the operation of the system into two different phases:

- Cooling to Storage (CtS): charging phase;
- Heat from Storage (HfS): discharging phase.

This distinction is fundamental because in a CAES system, the compressor and turbine never operate simultaneously, as happens in a normal gas cycle. Therefore, the two phases represent the two moments of operation of the system: during the CtS phase, the compressor works by storing air in the underwater tanks, while during the HfS phase, the turbine works by expanding the stored air to produce energy. This decoupling is typical of storage systems, which store energy when it is abundant or convenient, and release it when needed or if the market is favourable.

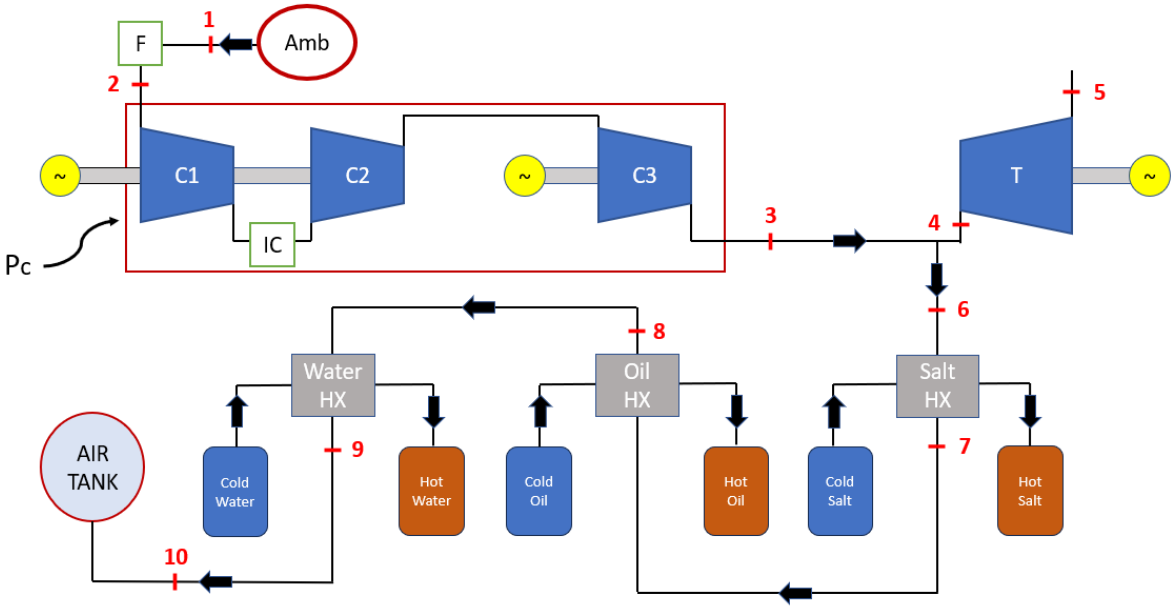

Figure 2.1: Plant scheme and charging mode (CtS).

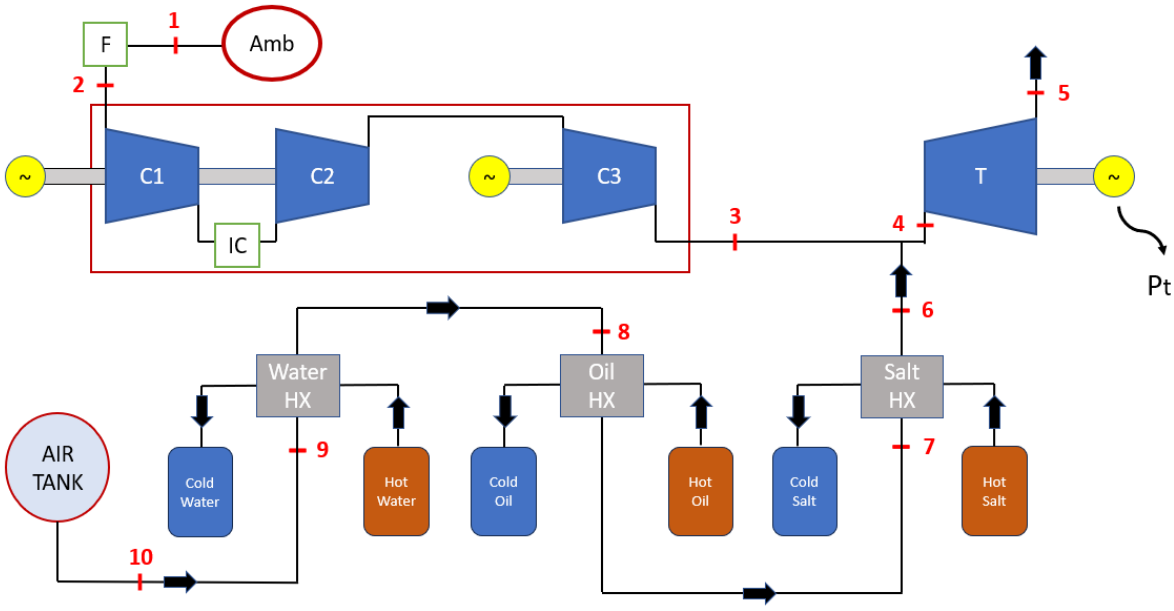

Figure 2.2: Plant scheme and discharging mode (HfS).

By following the Figure 2.1 it is possible to better understand the path of the air through the system in charging mode. Starting at point 1, the ambient air is purified by the air filter, reaching the inlet of the compressor train at point 2. Then, the compressors increase its pressure up to underwater pressure, plus the pressure drop to be covered through the system, resulting in an increase of its temperature up to the so-called compressor outlet temperature (COT). Thanks to a system of valves, air flows from point 3, the compressor outlet, to the first heat exchanger at point 6. At this point the air undergoes the cooling process, and its thermal energy is stored in the TES. From the air-salt heat exchanger, passing through the air-thermal oil heat exchanger, the air

reaches the outlet of the last HX, the air-sea water one, with a temperature close to that of ambient air. It then arrives at the inlet of the pipeline that connects the system on shore with the underwater tanks at point 10, where the air is stored at constant pressure. The thermal fluids in this phase flow from the low temperature tanks through the HXs, and heating ends up in the hot tanks. This heat is then used to warm up the air before the expansion in the turbine.

The opposite path is taken by the air in discharging mode (Figure 2.2). Thus, from the underwater tanks in point 10, the HXs are reached in point 9 and crossed in reverse way until point 6, where again a system of valves allows the air to flow through the turbine. During this phase the air is heated from the sea water temperature up to the turbine inlet temperature (TIT), thanks to the energy stored in the TES in the previous phase.

In this thesis the UW-CAES system is seen as part of an integrated system with an off-shore wind farm (Figure 2.3), even if the latter will not be analysed. In fact, the CAES system will be investigated considering projects of off-shore wind farm already presented in Italy, trying to carry out its design and operation on the bases of the wind farm power output forecast.

Now that has been shortly presented the operation of the plant and how the components interact to make it possible to work, a detailed explanation on their main aspects is needed to understand their design criteria.

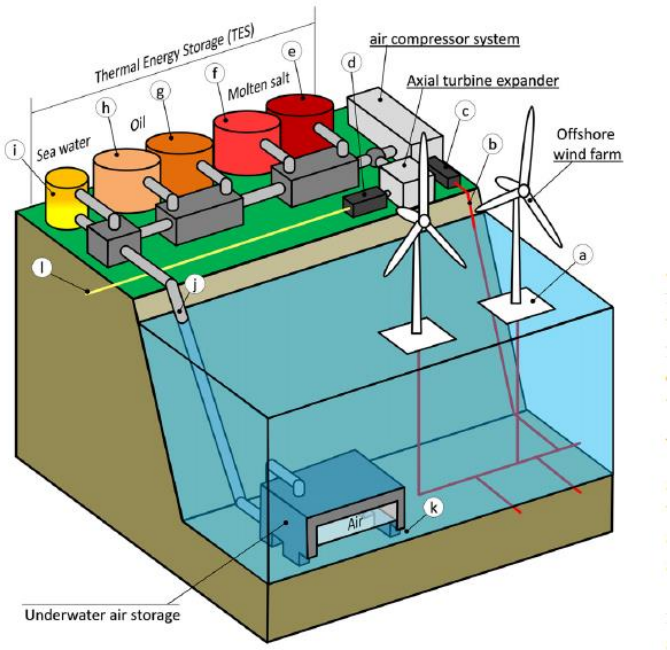

Figure 2.3: UW-CAES configuration coupled to an off-shore wind farm. [10]

2.1. Turbomachines

Compression train and turbine are two crucial components of a CAES plant. The former allows to store energy as compressed air, driven by an electric motor that absorbs electricity provided by the off-shore wind farm. The latter allows to expands the stored air to drive an electric generator that produces electricity.

The compressor train is designed to reach the desired pressure and can be composed by more compressors in series. In order to decrease its work consumption, an intercooler is introduced, that has to be designed also to reach the right temperature at the compressor outlet (COT). This is necessary to improve the following heat exchange process basing on the thermal fluids' characteristics. The layout of the compression train and the assumptions to perform calculations are taken from a previous work [11]. Its work conditions depend by the power output of the off-shore wind farm at which the UW-CAES system is coupled, thus it often works in off-design condition, differently by the turbine that, for sake of simplicity, is designed to work always at full power. The only aspect that must be paid attention to is the turbine outlet temperature (TOT) that must be higher than 5°C to avoid freezing phenomena.

For the intercooler a Shell-and-Tube heat exchanger is assumed, with sea water as cooling fluid flowing inside the tubes and the air in the shell side. Since the sea water is reinjected into the sea, the Italian legislation imposes limits to its maximum temperature, that is fixed to 35°C by "decreto legislativo 3 aprile 2006, n. 152" [12]. This constrain is important to determine the sea water mass flow rate necessary to cool down the air without exceed this limit.

Table 2.1: Assumption for performance calculations of turbomachines.

Parameter	Value	Unit
T_{amb}	15	°C
p_{amb}	101325	Pa
cp_{air}	1050	J/(kg·K)
η_{o-el}	95%	[-]
$\eta_{C,nom}$	85%	[-]
$\eta_{T,nom}$	90%	[-]
$\Delta p_{\%,F}$	1%	[-]

Table 2.2: Assumption for performance calculation of intercooler.

Parameter	Value	Unit
$T^{in}_{sw,IC}$	14	°C
$\Delta T_{pp,IC}$	10	°C
$\Delta T^{max}_{sw,IC}$	21	°C
$\Delta p_{\%,IC}$	1%	[-]

Other than the listed assumptions in Table 2.1 and Table 2.2, the following are made:

- Heat losses are neglected;
- At the inlet of the heat exchanger on each fluid side, the flow velocity and temperature of both fluids are considered uniform over the flow cross section;
- The fluid flow rate is uniformly distributed through the heat exchanger on each fluid side in each pass.

2.2. T.E.S.

The key component that contributes to the adiabatic nature of this CAES system is the Thermal Energy Storage (TES). In fact, the TES's purpose is to use thermal fluids to store the energy of the high-temperature air stream that exits the final compression stage. The air must be cooled from a high temperature over 600°C, to the ambient temperature before being stored, otherwise the heat will be lost. In that way, the stored energy can be used to heat up the air before expansion through the turbine without integrating any fuel. Hence, it permits the decoupling between the compression and expansion phases.

Three distinct high performance heat transfer fluids (TF) must be used, following previous work [11]:

- Molten Salts – 60% $NaNO_3$, 40% KNO_3 [13];
- Diathermic Oil [14];
- Sea water.

The thermodynamic properties of these fluids, shown in Table 2.3, are taken from the previous work, except for diathermic oil and molten salt densities, and specific heat of diathermic oil, that are evaluated as integral average in the range of temperature of work of the corresponding functions given by [13] and [14].

Table 2.3: Thermodynamic properties of thermal fluids. [11] [13] [14]

Parameter	Solar Salt	Diathermic Oil	Sea Water	Unit
T_{max}-T_{min}	600-290	290-80	80-30	°C
ρ	1808.8	757.9	985.7	kg/m^3
cp	1559	2490.8	4179.2	J/(kg·K)
k	0.5275	0.1071	0.464	W/(m·K)
μ	0.0015	$9.787 \cdot 10^{-4}$	$5.0363 \cdot 10^{-4}$	Pa·s
Pr	4.3046	19.56	3.2609	[-]

The TES results then composed by three sequential storage units, with a cold and a hot tank for each fluid. In fact, during CtS phase each TF flows from the cold to the hot one through an HX, storing thermal energy, and during HfS phase they release it flowing in the opposite direction from hot to cold tank. The range of their operating temperature depends by physical constraints such as evaporation temperature for the sea water, that imposes its T_{max}, fire and cracking phenomenon for the diathermic oil,

that are composed by synthetic oils, and solidification temperature and unstable behaviour that limit the solar salt T_{min} and T_{max} respectively. The tanks used to store the TFs are supposed of being cylindrical structures with a diameter and height of 20 meters, and with negligible heat losses.

2.3. Heat exchangers

Other than the already mentioned IC, the plant presents three heat exchangers that are used to cool down the air temperature during CtS phase, from the COT at the compressor out to the sea water temperature. The same HXs are then used to heat up the air during HfS phase, from the sea water temperature at which it is stored in the underwater tanks, to the TIT at the turbine intake. As done for the IC, Shell-and-Tube type is used also in this case, with the thermal fluids that are supposed to flow inside the tubes while the air in the shell side. Their design depends by the air flow characteristic obtained by the operation of the compressor in design mode, other than the thermal fluids characteristic. The following assumptions are valid [11]:

- $\Delta T_{pp,HX}$ of 25°C;
- $\Delta p_{\%,HX}$ of 1%;
- Negligible heat loss;
- Negligible tube wall thermal resistance and fouling effect;
- Fully developed conditions for both air and thermal fluids.

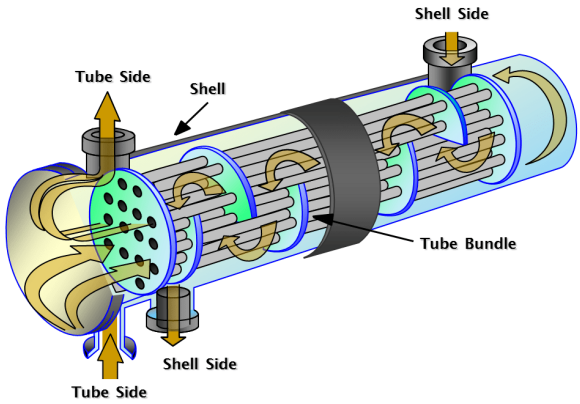

Figure 2.4: Example of a Shell and Tube heat exchanger [15].

In addition to these three HXs, another is used to transfer energy from solar salt to thermal oil when a lack of energy stored in the oil tanks would prevent the functioning of the plant in HfS mode.

2.4. Underwater air storage system

The underwater tanks constituting the air storage system is one of the key components of the UW-CAES system discussed in this work, making it innovative respect the CAES

systems already existing. The air storage tanks can be either flexible and closed, allowing the internal fluid to be pushed by the external pressure on the walls, or rigid and communicating with the seawater, allowing water to partially fill the tank while maintaining a constant internal pressure. In order to give more flexibility to the system, this storage is often made up of several units that are attached to the seafloor. In the tanks, compressed air is held at a pressure equivalent to the hydrostatic pressure of the surrounding water, therefore, their design is determined by the depth at which they are placed below the water surface. The two different storage solutions adopted in this thesis are taken from a previous work in which their characteristics are deeply discussed [4].

Energy Bags taken from space application and presented by NASA, are chosen as flexible air storage. The compressed air is stored in flexible fabric structures, of 36000 m^3 as maximum volume, anchored to the seabed, that during charging phase will expand and will contract during discharging phase, keeping constant the air pressure. An example is shown in Figure 2.5(a).

Regarding tanks with a rigid structure instead, Rigid Caissons made by concreate is taken in consideration (Figure 2.5(b)), with a volume of 5000 m^3 per tank. They are characterized by an open-ended structure that allows to the surrounding seawater to keep constant the air pressure entering inside during HfS phase and flowing out during CtS phase. The most important aspect of this kind of tanks is that they can be sized as gravity base structures, resisting to the buoyancy without the need of additional anchor or piles.

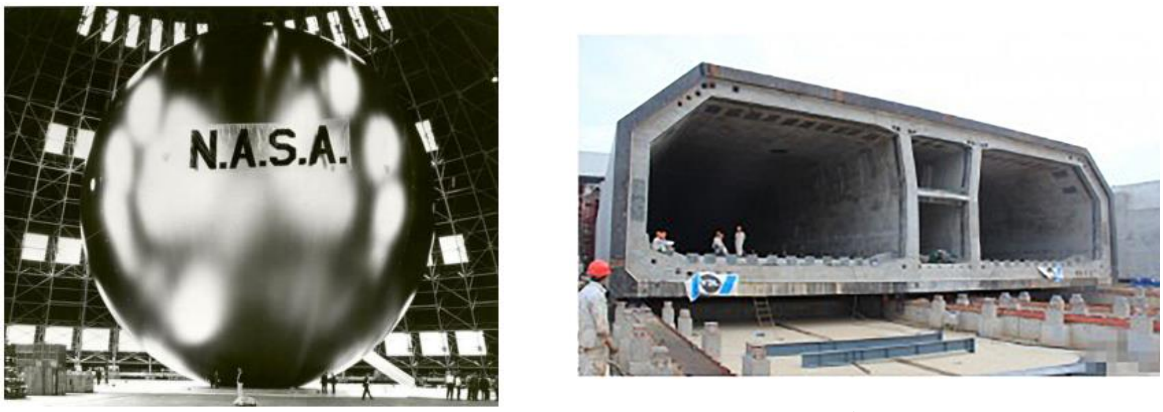

(a) (b)

Figure 2.5: (a) NASA Energy Bag; (b) Rigid Caisson.

The storage temperature is considered at 5°C, in equilibrium with the seawater one at seabed depth, and for the evaluation of the underwater pressure a sea water density ρ_{SW} of 1025 kg/m^3 is assumed. Furthermore, possible pressure losses resulting from the flow of air between the air tanks and the pipeline are neglected.

2.5. Pipeline

The pipeline is designed to connect the facility on the coast, consisting of turbomachines and a TES system, with the subsea air storage system. Since the latter may be located far from the coast, the pipeline design must consider this distance because resulting pressure losses could significantly impact the plant's operation. In this thesis, its sizing is based on previous work [4], which thoroughly examined the pipeline's resistance to internal and external loads and the balancing of buoyancy forces. The materials considered for its construction are carbon steel for the pipeline, with an inner surface roughness ϵ of $2 \cdot 10^{-4}$ m, and a concrete coating as ballast. In Chapter 3 their design is presented.

The air flowing inside the pipeline is considered to be in thermal equilibrium with the surrounded water at 5°C, neglecting the heating effect given by friction.

2.6. Integrated system

As already mentioned, the UW-CAES system is assumed to be coupled with an off-shore wind farm. This connection can be realised in different ways, for example by considering the turbomachines placed on land and the air tanks, instead, where the wind farm is located, or by using an off-shore platform to place everything close to the wind farm, thus reducing the pipeline length almost to zero. In any case, one of the most important parameters to be taken into account is the depth of the sea, as it determines the underwater pressure at which air is stored. Therefore, the choice of the off-shore wind farm must be made considering the characteristics of its location, both in terms of sea depth and distance from the coast. Some possible configurations are shown in Figure 2.6.

In configuration (a) the layout with the CAES plant on land is shown. In this case, the air storage system can be positioned close to the off-shore wind farm or not, and the pipeline length depends by the distance between CAES and the air tanks.

Configuration (b) shows the case where an off-shore platform is used to place the CAES close to the air storage system, thus reducing the pipeline length essentially to the sea depth. The system can be placed close to the wind farm, but it is not a constrain.

Finally, another layout similar to the first one is shown in configuration (c), in which the location of the underwater tanks is constrained to that of the off-shore wind farm, as the tanks are used as ballasts of the floating wind turbines. This requires the use of tanks with a rigid structure, such as rigid caissons.

In this work, case (a) is taken into account, by locating the air tanks close to the wind farm.

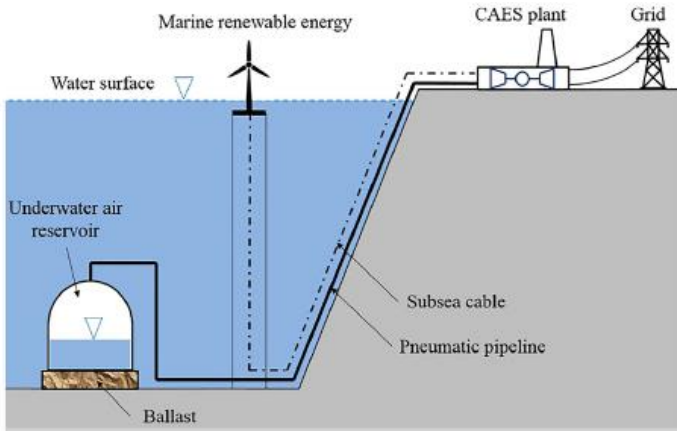

(a)

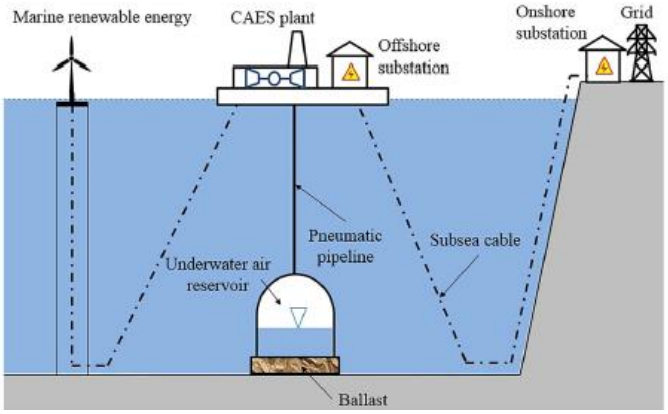

(b)

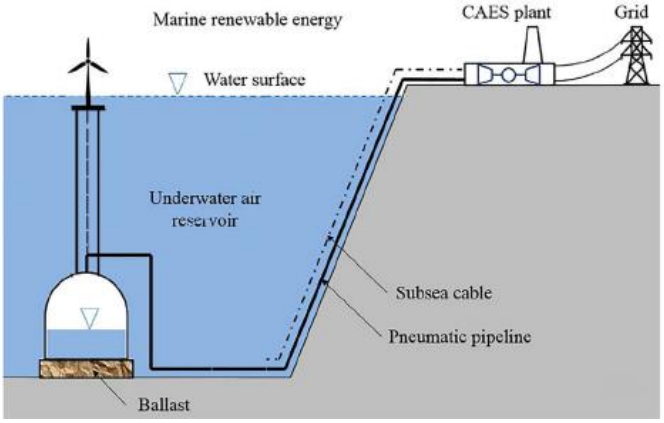

(c)

Figure 2.6: Possible configurations of UW-CAES and off-shore wind farm as integrated system. [4]

3 Operation Design

Basing on the characteristics of the site where the wind farm and the UW-CAES are located, the evaluation of the plant in design mode is conducted in order to size the main components and determine the magnitude of the mass and thermal flows that the plant faces. These results are subsequently used to evaluate the actual operating conditions of the plant, through a simulation of its annual operation as shown in the next chapter.

The design of each component of the UW-CAES plant has been carried out with a MatLab model. This is necessary to solve the system of equations that takes into account how the different parts of the plant influence each other. In order to assess the real conditions of air as a real gas at different points in the thermodynamic cycle, the CoolProp library was used.

The model is divided into two parts that analyse the two different phases: Charging (CtS) and Discharging (HfS). First at all, the constrains and the site specifics are defined, then the model can run.

3.1. Charging phase

Giving the site specifics like sea depth $d\ [m]$, the hydrostatic pressure $p\ [Pa]$ at which the air has to be stored can be calculated:

$$p_{air\ tank} = p_{amb} + \rho_{sw}\ g\ d \tag{3.1}$$

where p_{amb} is the ambient pressure in Pa, ρ_{sw} is the sea water density in kg/m^3 and g is the gravity constant equal to 9.81 m/s^2.

At this point, it's possible to analyse how the compression train works to ensure that the air tanks can be filled, considering that air pressure has to be increased above the $p_{air\ tank}$ to cope with pressure drops, mainly through heat exchangers and pipeline.

The main equations are the following:

$$P_c = \frac{\dot{m}_{air}\ \Delta h_C^{tot}}{\eta_{o-el}} \tag{3.2}$$

$$p_C^{out} = p_{air\ tank} + \Delta p_{pipe} + \sum \Delta p_{HX,i} \tag{3.3}$$

$$\Delta p_{pipe} = 8\, f \frac{\dot{m}_{air}^2\, L}{\rho_{av}\, \pi^2\, D^5} \tag{3.4}$$

$$f = \frac{1.325}{\left[ln\left(\frac{\varepsilon}{3.7\, D} + \frac{5.74}{Re^{0.9}}\right)\right]^2} \tag{3.5}$$

$$Re = \frac{4\, \dot{m}_{air}}{\pi\, D\, \mu} \tag{3.6}$$

Where the unknowns are:

- air mass flow rate $\dot{m}_{air}$ $\left[\frac{kg}{s}\right]$;
- enthalpy variation across the compressor train Δh_C^{tot} $[\frac{J}{kg}]$;
- air pressure at the compressor train outlet p_C^{out} $[Pa]$;
- pressure drops through the three heat exchangers $\sum \Delta p_{HX,i}$ $[Pa]$ and pipeline Δp_{pipe} $[Pa]$;
- friction factor f $[-]$;
- average air density across pipeline $\rho_{av}[\frac{kg}{m^3}]$;
- Reynolds number Re $[-]$.

The $p_{air\ tank}$ was already presented in the Equation (3.1) and the other parameters are known, since they represent plant characteristics, such as:

- nominal power P_c $[W]$ of compressor train;
- organic-electric efficiency η_{o-el} of compression train, including gearbox and electric motors;
- pipeline length L $[m]$ that depends on the distance from the shore;
- pipeline inner diameter D $[m]$;
- roughness of pipeline inner wall ε $[m]$;
- air viscosity μ $[Pa \cdot s]$.

In general, the friction factor f is a complex function of Re and ε/D, but for turbulent flows, it can be written as in Equation (3.5) if the following conditions are satisfied:

$$\begin{bmatrix} 5000 \leq Re \leq 10^8 \\ 10^{-6} \leq \frac{\varepsilon}{D} \leq 10^{-2} \end{bmatrix}$$

The Equation (3.6) is obtained starting from the definition of Reynolds number, Equation (3.7), and replacing the air velocity from the mass flow rate across a pipe, defined in Equation (3.8):

$$Re = \frac{\rho\, v\, D}{\mu} \tag{3.7}$$

$$\dot{m} = \rho \, v \, \pi \frac{D^2}{4} \tag{3.8}$$

where v is the fluid velocity in [m/s].

For sake of simplicity the pressure drops through each of the three heat exchangers are fixed equal to a fraction of the respective inlet pressures, then they can be calculated as follows:

$$\Delta p_{HX,1} = p_C^{out} \cdot \Delta p_{\%,HX} \tag{3.9}$$

$$\Delta p_{HX,2} = p_C^{out} \cdot \left(1 - \Delta p_{\%,HX}\right) \cdot \Delta p_{\%,HX} \tag{3.10}$$

$$\Delta p_{HX,3} = p_C^{out} \cdot \left(1 - \Delta p_{\%,HX}\right)^2 \cdot \Delta p_{\%,HX} \tag{3.11}$$

The average density of air across the pipeline ρ_{av} is evaluated as an arithmetic mean between the inlet and the outlet one. To do that, the respective densities are computed as function of the sea water temperature T_{sw} [K] and pressures by means of CoolProp, knowing that the air pressure at pipeline inlet is equal to pressure in the air tanks plus pressure drop across the pipeline.

$$p_{pipe}^{in} = p_{air\ tank} + \Delta p_{pipe} \tag{3.12}$$

$$\rho_{pipe}^{in} = CoolProp\left(T_{sw},\ p_{pipe}^{in}\right) \tag{3.13}$$

$$\rho_{pipe}^{out} = CoolProp\left(T_{sw},\ p_{air\ tank}\right) \tag{3.14}$$

$$\rho_{av} = \frac{\rho_{pipe}^{in} + \rho_{pipe}^{out}}{2} \tag{3.15}$$

Since the air has to flow through the entire pipeline, that is underwater for almost all its length, except for the first part on shore from the sea water heat exchanger to the sea, the air at the pipeline inlet is assumed to be in thermal equilibrium with the sea water, then with a temperature equal to T_{sw}.

The last unknown that needs to be analyzed in detail is the Δh_C^{tot}, that represents the enthalpy variation across all the different stages of the compressor train, considering that is dived into three main parts in series, with an intercooler between the first and second one, as investigated in the previous work [11].

To better understand what is involved, Figure 3.1 shows the intercooled compression phase on the thermodynamic diagram T-s (temperature and entropy):

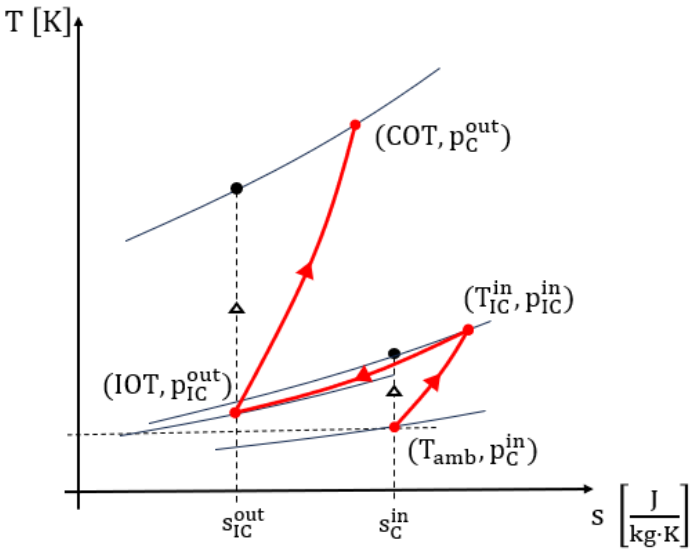

Figure 3.1: Intercooler effect on compressor work.

where IOT and COT respectively stand for Intercooler Outlet Temperature and Compressor Outlet Temperature. Both are set, during the plant design, to guarantee the best performance of the plant, determining the necessary sea water flow rate to cool down the air up to IOT.

Regarding the air temperature coming out of the compress, to maximize the heat exchange between the air and the different thermal fluid used in the three HXs, the COT is set equal to 625°C. This value can be easily found knowing that the pinch point of the HX, $\Delta T_{pp,HX}$, is assumed 25°C and the maximum temperature the solar salt can face is 600°C, otherwise at higher temperature its behaviour becomes unstable. In this way it is possible to minimize losses during the whole heat transfer process.

Similarly, since a counterflow air-water heat exchanger is used as IC, the air temperature at the end of the intercooling process is equal to 24°C, assuming a $\Delta T_{pp,IC}$ of 10°C and a sea water temperature $T_{sw,IC}^{in}$ of 14°C. This last temperature is different from the one assumed for sea water when air properties at pipeline inlet are evaluated, because in this case water close to the coast is used.

This plant complication, with the introduction of an IC, is needed firstly to reduce the work of the compressor train and so its energy consumption, then to guarantee a suitable temperature of the air at the compressor outlet, to perform a better cooling process with thermal fluids from a thermodynamic point of view.

In the process shown in Figure 3.1, only the inlet conditions of the compressor are already known:

$$\begin{cases} h_C^{in} = CoolProp\left(T_{amb},\, p_c^{in}\right) \\ s_C^{in} = CoolProp\left(T_{amb},\, p_c^{in}\right) \end{cases} \tag{3.16}$$

where the inlet pressure of the compressor depends on the pressure drop across the filter.

$$p_C^{in} = p_{amb}\left(1 - \Delta p_{\%,F}\right) \tag{3.17}$$

At this point the enthalpy variation across the compressor train can be performed as shown in the Equation (3.18):

$$\Delta h_C^{tot} = (h_C^{out} - h_{IC}^{out}) + \left(h_{IC}^{in} - h_C^{in}\right) \tag{3.18}$$

Starting from the compressor outlet, with some equations it is possible to find out all the required enthalpies:

$$h_C^{out} = CoolProp(COT,\, p_C^{out}) \tag{3.19}$$

$$h_{C,is}^{out} = (h_C^{out} - h_{IC}^{out}) \cdot \eta_{C,nom} + h_{IC}^{out} \tag{3.20}$$

$$h_{C,is}^{out} = CoolProp(p_C^{out},\, s_{IC}^{out}) \tag{3.21}$$

$$h_{IC}^{out} = CoolProp(IOT,\, s_{IC}^{out}) \tag{3.22}$$

$$p_{IC}^{out} = CoolProp(IOT,\, s_{IC}^{out}) \tag{3.23}$$

$$p_{IC}^{in} = \frac{p_{IC}^{out}}{\left(1 - \Delta p_{\%,IC}\right)} \tag{3.24}$$

$$h_{IC}^{in} = \frac{h_{IC,is}^{in} - h_C^{in}}{\eta_{C,nom}} + h_C^{in} \tag{3.25}$$

$$h_{IC,is}^{in} = CoolProp\left(p_{IC}^{in},\, s_C^{in}\right) \tag{3.26}$$

where $\eta_{C,nom}$ [-] is the nominal adiabatic efficiency of the compressor. Furthermore, the difference between p_{IC}^{in} and p_{IC}^{out} give the pressure drop Δp_{IC} across the intercooler.

All the equations from (3.2) to (3.26), are iteratively solved together in a system by means of the function *fsolve* on MatLab. In addition to the unknowns already mentioned, other important parameters are calculated, such as the total compression ratio of compressor train $\beta_{C,tot}$, and the compression ratio before and after the intercooler $\beta_{C1}$and β_{C2}.

The only aspect that still needs to be analysed in this first portion of the plant, is the heat transfer exchange through the intercooler.

During nominal conditions design, it is possible to evaluate the exchanged thermal power Q_{IC} $[W]$, the sea water mass flow rate $\dot{m}_{sw,IC}$ $[\frac{kg}{s}]$ and the parameter $(UA)_{IC}^{nom}$ $[\frac{W}{K}]$ to size the intercooler, solving the following energy balance:

$$\begin{cases} Q_{IC} = \dot{m}_{air}\, cp_{air}\left(T_{IC}^{in} - IOT\right) \\ Q_{IC} = \dot{m}_{sw,IC}\, cp_{sw}\, \Delta T_{sw}^{max} \\ Q_{IC} = (UA)_{IC}^{nom}\, \Delta T_{mln}^{IC} \end{cases} \tag{3.27}$$

In particular, cp_{air} and cp_{sw} are the specific heat of air and sea water respectively in [J/kg K], A is the heat exchange surface in [m^2], U is the overall heat transfer coefficient in [W/m^2 K], and ΔT_{sw}^{max} is the maximum temperature variation allowed for sea water to respect Italian legislation. Regarding T_{IC}^{in} can be easily found with CoolProp, since at least two thermodynamic properties are already known, such as the enthalpy and pressure at the inlet of the IC. The logarithmic mean temperature in the last equation of the system is expressed as:

$$\Delta T_{mln}^{IC} = \frac{\left(T_{IC}^{in} - T_{sw,IC}^{out}\right) - \left(IOT - T_{sw,IC}^{in}\right)}{\ln\left(\frac{T_{IC}^{in} - T_{sw,IC}^{out}}{IOT - T_{sw,IC}^{in}}\right)} \tag{3.28}$$

After the description of this first part of the plant, the Thermal Energy Storage (TES) can be analysed, knowing the air mass flow rate in nominal conditions that have to be cooled and its temperature at the beginning. Since the COT is a constrain that is guaranteed by the IC, in design conditions the temperature of the air at the inlet of the first heat exchanger, is always known. Furthermore, it has been set to have the best performance during the heat exchange, in fact is equal to the maximum temperature the solar salt can face, plus the chosen pinch point for these heat exchangers.

The energy balance for each heat exchanger has been conducted keeping constant and equal the thermal capacity between air and thermal fluid, so that the temperature variations are the same, and with constant specific heats for both fluids involved in the heat exchange process. In this way, for each heat exchanger, the process can be drawn with parallel straight lines on the T-Q diagram as shown in Figure 3.2.

$$\begin{cases} Q_{HX} = \dot{m}_{air}\, cp_{air}\, \Delta T_{air} \\ Q_{HX} = \dot{m}_{tf}\, cp_{tf}\, \Delta T_{tf} \\ Q_{HX} = (UA)_{HX,CtS}^{nom}\, \Delta T_{mln} \end{cases} \tag{3.29}$$

Since, in order to have a constant thermal capacity, the following equality has to be satisfied:

$$\dot{m}_{air}\, cp_{air} = \dot{m}_{tf}\, cp_{tf}$$

and the range of temperature variation for the thermal fluids are known from the previous chapter, the ΔT_{air} is equal to the one of the thermal fluids, as already told, and the outlet temperature of air at the exit of each HX can be performed.

The logarithmic mean temperature is equal to the pinch point because the temperature difference between the two fluids is constant and equal to it during the whole process for each heat exchanger. Then, from the energy balance for each HX, the mass flow rate of thermal fluids and the UA parameters can be found for nominal condition in CtS mode.

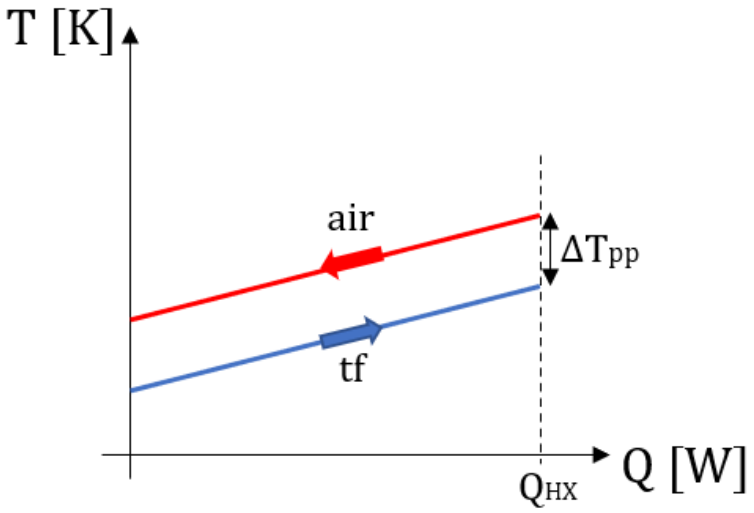

Figure 3.2: Heat exchange process during CtS phase.

By means of CoolProp is possible to calculate the properties of the air at the mean temperature and pressure between inlet and outlet of each HX, in particular:

- air viscosity μ $[Pa \cdot s]$;
- thermal conductivity k $[\frac{W}{m\ K}]$;
- specific heat capacity cp $[\frac{J}{kg\ K}]$.

Then, the Prandtl number Pr $[-]$ can be obtained as follow:

$$Pr = \frac{\mu\ cp}{k} \tag{3.30}$$

These properties are necessary to understand how the HXs work in all the others condition, outside of design.

Knowing how the plant works in nominal conditions in CtS mode, the analysis of the HfS mode can be carried out.

3.2. Discharging phase

In this case, the air flows in opposite directions from the air tanks to the turbine, passing through the heat exchangers to be heated up. But before starting with the sizing of the air tanks, the heating process and the expansion through the turbine have to be analysed. Then, knowing how much air the turbine needs, it is possible to size

the air tanks depending on which kind of storage the CAES system has to provide, daily or seasonal.

First at all, the pressure drop across the pipeline has to be evaluated, because the air flows from the air tanks to the TES through the pipeline in reverse way respect to the CtS phase. As proposed in a previous work [16], the turbine dimension factor (TDF) is introduced to correlate the air mass flow rate during CtS and HfS phases:

$$TDF = \frac{\dot{m}_{Nom,HfS}}{\dot{m}_{Nom,CtS}} = \frac{\dot{m}_{turbine}}{\dot{m}_{compressor}} \tag{3.31}$$

It makes easier the evaluation of different working conditions of the plant, just chancing the value of this factor. With a set value of TDF, the air mass flow rate that expands through the turbine is defined, and with the already presented Equations (3.6) and (3.5) is possible to evaluate the Reynolds number and the friction factor f that are necessary to iteratively solve the following system of equations:

$$\begin{cases} p_{pipe}^{out} = p_{air\ tank} - \Delta p_{pipe} \\ \Delta p_{pipe} = 8\, f \dfrac{\dot{m}_{air}^2\, L}{\rho_{av}\, \pi^2\, D^5} \\ \rho_{av} = \dfrac{\rho_{air\ tank} + \rho_{pipe}^{out}}{2} \\ \rho_{pipe}^{out} = CoolProp\left(T_{sw}, p_{pipe}^{out}\right) \end{cases} \tag{3.32}$$

Where the unknown are the pressure and density of the air at the end of the pipeline p_{pipe}^{out} $[Pa]$ and ρ_{pipe}^{out} $\left[\frac{kg}{m^3}\right]$, that means at the inlet of the sea water heat exchanger, the pressure drop Δp_{pipe} $[Pa]$ and the average density of air across the pipeline ρ_{av} $\left[\frac{kg}{m^3}\right]$.

The air density at the inlet of the pipeline is considered equal to the one of air inside the air tanks, neglecting the pressure drops due to the presence of valves and pipes that connect them with the main pipeline. Then, the $\rho_{air\ tank}$ is calculated as shown in the Equation (3.14).

At the end of the pipeline, air starts the heating process to increase its temperature from T_{sw} at which is stored, to the turbine inlet temperature TIT. At the same time, the thermal fluids decrease their temperature from the maximum to minimum one of their possible ranges, as presented in the previous chapter. Possible air temperature increases before reaching the first HX due to friction, are neglected for sake of simplicity.

The thermal energy storage, thanks to the heat stored during the CtS phase, can provide the required energy to heat up the air, starting with the sea water that provides heat at low temperature, then thermal oil and solar salt in the end to achieve high temperature before the air expands through the turbine. Contrary to the cooling phase,

now hot thermal fluid tanks are emptied, and cold tanks are filled, since the thermal fluids cool down to heat up the air, as shown in the Figure 3.3. To do that, the same HXs as in the previous phase are used, then a process with different starting point condition has to be done with the same heat exchanger modules, and therefore with the same heat exchange surface. This implies that the UA parameter in the energy balance is bound to the same correspondent parameter in CtS phase, hence another variable must change to ensure the same number of equations and unknowns. In fact, now the outlet air temperature is free to change, and the process will no longer be depicted with parallel straight lines on the T-Q diagram.

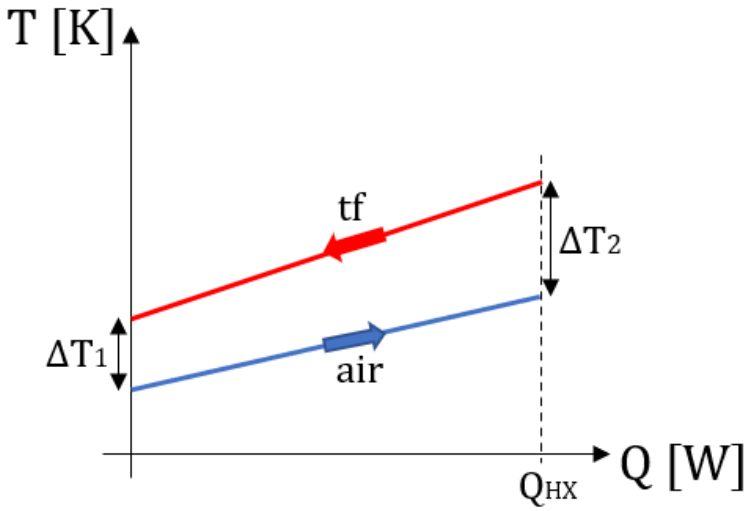

Figure 3.3: Heat exchange process during HfS phase.

By adapting the Equation (3.29) for each HX in the direction in which air flows, substituting the air mass flow rate with the one in HfS phase, it is possible to find the air temperature at the outlet of each HX, the thermal fluid flow rates and the exchanged thermal powers.

$$\begin{cases} Q_{HX} = \dot{m}_{air}\, cp_{air} \left(T_{air}^{out} - T_{air}^{in}\right) \\ Q_{HX} = \dot{m}_{tf}\, cp_{tf}\, \Delta T_{tf} \\ Q_{HX} = (UA)_{HX,HfS}^{nom}\, \Delta T_{mln} \end{cases} \tag{3.33}$$

with:

$$\Delta T_{mln} = \frac{\left(T_{tf}^{out} - T_{air}^{in}\right) - \left(T_{tf}^{in} - T_{air}^{out}\right)}{ln\left(\frac{T_{tf}^{out} - T_{ait}^{in}}{T_{tf}^{in} - T_{air}^{out}}\right)} \tag{3.34}$$

But since the available surfaces for the HXs are constant and the heat transfer properties can change, the UA parameters have to be found before solving the energy balance. To do that, the Dittus Boelter equation and the Nusselt number expression are considered to carry out how the global heat transfer coefficient changes:

$$\begin{cases} Nu = 0.023 \cdot Re^{4/5} \cdot Pr^{n} \\ Nu = \dfrac{h\,D}{k_f} \end{cases} \tag{3.35}$$

where Nu is the Nusselt number, Re the Reynolds number, Pr the Prandtl number, h $[\frac{W}{m^2\,K}]$ is the convective heat transfer coefficient between the surface and fluid, D $[m]$ the pipe diameter of the heat exchanger, and k_f $[\frac{W}{m\,K}]$ the thermal conductivity of the fluid.

This correlation is valid for fully developed turbulent flow in smooth circular tubes and for the following range of conditions [17]:

$$\begin{bmatrix} 0.7 \lesssim Pr \lesssim 160 \\ Re \gtrsim 10000 \\ \dfrac{L}{D} \gtrsim 10 \end{bmatrix}$$

The n exponent of the Pr number is equal to 0.4 when the fluid inside the tubes is heated up, in other words during HfS phase, instead is equal to 0.3 when the fluid is cooled down, then during CtS phase.

Neglecting the tube wall thermal resistance and the fouling effect, from the Equation (3.35) is possible to obtain the h for both fluids during the heat transfer process, air and thermal fluid, and then the global heat transfer coefficient with the following equation:

$$\frac{1}{U} = \frac{1}{h_{air}} + \frac{1}{h_{tf}} \tag{3.36}$$

Since:

$$Nu \propto h; \qquad Re = \frac{\rho\, v\, D}{\mu}; \qquad \dot{m} = \rho\, v\, A;$$

the ratio between the convective coefficient in HfS and CtS mode can be expressed as:

$$\frac{h_{HfS}}{h_{CtS}} \propto \frac{Nu_{HfS}}{Nu_{CtS}} = \frac{\left(Re^{4/5} \cdot Pr^{0.4}\right)_{HfS}}{\left(Re^{4/5} \cdot Pr^{0.3}\right)_{CtS}}$$

$$\frac{h_{HfS}}{h_{CtS}} \propto \left(\frac{\dot{m}_{HfS}\, D \,/\, \mu_{HfS}\, A}{\dot{m}_{CtS}\, D \,/\, \mu_{CtS}\, A} \right)^{4/5} \cdot \frac{\left(Pr_{HfS}\right)^{0.4}}{\left(Pr_{CtS}\right)^{0.3}}$$

Considering that the same HXs are used and with the TDF introduced in the Equation (3.31), the UA relation can be carried out with the following equation:

$$(UA)_{HfS} = (UA)_{CtS} \cdot \left(TDF \cdot \frac{\mu_{CtS}}{\mu_{HfS}}\right)^{4/5} \cdot \frac{(Pr_{HfS})^{0.4}}{(Pr_{CtS})^{0.3}} \cdot \frac{k_{f,HfS}}{k_{f,CtS}} \tag{3.37}$$

The transition from Equation (3.36) to (3.37) is possible by making the assumption to consider only the air side of the HXs for the evaluation of the UA parameters, due to the fact that air has a greater influence on the U variation, thus that is the limiting side. Furthermore, assuming that air viscosity, conductivity and Pr number are constant because of the small dependence on temperature and pressure, the UA value mainly depends on TDF during the HfS phase in nominal condition.

At the end of the heating process, the air temperature and pressure at which the expansion starts are reached, respectively defined as Turbine Inlet Temperature (TIT) and Turbine Inlet Pressure (TIP). In particular, the pressure can be carried out taking into account the procedure followed during the CtS phase from Equation (3.9) to (3.11), to calculate the pressure drops across all the heat exchangers.

Hence, the turbine can be sized based on the mass flow rate of air that flows during the HfS phase and knowing the characteristics of the main points of the expansion process:

- turbine inlet: TIT and TIP;
- turbine outlet: ambient pressure and a turbine outlet temperature (TOT) higher than 5°C, to avoid freezing phenomena on the blades of the last stages of the turbine.

The turbine size in term of power can be obtained with:

$$P_t = \dot{m}_{air}\, \Delta h_T\, \eta_{o-el} \tag{3.38}$$

where $\Delta h_T \left[\frac{J}{kg}\right]$ is the enthalpy variation across the turbine and $\eta_{o-el}\,[-]$ is the organic-electric efficiency of the electric generator, that allows to convert the mechanical energy into electric energy.

$$\Delta h_T = h_T^{in} - h_T^{out} \tag{3.39}$$

Enthalpy and entropy at turbine inlet can be easily obtained by means of CoolProp as function of TIT and TIP. Then, enthalpy at the outlet of the turbine as a result of an isentropic expansion, is function of ambient pressure and the turbine inlet entropy.

$$h_T^{in} = CoolProp(TIT, TIP) \tag{3.40}$$

$$s_T^{in} = CoolProp(TIT, TIP) \tag{3.41}$$

$$h_{T,is}^{out} = CoolProp\left(s_T^{in}, p_{amb}\right) \tag{3.42}$$

In this way, knowing the nominal adiabatic efficiency of the turbine $\eta_{T,nom}$, h_T^{out} is carried out with the following expression:

$$h_T^{out} = h_T^{in} - \left(h_T^{in} - h_{T,is}^{out}\right) \cdot \eta_{T,nom} \tag{3.43}$$

The procedure outlined so far, can be better understood by observing the expansion process through the turbine on the T-s diagram in the Figure 3.4, with the characteristic points analysed above.

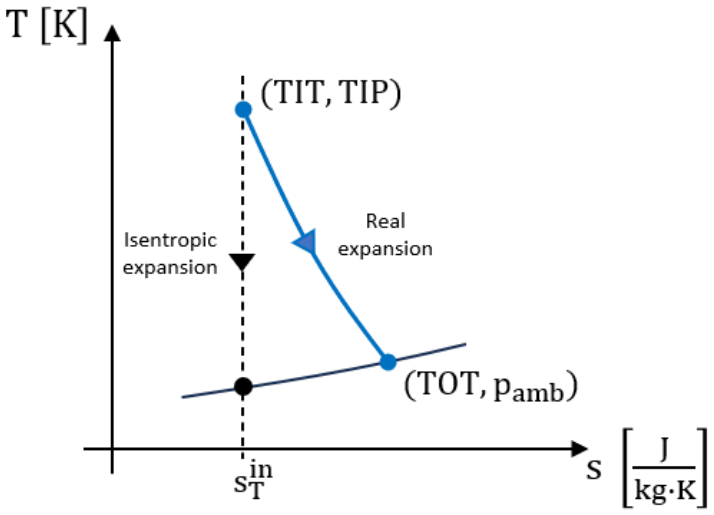

Figure 3.4: Air expansion through turbine.

The air turbine outlet temperature can be calculated at this point, checking that is not lower than the freezing point:

$$TOT = CoolProp(h_T^{out}, p_{amb}) \tag{3.44}$$

3.3. Pipeline

The pipeline is a key component of the system, as it is needed to bring the compressed air from land to the submarine tanks and vice versa, which must be located far from the coast in order to have adequate depth and therefore storage pressure.

The main parameters to be dimensioned are length, wall and coating thickness, after the selection of pipe diameter. The length depends on the site location and thus on how far from the coast the air tanks are placed. An approximative evaluation can be done considering a first seabed stretch with an α slope and a second stretch with zero slope.

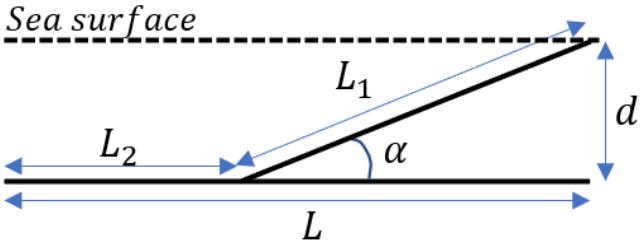

Figure 3.5: Pipeline design.

Then the total length of the pipeline L_{tot} can be calculated knowing seabed slope and site location specifics, such as distance L from the shore and depth d.

$$L_1 = \frac{d}{\sin \alpha} \tag{3.45}$$

$$L_2 = L - L_1 \cdot \cos \alpha \tag{3.46}$$

$$L_{tot} = L_1 + L_2 \tag{3.47}$$

One of the most crucial and essential steps in the design of subsea pipelines is the decision of wall thickness since it is affected by operating pressure and external hydrostatic pressure. While the air pressure is at its highest at the inlet of the pipeline during the compression phase due to pressure drops, the hydrostatic pressure is at its lowest. On the other hand, hydrostatic and operating pressure are almost equal at the end of the pipeline. Then, wall thickness has to be evaluated at the inlet, where the pipeline faces the highest load.

The following procedure takes into account the internal pressure only, as already proposed by [4]. In general, for oil and gas pipelines, the thickness of the pipe wall is determined in such a way that the hoop stress, which is the maximum stress in the pipe, is kept below a particular permissible stress. Using the thin wall approximation (D/t>20), the following expression have to be satisfied: [18]

$$\frac{pD_o}{2t} < S \tag{3.48}$$

considering p $[psi]$ the internal design pressure, D_0 and D $[in]$ the outer and inner pipe diameter respectively, t $[in]$ the wall thickness and S $[psi]$ the maximum permissible stress, that is the [ASME B31.8] for gas pipeline.

$$S = 1000\, S_y\, F\, E\, T \tag{3.49}$$

All the parameters used in this last correlation, are strongly dependent on the characteristics of the pipeline. In this case the used values are presented in the Table 3.1:

Table 3.1: Required coefficients for Equation (3.49)

Symbol	Parameter	Value	Characteristic
Sy [kpsi]	Specified minimum yield stress	39.067	Derived from trend data: A 106 Gr.B ,41 °F
F [-]	Design factor	0.8	Class 1 Div.1: like deserts, isolated land
E [-]	Weld joint factor	1	ASTM A 53, A106. Pipe Class: Seamless
T [-]	Temperature derating factor	1	Temperature < 250 °F

Defining the stress σ $[psi]$ as:

$$\sigma = p \cdot \left(\frac{D_o}{2\,t} - y\right) \tag{3.50}$$

in which y is a temperature coefficient equal to 0.4 in case of t < D/6 and for materials at temperature lower than 900 °F.

Then, imposing the stress equal to the admissible one, and considering that the outer diameter D_o is equal to the inner diameter D plus two times the wall thickness t, the minimum required wall thickness can be carried out with the following relation:

$$t = \frac{p\,D}{2 \cdot (S\,E + p\,y - p)} \tag{3.51}$$

The conversion factors, 39.37 in/m and 6894.757 Pa/psi, are used to pass from the used units of measure to those of the IS.

With regard to the pipeline coating, typically submarine pipelines have a concrete coating in order to add weight to the steel pipeline itself, to balance the buoyancy force and improve stability on the seabed. The dimension process of this coating layer presented by [4] [19], can be better understood taking a look to Figure 3.6.

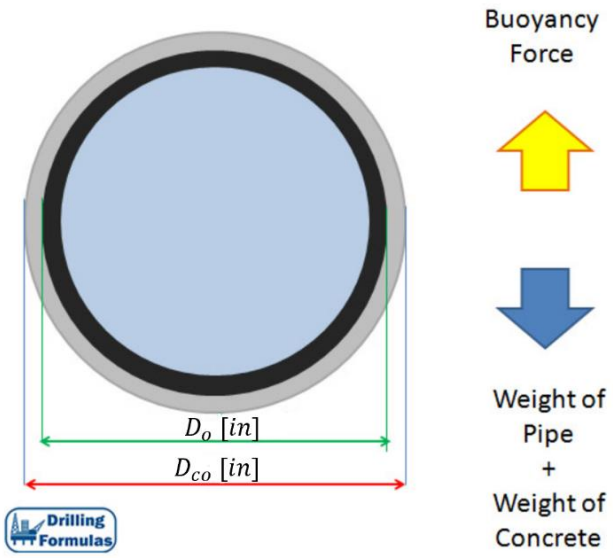

Figure 3.6: Forces acting on the pipeline [19].

Where D_o has been already introduced as the outer diameter of the steel pipeline and now is the inner diameter of the concrete coating, instead the D_{co} is its outer diameter.

All the other parameters used in the next equations are given and listed in the Table 3.2 below:

Table 3.2: Given information to compute concrete coating thickness [19].

Parameter	Symbol	Unit	Value
Steel pipe weight	W_{SP}	lb/ft	145
Fresh water density	ρ_{fw}	lb/ft³	64.2
Sea water density	ρ_{sw}	lb/ft³	65.52
Concrete specific gravity	SG	-	2.8
Required net down force	-	lb/ft	200

The first step is to evaluate the buoyancy force at which the pipeline is exposed:

$$F_b = \frac{\pi}{4} \cdot \left(\frac{D_{co}}{12}\right)^2 \cdot \rho_{sw} \tag{3.52}$$

It is necessary to divide the diameter by 12, simply to change the unite of measure form $[in]$ to $[ft]$. Then, the weight of concrete can be written:

$$W_c = \frac{\pi}{4}\left(\left(\frac{D_{co}}{12}\right)^2 - \left(\frac{D_o}{12}\right)^2\right) \cdot SG \cdot \rho_{fw} \tag{3.53}$$

In order to obtain the unknown, in other words the necessary D_{co} from which the coating thickness can be derived, the balance of forces shown in Equation (3.54) has to be computed:

$$Net\ down\ force = (W_{SP} + W_c) - F_b \tag{3.54}$$

And by doing so, the thickness is easily derived:

$$t_c = \frac{D_{co} - D_o}{2} \tag{3.55}$$

3.4. Air storage

Air storage dimensioning consists in determining the number of air tanks required to store the desired amount of energy. In this work, sizing was based on the continuous operating hours at full load to be guaranteed for the turbine. Hence, if the turbine has to work with a certain air mass flow rate for at least a fixed period of time, this necessary mass of air has to be provided by the air storage. Depending on the depth of site, air tanks pressure changes and thus air density, leading to different necessary total volume and then number of tanks.

$$V_{air}^{tot} = \frac{3600 \cdot \dot{m}_{air} \cdot h_{max,T}}{\rho_{air\ tank}} \tag{3.56}$$

$$N_{tanks} = \frac{V_{air}^{tot}}{V_{tank}} \tag{3.57}$$

In the equations above, $h_{max,T}$ $[h]$ represents the main variable for this dimensioning: hours of continuous turbine operation. The result of the Equation (3.57) must be rounded up to have a finite number of tanks. Obviously, this number depends also on the specific kind of air tanks being considered, because $V_{tank}[m^3]$ changes with it.

4 Operation Off Design

In this chapter the operation of the plant out of design conditions will be evaluated. This allows to define how the plant works during a certain period of time, for example a year, considering that many aspects can influence it by the hour. Obviously, the components of the plant are already sized, as result of the operation in design from Chapter 3, hence the new operation conditions are constrained to the size of air storage, compressor, turbine, heat exchangers and intercooler surface.

Furthermore, other external constrains need to be taken into account, such as the availability of wind, that allows to the off-shore wind farm to generate electric energy to run the compressor, and the electric energy price on the basis of which the convenience of storing energy with the UW-CAES is assessed.

Also, in this case the plant working conditions have been estimated with a specifically written MatLab model, considering the two different modes in which it can run: CtS and HfS. The results obtained from this analysis allow to establish how compressors and turbine work, in terms of equivalent hours and number of start-ups, calculating how much energy the CAES systems stores and produces, that is fundamental to assess the economic feasibility of the system.

4.1. Operational Constrains

During plant design, the two phases could be separated and analysed independently, but now operation in one or the other mode, or even plant shutdown, is determined hour by hour on the basis of a series of constraints:

- wind availability;
- electric energy price;
- amount of stored air;
- amount of stored thermal energy.

The availability of wind leads to a power output from the wind farm, depending on its size. The compressor of the UW-CAES was sized with a nominal power that is a fraction of the off-shore wind farm power. Then, hour by hour, it is necessary to control if the power output from the wind farm is at least higher than the minimum power at which the compressor can run. At that point, if the compressor can run, it will work following a certain efficiency curve, that for simplicity was taken from a previous thesis as an example of a possible real case. [11]

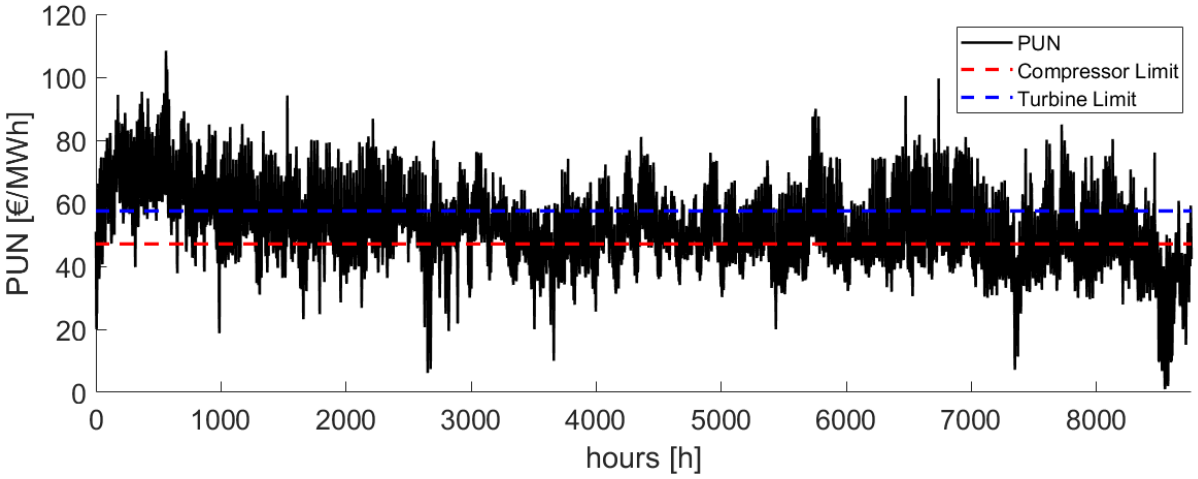

Figure 4.1: PUN 2019 with compressor and turbine limits determined with a margin of ±10% on the annual mean value.

Regarding the energy price, the PUN (Prezzo Unico Nazionale) trend during the year under consideration is taken. It represents the price at which electric energy is sold in the Italian Power Exchange, in other words in the wholesale market. Firstly, a logic based on the yearly mean value of PUN has been investigated to determine the start-up of compressor or turbine, considering a certain margin around it. But this led to a limited number of plant operating hours, due to the seasonality and fluctuation of the energy price. In fact, as can be seen in Figure 4.1 that is just an example of the PUN trend during 2019, the first part of the year (winter) is characterized by higher energy price that limit the compressor work. But in general, considering the mean value of the PUN is difficult to follow its fluctuation.

Hence, another logic has been evaluated trying to follow the energy price trend. Basing on the size of the air storage, that determine the period of time over which the UW-CAES system can act using or producing energy, a certain range of hours is taken as reference. Then, hour by hour the PUN [€/MWh] is compared with the mean value over this period around the hour under consideration, hence a trend that represents the activation limits of compressor and turbine can be traced as shown in Figure 4.2. If the price is lower than this mean value minus a certain margin (red curve), it is worthwhile to run the compressor because energy is cheap. If the price is higher than this mean value plus a certain margin (blue curve), it is worthwhile to run the turbine because higher gains can be made. Otherwise, when the PUN is between these two operational limits, the plant does not work.

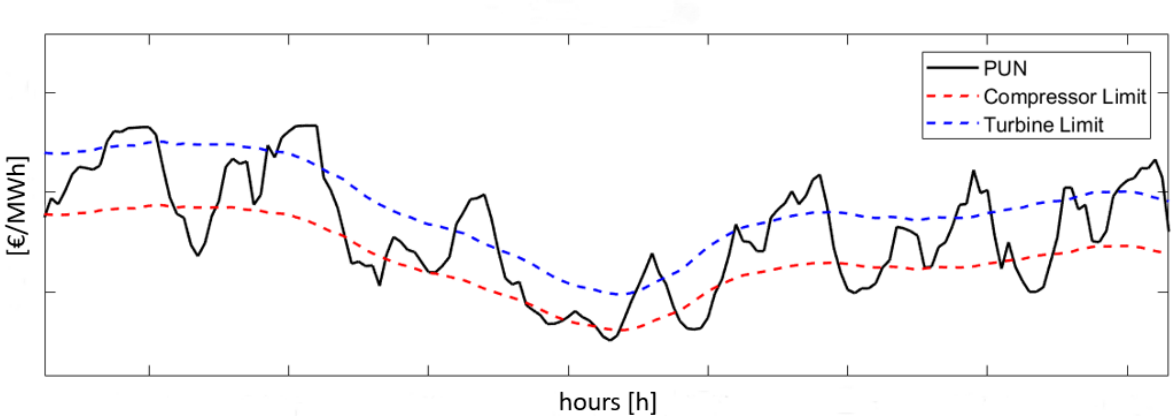

Figure 4.2: Example of the used logic to assess the convenience of compressor or turbine activation with a margin of ±10% on the periodic mean value.

The amount of air and thermal energy that are stored, influence the operation of the plant because if the air tanks are full, the compressor cannot work even if the other constrains are satisfied, but at the same time, if there is not enough stored air, the turbine cannot operate producing electric energy. The same happens looking at the TES side, where the compressor cannot work if there are not enough thermal fluids inside cold tanks, and the turbine cannot work if there are not enough thermal fluids inside hot tanks.

In the following Figure 4.3, it is possible to better understand the influence of different operational constrains on the plant and how the written model on MatLab works.

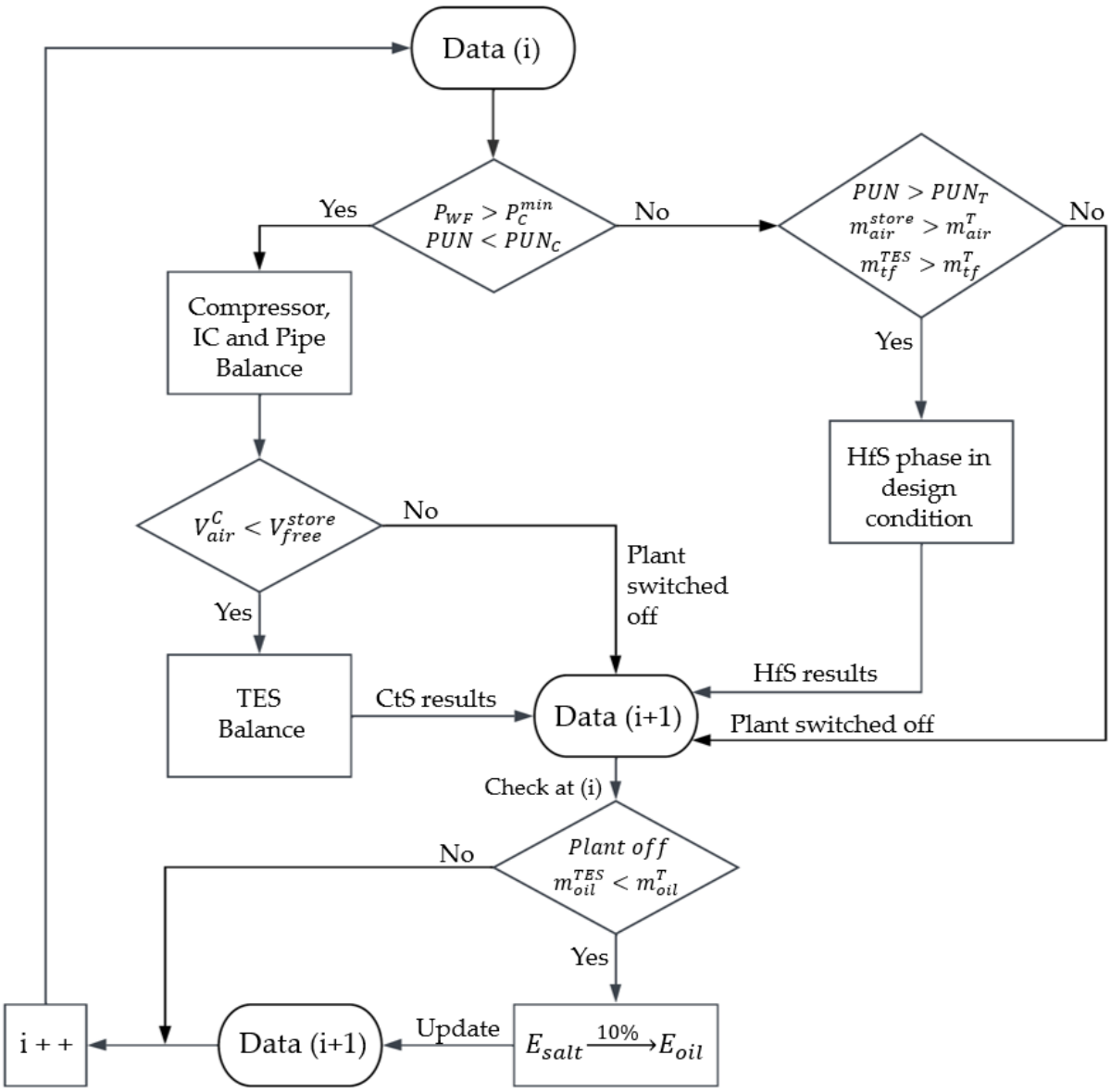

Figure 4.3: Flow chart of plant operation in off design condition.

Where rhombuses contain the constrains based on which decisions are made, instead rectangles represent the equations that are solved to get the results of the processes.

During a whole year, for each hour, it is firstly evaluated if the compressor can work, checking if the energy price PUN is cheap enough and the amount of power given by the off-shore wind farm is high enough to activate the compressor. If these constrains are satisfied, a system of equations, taking into account the compressor, intercooler and pressure drops across heat exchangers and pipeline, is carried out to mainly calculate the amount of air mass that the compressor elaborates during that hour. This is necessary to ensure that there is sufficient space in the air tanks to store it. In that case, the plant can work in CtS mode, and all the results get from the first system of

equations can be saved, other than the air mass flow rate. Then the second system of equation to carry out the heat transfer process through thermal energy storage is done, in other words the energy balance at the three heat exchangers. All this process allows to solve the system in off design condition during the compression phase, similarly to what has been done during the plant design.

Otherwise, if the first two constrains are not satisfied, the model checks if there are the condition to run the turbine expanding the stored air. To do that, firstly the convenience is evaluated comparing the energy price with the threshold above which a higher gain can occur. Then the availability inside the underwater air tanks of the required air by the turbine, and hot thermal fluids to warm up the air before the expansion, is verified. If the expansion can take place, all the results given by the design in HfS phase are used, since the turbine always works in design condition. This is done to guarantee the best performances both during heat transfer and expansion through the turbine, in order to minimize losses that adversely affect income.

Or else, when both compressor and turbine cannot operate, the plant is switched off. In all these cases, the used data are updated with the results given by the illustrated operation analysis, to be used for the plant evaluation during the next hour. But since thermal oil has a lower specific heat coefficient than solar salt, against a similar temperature variation to meet, its consumption during the heating process is higher and its production during cooling process is lower. Then, can happen that the turbine does not work only because there is not enough hot thermal oil to provide energy to heat up the air. This problem has already been addressed in previous works [11].

The introduction of another heat exchanger, gives the possibility to increase the energy stored by thermal oil, using the higher availability of energy stored in hot solar salt. In that way the plant can be prepared to work in expansion phase during the following hour, if the other constrains are satisfied.

At the end of this process, an update of the data is necessary, and the model is ready to carry out the same process again, for all the 8760 hours during a year. In particular, the cumulative air mass and thermal fluids mass are carried out for each hour. The former to monitor the progress of air tanks filling status, that influences the switching on of the turbine and compressor. The latter, on the other hand, is used both to check the filling status of the tanks of thermal fluids, which if empty on the hot side do not allow operation in HfS mode, and to assess during the year what is the maximum quantity of thermal fluids required so as to establish the number of tanks needed. In fact, the number of tanks of the TES is not decided during the design but is assessed afterwards, leaving an extra degree of freedom. To do that, the solar salt and thermal oil density are carried out by means of the corresponding equations discussed in previous chapter, and knowing the maximum mass that accumulates during the year, the occupied volume is calculated. Then, considering the size of the chosen thermal tanks, the number is found out.

Now that it is clear how the model establishes the plant operating conditions, basing on the different constrains that have to be taken into account, it is possible to deeply analyse the charging phase and highlight differences with used methods during the plant design. Expansion phase will not be analysed since the plant works always in design conditions in this configuration.

4.2. Charging phase

Once all the above requirements for compression operation are met, the plant can work in CtS phase. It's important to analyse the behaviour of the various components when it works in off-design conditions throughout the year.

The procedure followed for the analysis of the various components of the plant is based on the one already discussed for the design, but this time the compressor will not always operate under nominal conditions, since the availability of power from the wind farm changes according to the availability of wind, then the air mass flow rate processed will vary accordingly. Since the heat exchanger surface of the intercooler remain the same as the design, the air temperature at the outlet of the intercooler, IOT, cannot be controlled as a constraint. However, the temperature that air must have at the exit of the compressor train is kept fixed, in order to always maintain the best conditions for the subsequent heat exchange during air cooling.

Basing on the available power the compressor can absorb, its efficiency is determined by interpolation of data obtained in previous work [11], as shown in Figure 4.4, for a compressor block with a total power of 75 MW, made by three compressor trains in parallel with two shaft for each train.

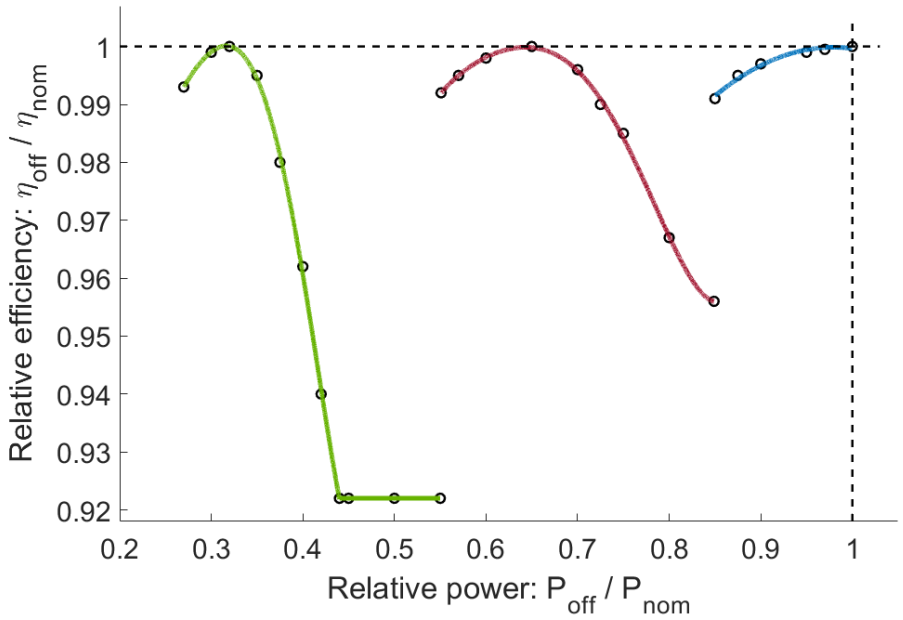

Figure 4.4: Data interpolation to perform compressor efficiency trend.

The efficiency trend of the compressor is represented by three different curves because it is obtained changing the number of compressor trains in operation to have a higher efficiency. Going from left to right, in other words increasing the power of the compressor, it is necessary to operate with more compressor trains in parallel. In fact, in the previous thesis it has been found that smaller compressors better suited these kinds of plants, because otherwise cannot be possible to reach a wide range of part load condition. When operating with one compressor train it is not convenient anymore to increase power absorbed due to a decrease of efficiency, another compressor train is activated, and the red curve follows. The same for the blue curve on the right when all the three compressor trains in parallel are switched on.

Then, knowing the absorbed power by the compressor and consequently its efficiency, all the equations used in the plant design from Equation (3.2) to (3.26) are solved again, keeping in mind that some changes need to be made. In particular, in the Equation (3.20) and (3.25), the nominal efficiency of the compressor has to be substituted with the efficiency in off design $\eta_{C,off}$ for part load.

Now also the intercooler outlet temperature IOT is an unknown, and for this reason to solve the system of equation is necessary to add the equations regarding the energy balance at the IC, in which the parameter UA is obtained with the same approach used in the HXs during the HfS phase with the Equation (3.37).

In the following Table 4.1 are listed all the equations that are solved together in a unique system during the off design:

Table 4.1: System of equations to solve the Compressor-IC-Pipeline balance in off-design.

Meaning	Equation
Compressor power	$P_c = \frac{\dot{m}_{air}\,\Delta h_C^{tot}}{\eta_{o-el}}$ (4.1)
Pressure at compressor outlet	$p_C^{out} = p_{air\ tank} + \Delta p_{pipe} + \sum \Delta p_{HX,i}$ (4.2)
Pressure drop across the pipeline	$\Delta p_{pipe} = 8\, f \frac{\dot{m}_{air}^2\, L}{\rho_{av}\, \pi^2\, D^5}$ (4.3)
Friction factor	$f = \frac{1.325}{\left[ln\left(\frac{\varepsilon}{3.7\,D} + \frac{5.74}{Re^{0.9}}\right)\right]^2}$ (4.4)

Reynolds number	$Re = \frac{4\,\dot{m}_{air}}{\pi\, D\, \mu}$	(4.5)
Pressure drop across salt HX	$\Delta p_{HX,1} = p_C^{out} \cdot \Delta p_{\%,HX}$	(4.6)
Pressure drop across oil HX	$\Delta p_{HX,2} = p_C^{out} \cdot (1 - \Delta p_{\%,HX}) \cdot \Delta p_{\%,HX}$	(4.7)
Pressure drop across water HX	$\Delta p_{HX,3} = p_C^{out} \cdot \left(1 - \Delta p_{\%,HX}\right)^2 \cdot \Delta p_{\%,HX}$	(4.8)
Pressure at pipeline inlet	$p_{pipe}^{in} = p_{air\ tank} + \Delta p_{pipe}$	(4.9)
Air density at pipeline inlet	$\rho_{pipe}^{in} = CoolProp\left(T_{sw},\ p_{pipe}^{in}\right)$	(4.10)
Air density at pipeline outlet	$\rho_{pipe}^{out} = CoolProp(T_{sw},\ p_{air\ tank})$	(4.11)
Mean air density across pipeline	$\rho_{av} = \frac{\rho_{pipe}^{in} + \rho_{pipe}^{out}}{2}$	(4.12)
Enthalpy variation across the compressor	$\Delta h_C^{tot} = (h_C^{out} - h_{IC}^{out}) + \left(h_{IC}^{in} - h_C^{in}\right)$	(4.13)
Compressor outlet enthalpy	$h_C^{out} = CoolProp(COT,\ p_C^{out})$	(4.14)
Isentropic compressor outlet enthalpy	$h_{C,is}^{out} = (h_C^{out} - h_{IC}^{out}) \cdot\ \eta_{C,off} + h_{IC}^{out}$	(4.15)

Isentropic compressor outlet enthalpy	$h_{C,is}^{out} = CoolProp(p_C^{out},\ s_{IC}^{out})$	(4.16)
Intercooler outlet enthalpy	$h_{IC}^{out} = CoolProp(IOT,\ s_{IC}^{out})$	(4.17)
Intercooler outlet pressure	$p_{IC}^{out} = CoolProp(IOT,\ s_{IC}^{out})$	(4.18)
Intercooler inlet enthalpy	$h_{IC}^{in} = \frac{h_{IC,is}^{in} - h_C^{in}}{\eta_{C,off}} + h_C^{in}$	(4.19)
Intercooler inlet temperature of air	$T_{IC}^{in} = CoolProp\left(h_{IC}^{in}, p_{IC}^{in}\right)$	(4.20)
Pressure drop across the intercooler	$\Delta p_{IC}^{off} = \Delta p_{IC}^{nom} \cdot \left(\frac{\dot{V}_{off}}{\dot{V}_{nom}}\right)^2_{air,IC}$	(4.21)
Intercooler inlet pressure	$p_{IC}^{in} = p_{IC}^{out} + \Delta p_{IC}^{off}$	(4.22)
Intercooler inlet density of air	$\rho_{IC}^{in} = CoolProp\left(T_{IC}^{in},\ p_{IC}^{in}\right)$	(4.23)
Air volumetric flow rate at IC inlet	$\dot{V}_{air,IC}^{in} = \frac{\dot{m}_{air}}{\rho_{IC}^{in}}$	(4.24)
Enthalpy at IC inlet with isentropic compression	$h_{IC,is}^{in} = CoolProp\left(p_{IC}^{in},\ s_C^{in}\right)$	(4.25)
IC logarithmic mean temperature	$\Delta T_{mln}^{IC} = \frac{\left(T_{IC}^{in} - T_{sw,IC}^{out}\right) - \left(IOT - T_{sw,IC}^{in}\right)}{ln\left(\frac{T_{IC}^{in} - T_{sw,IC}^{out}}{IOT - T_{sw,IC}^{in}}\right)}$	(4.26)

Thermal power at air side	$Q_{IC} = \dot{m}_{air}\, cp_{air}\left(T_{IC}^{in} - IOT\right)$	(4.27)
Thermal power at water side	$Q_{IC} = \dot{m}_{sw,IC}\, cp_{sw}\, \Delta T_{sw}^{max}$	(4.28)
Thermal power balance for IC in off design	$Q_{IC} = (UA)_{IC}^{off}\, \Delta T_{mln}^{IC}$	(4.29)
UA variation for IC based on design condition	$(UA)_{IC}^{off} = (UA)_{IC}^{nom} \cdot \left(\frac{\dot{m}^{off}}{\dot{m}^{nom}}\right)_{air}^{\frac{4}{5}} \cdot \frac{\left(Pr_{off}\right)^{0.4}}{(Pr_{nom})^{0.3}}$	(4.30)

The Equation (4.21) shows as the pressure drops across the IC can be evaluated in off design basing on the one obtained with nominal conditions. It is obtained from the Darcy Weisbach equation, neglecting the variation of friction factor and air density across the IC between design and off design:

$$\Delta p = f\, \rho \frac{v^2}{2} \frac{L}{D} \tag{4.31}$$

Where L/D is the ratio between length and diameter of IC pipes, instead $v\ \left[\frac{m}{s}\right]$ is the fluid velocity inside pipes, that can be written as:

$$v = \frac{\dot{V}}{A} \tag{4.32}$$

with $A\ [m^2]$ cross section of pipes and $\dot{V}\ \left[\frac{m^3}{s}\right]$ volumetric flow rate.

For sake of simplicity, the same is not done with the HXs to cool down the air, because otherwise it was necessary to calculate the air density at the inlet of each of them, to carry out the volumetric flow rate from the air mass flow rate as done with Equation (4.23) and (4.24). Then to avoid further complicating the system of equation, the pressure drops across those HXs is considered a percentage of the inlet pressure.

After this balance, it is possible to continue with the next step, the air cooling process through the three HXs storing the thermal energy inside TES. In off-design, as already explained for the IC, the heat exchange surface is set and hence the UA parameter can be found for each HXs with the following equation:

$$(UA)_{CtS}^{off} = (UA)_{CtS}^{nom} \cdot \left(\frac{\dot{m}^{off}}{\dot{m}^{nom}}\right)_{air}^{\frac{4}{5}} \cdot \frac{(Pr_{off})^{0.4}}{(Pr_{nom})^{0.3}} \cdot \frac{k_{f,off}}{k_{f,nom}} \tag{4.33}$$

The results are used in the energy balance, where the air temperature variation is not equal anymore to the one of the thermal fluids, because the third equation define the thermal power exchanged, and given a certain air mass flow rate the air temperature at the HX outlet have to be free to change, then is an unknown. This leads to processes that cannot be represented with parallel straight lines on the T-Q diagram, as occurred during design (Figure 3.2).

$$\begin{cases} Q_{HX} = \dot{m}_{air}\, cp_{air}\, (T_{air}^{in} - T_{air}^{out}) \\ Q_{HX} = \dot{m}_{tf}\, cp_{tf}\, \Delta T_{tf} \\ Q_{HX} = (UA)_{CtS}^{off}\, \Delta T_{mln} \end{cases} \tag{4.34}$$

Since the air and thermal fluids temperature variations are not the same, the logarithmic mean temperature has to be found with the following:

$$\Delta T_{mln}^{IC} = \frac{(T_{air}^{in} - T_{tf}^{out}) - (T_{air}^{out} - T_{tf}^{in})}{ln\left(\frac{T_{air}^{in} - T_{tf}^{out}}{T_{air}^{out} - T_{tf}^{in}}\right)} \tag{4.35}$$

Obviously, at the inlet of the first heat exchanger, the solar salt HX, the air temperature is the one at the outlet of the compressor, that is the COT.

4.3. Oil-Salt heat exchanger

The faster consumption of thermal oil during expansion phase, respect to solar salt, imposes the system switching off. This limits the possibility to make the plant profitable, since hours of operation during the year drop. To avoid this problem another heat exchanger, other than the three main HXs used both during CtS and HfS phases, is introduced to transfer part of the energy stored in the hot salt to the oil. This helps to balance the stored energy between solar and oil tanks, making possible a better exploitation of the energy released by the air during its cooling phase.

When the system is switched off due to this luck of energy required from the thermal oil, this heat exchanger comes into operation, knowing the amount of stored hot solar salt in term of mass, and thus of energy. The design of this component is not done in this work, but the idea is that is possible to transfer energy from a fluid to another. Then 10% of the available energy stored in the solar salt is given to the thermal oil.

$$E_{Salt}(i) = m_{Salt}\,(i)\, cp_{Salt}\, \Delta T_{Salt} \tag{4.36}$$

$$E_{Oil}^{transf} = 0.1 \cdot E_{Salt}(i) \tag{4.37}$$

Where $m_{Salt}\ [kg]$ is the mass of stored salt in the hot tank at the time (i) under consideration.

Hence, this transfer of energy leads to a change in the mass of oil and salt stored in hot tanks, and consequently in cold tanks, that need to be carried out to update these values in order to proceed with the evaluation of the plant operation in the following hour $(i + 1)$. The new masses of fluids in the hot tanks can be assessed as follow:

$$\begin{cases} m_{Salt}(i+1) = m_{Salt}(i) - \dfrac{E_{Oil}^{transf}}{cp_{Salt}\ \Delta T_{Salt}} \\ m_{Oil}(i+1) = m_{Oil}(i) + \dfrac{E_{Oil}^{transf}}{cp_{Oil}\ \Delta T_{Oil}} \end{cases} \tag{4.38}$$

In the same way the energy stored in the hot tanks can be carried out:

$$\begin{cases} E_{Salt}(i+1) = E_{Salt}(i) - E_{Oil}^{transf} \\ E_{Oil}(i+1) = E_{Oil}(i) + E_{Oil}^{transf} \end{cases} \tag{4.39}$$

4.4. Performance parameters

At the end of the simulation of the operation of the plant over a whole year, it is possible to investigate how the plant worked checking some parameters used to compare different technologies. The energy absorbed by the compressor and produced by the turbine is given as a result knowing when they run and at which power. Then it is possible to carry out the equivalent hours of operation for both compressor and turbine, that represents the amount of time in hours, the respective machines have to work at nominal condition to absorb or produce the same amount of energy absorbed or produced during a year:

$$h_{eq} = \frac{E}{P_{nom}} \tag{4.40}$$

in which $E\ [MWh]$ represent the energy and $P_{nom}\ [MW]$ the nominal power of the respective machines.

At the same time, it is important to check the number of compressor and turbine start-ups, because it cannot be too high in order to not stress to much the different parts of the machines.

Another important index of performance for this kind of system is the round trip efficiency (RTE), calculated as the ratio between the total energy produced by the

turbine and the total energy absorbed by the compressor. In this work, the residual energy stored in the subsea air tanks at the end of the year is also considered for the RTE evaluation, as this energy could be utilised by the turbine if the analysis were carried out by changing the initial conditions, for example starting with the subsea reservoirs already filled. This latter case would represent a random year in the lifetime of the plant, instead of starting with empty tanks as in the first year of operation.

Knowing the amount of air still stored underwater at the end of the year, it is possible to calculate the amount of energy that could be extracted expanding it through the turbine:

$$E_t^{end} = \frac{m_{cum}^{end}}{\dot{m}_t \cdot 3600} \cdot P_t \tag{4.41}$$

Where the first term of the equation expresses the necessary hours of turbine operation to empty the air tanks. In fact, the air mass flow rate through the turbine $\dot{m}_t$ $\left[\frac{kg}{s}\right]$ is there converted into $\left[\frac{kg}{h}\right]$ by 3600, that represents the seconds in one hour.

At this point, the RTE $[-]$ can be assessed:

$$RTE = \frac{E_t + E_t^{end}}{E_c} \tag{4.42}$$

Another aspect that can be analysed is the impact of the UW-CAES system on the possible coupled wind farm, in terms of energy flows to the electric grid. From forecasts of wind profiles on a certain site and then of the power outputs from the wind farm, is possible to calculate the energy that the wind farm could produce and feed into the grid. But if the wind farm provides energy to the compressor of the CAES system to run, the total energy feed into the grid is lower due to the efficiency of the CAES system itself:

$$E_{grid} = E_{WF} - E_c + E_t \tag{4.43}$$

These considerations are necessary because they influence the economic feasibility of the plant, treated in the Chapter 5.

5 Economic Model

The economic feasibility of the UW-CAES system must be investigated, as happen for any kind of plant that is proposed before the construction. Furthermore, even though there are CAES plants already in operation in the world, the underwater category proposed in this work is not a reality yet, then an economic analysis is even more important. Taking into account available data in literature, regarding the costs of the different components of the plant under investigation that are already used in other plants, it is possible to estimate the investment cost of the whole system and the operational and maintenance costs (O&M) for each component. Then some economic parameters are used to assess the feasibility of the plant, making possible a comparison with other kinds of solutions already available on the market.

5.1. Capital Expenditure: CAPEX

The capital expenditure represents the investment, and then the cash flow, from the purchase of a technology or service that a company has to face. With a literature review is possible to assess the CAPEX of each component and then of the entire system:

$$C_{inv} = C_{turbomachinery} + C_{HX} + C_{TES} + C_{air\ tank} + C_{pipeline} + C_{other} \tag{5.1}$$

Since costs change year by year due to inflation, to actualize them from old publications, the Chemical Engineering Plant Cost Index (CEPCI [20]) has been chosen in this work. It is done by multiplying and dividing the cost for the CEPCI value of the last year 2022, since currently is the last one available, and the one referring, for simplicity, to the year of the publication from which data are taken:

$$C_{actualized} = C \cdot \frac{CEPCI_{2022}}{CEPCI_{publication\ year}} \tag{5.2}$$

Since all the available data taken from previous work refer to publication made in 2014, except for pipeline that refers to 2006, these two values of CEPCI are used, that are respectively 576.1 and 499.6. Instead, the CEPCI value in 2022 is 816.

The costs calculated in the following are in [€].

5.1.1. Turbomachinery

$$C_{turbomachin} = C_{axial} + 2\ C_{radial} + C_{turb} + C_{alt} + C_{transf} + C_{gb} \tag{5.3}$$

All the components included in the compressor train need to be taken in consideration, other than the turbine. Hence, for the compressor used in this work, the costs of the two radial and the axial components are investigated. These costs are not linear, but they depend on the power and air mass flow rate [21] [4]:

$$C_{axial} = 450 \cdot \frac{P_C}{\dot{m}_{air}^{0.31}} \tag{5.4}$$

$$C_{radial} = 6490 \cdot P_C^{0.62} \tag{5.5}$$

$$C_{turb} = 500 \cdot \frac{P_T}{\dot{m}_{air}^{0.363}} \tag{5.6}$$

Where the turbine and compressor power are expressed in [kW], except in Equation (5.5) in which the P_C is in [hp], and air mass flow rate is in [kg/s].

But each part of the compressor has a different size, than the fraction of power attributed to each part has to be evaluated to assess its cost. Since the air mass flow rate is constant through the compressor, the power is proportional to the enthalpy variation across each stage. Thus, knowing the thermodynamic properties of the air at the inlet and outlet of the axial compressor, that operate between ambient conditions and IC inlet, the enthalpies can be evaluated by means of CoolProp, and the fraction f_1 [−] can be carried out with Equation (5.8). Following the same procedure and considering the two radial stages after the IC designed to share the remaining enthalpy variation up to compressor outlet condition, the other fraction f_2 [−] can be assessed with Equation (5.9). In this way the power of the two radial compressors is assumed to be the same.

$$\Delta h_C^{tot} = \Delta h_1 + \Delta h_2 + \Delta h_3 \tag{5.7}$$

$$f_1 = \frac{\Delta h_1}{\Delta h_1 + \Delta h_2 + \Delta h_3} \tag{5.8}$$

$$f_2 = \frac{\Delta h_2}{\Delta h_1 + \Delta h_2 + \Delta h_3} \tag{5.9}$$

The Equation (5.3) can be reformulated as follow:

$$C_{turbomachin} = f_1\ C_{axial} + 2\ f_2^{0.62}\ C_{radial} + C_{turb} + C_{alt} + C_{transf} + C_{gb} \tag{5.10}$$

For the other necessary components to turbomachinery to convert mechanical energy to electrical energy, the costs are not linear but they follow a certain economy of scale. Then taking into account a reference case is possible to scale their cost:

$$C_{alt} = C_{alt,ref} \cdot \left(\frac{P_t}{P_{alt,ref}} \right)^{0.9} \tag{5.11}$$

$$C_{alt} = C_{transf,ref} \cdot \left(\frac{P_t}{P_{transf,ref}} \right)^{0.9} \tag{5.12}$$

$$C_{gb} = c_{gb} \cdot P_C \tag{5.13}$$

Where all the powers are expressed in MW. The other parameters are listed below in the Table 5.1.

Table 5.1: Reference value to determine costs of alternator, transformer and gearbox. [22]

Parameter	Value	Unit
$\boldsymbol{P_{alt,ref}}$	80	MW
$\boldsymbol{C_{alt,ref}}$	3000000	€
$\boldsymbol{P_{transf,ref}}$	80	MW
$\boldsymbol{C_{transf,ref}}$	800000	€
$\boldsymbol{c_{gb}}$	5000	€/MW

5.1.2. Heat exchangers

In the UW-CAES plant under investigation there are five heat exchangers used, one to cool down air before axial and radials compressor, the inter cooler, and four to store energy in CtS phase or use it in HfS phase. In particular, these last four HXs are divided into three common HXs, air-salt, air-oil and air-water, and another one, salt-oil, used to compensate the lack of thermal energy stored inside oil tanks. For sake of simplicity the salt-oil heat exchanger is not investigated in this work and then its cost is not considered. Then, investment costs for these components can be written as follow, by means of specific cost and the nominal power they can exchange given by the design:

$$C_{HX,i}^{TES} = c_{HX,i}^{TES} \cdot Q_{HX,i}^{TES} \tag{5.14}$$

$$C_{HX}^{IC} = c_{HX}^{IC} \cdot Q_{IC} \tag{5.15}$$

Keeping in mind that c_{HX}^{IC} and $c_{HX,Water}^{TES}$ are the same since they refer to two air-water HXs. The specific costs are taken from a previous work [11] and are listed in the following Table 5.2:

Table 5.2: Specific costs of different heat exchangers.

Parameter	Value	Unit
$c_{HX,Salt}$	100	€/kW
$c_{HX,Oil}$	40	€/kW
$c_{HX,Water}$	5	€/kW

The total investment for the purchase of all the HXs is given by summing all the above mentioned costs:

$$C_{HX} = C_{HX,Salt}^{TES} + C_{HX,Oil}^{TES} + C_{HX,Water}^{TES} + C_{HX}^{IC} \tag{5.16}$$

5.1.3. TES

The thermal energy storage cost includes the investment for the thermal fluids other than the thermal tanks, that are two for each fluid since one stores cold fluid and the other one hot fluid.

$$C_{TES} = \sum_{i=1}^{3} 2\, C_{tank,i} + C_{TF,i} \tag{5.17}$$

The cost associated to TFs can be easily calculated, knowing from the operation of the plant during a whole year the amount of necessary mass for each fluid:

$$C_{TF,i} = c_{TF,i} \cdot m_{TF,i} \tag{5.18}$$

Regarding the different tanks, the cost includes tank structure, insulation and foundation, and it is related to a reference case already adopted in previous work [11].

$$C_{tank,i} = N_{tank,i} \cdot c_{tank,ref,i} \cdot V_{ref,i} \left(\frac{V_i}{V_{ref,i}} \right)^{0.7} \tag{5.19}$$

$$c_{tank,ref,i} = c_{tank,i} + c_{ins,i} + c_{fund,i} \tag{5.20}$$

Where $N_{tank,i}$ is the number of tanks required for each side, cold and hot, considering its size V_i $[m^3]$ and the maximum amount of TF stored during a year. All the necessary data such as reference value and specific cost are listed in the Table 5.3.

Table 5.3: Reference costs for TES.

Parameter	Solar Salt	Thermal Oil	Unit
c_{TF}	0.7	2	€/kg
c_{tank}	350	168	€/m^3
c_{ins}	134	72	€/m^3
c_{fund}	449	250	€/m^3
V_{ref}	2195	3330	m^3

The water cost is neglected, and its total tank specific cost is assumed 500 €/m³, including tank structure, insulation and foundation.

5.1.4. Air tank

The cost of air tanks has been analysed in detail in previous work [4], where different structure to store air underwater has been investigated. Here, as already mentioned in Chapter 2, energy bags and concreate caissons are considered as possible options. Their cost, that includes ballast (or anchor), meridional tension-carrying material (straps or cables), and material other than engineering, manufacturing, and installation phases, has been related to the amount of energy that can be stored at a certain depth. Hence, the air tanks cost depends on the number of tanks that have to be installed, the specific cost per unit of energy stored referred to a reference case, and the amount of energy for which they are sized.

$$C_{Air\ tank} = c_{Air\ tank,ref} \cdot U_{ref} \cdot N_{Air\ tank} \cdot \left(\frac{U}{U_{ref}}\right)^{0.66} \tag{5.21}$$

Where the specific cost in $\left[\frac{€}{kWh}\right]$ and the energy $U_{ref}[kWh]$ are referred to a cost estimation done for air storage at 500 m depth. The number of tanks is evaluated basing on the hours of continuous turbine operation defined during the design of the UW-CAES plant. Instead, to carry out the energy U $[kWh]$ stored at the depth of the site under consideration, it is necessary to evaluate the recoverable energy per cubic metre of stored air through an adiabatic expansion, and hence the theoretical work that can be extracted form a fluid at a given pressure [7]:

$$u_{ad} = r\, p_{amb}\left(r^{((\gamma-1)/\gamma)} - 1\right)\left(\frac{\gamma - 1}{\gamma}\right) \tag{5.22}$$

Where r is the pressure ratio between storage (Equation (3.1)) and ambient pressure, and γ is the ratio between specific heat at constant pressure and specific heat at constant volume, that for dry air is equal to 1.4.

$$r = \frac{p_{air\ tank}}{p_{amb}} \tag{5.23}$$

$$\gamma = \frac{c_p}{c_v} \tag{5.24}$$

Using units of IS, the adiabatic energy u_{ad} from Equation (5.22) is measured in $[\frac{J}{m^3}]$, then the result has to be divided to $3.6 \cdot 10^6$ to express it in $\left[\frac{kWh}{m^3}\right]$. This is necessary for using it in Equation (5.21), in which specific costs are expressed basing on kWh.

From the adiabatic work, the real one can be calculated knowing turbine and organic-electric efficiency:

$$u = u_{ad} \cdot \eta_T \cdot \eta_{o-el} \tag{5.25}$$

With the total volume of air stored in the air tanks V_{air}^{tot}, already found with Equation (3.56) during the operation analysis of the plant on a whole year, it is possible to get the energy U related to the case under examination:

$$U = u \cdot V_{air}^{tot} \tag{5.26}$$

The costs are assessed for both systems considered in this work, with 30 €/kWh as specific cost for cement caissons storing air at 500 m depth, and 25 €/kWh for energy bags.

5.1.5. Pipeline

The pipeline cost contains materials, that constitutes the larger portion, labour, right of way, and miscellaneous, such as surveying, engineering, supervision, contingencies, allowances, overhead, and filing fees. In literature the estimating costs for pipeline construction are usually expressed as function of diameter and length.

$$C_{pipe} = c_{pipe} \cdot D_{max} \cdot L_{tot} \cdot 10^3 \tag{5.27}$$

In which the concreate outer diameter D_{co} is used as maximum diameter and has to be expressed in [in] (39.37 in/m conversion factor), the total length of the pipe in $[km]$, and the specific cost is 264 $\left[\frac{k€}{in \cdot km}\right]$. [4]

5.1.6. Others

They represent costs of construction, engineering, allowances, and labour needed for all the other components of the plant, except for the pipeline since they are already included in their cost definition. Furthermore, they include infrastructures where compressors, turbine and TES are located, other than cables to connect the plant with the electric grid.

They are considered around 30% of all the other investment costs.

5.2. Operational Expenditure: OPEX

The OPEX are the operating expenses related to the running of the plant during the year, thus measured in €/year. Since there are not real example of the kind of technology under investigation in this thesis, the literature does not report many indications on operation and maintenance costs. Hence, as shown in Table 5.4, costs of plants where similar components are used, are taken in consideration.

For turbomachinery, variable operational and maintenance costs are considered equal to 0.5 €/MWh in both charging and discharging mode, and a staff of 5 people is

assumed to be necessary for a total of 100 k€ per year. For off-shore pipeline, OPEX are obtained as percentage of total investment, equal to 4% of their CAPEX.

No information has been found regarding underwater air tanks, then the same percentage of pipeline (4% of CAPEX) has been considered. The OPEX of TES are accounted as 1% of its investment, instead for heat exchangers they are neglected.

Table 5.4: OPEX related to each component of the system.

Component	OPEX
Turbomachinery	0.5 €/MWh 100 k€/year
TES	1% of C_{TES}
Air Tank	4% of $C_{Air\ tank}$
Pipeline	4% of C_{pipe}

5.3. Economic parameters

The economic feasibility of the system under consideration was carried out by assessing the Levelized Cost of Storage (LCOS), that can be seen as the required average electricity price during discharging phase to cover the full lifetime costs of storage plant composed of operations and investments. The following equation provides a formulation of the given definition: [23]

$$LCOS = \frac{CAPEX + \sum_{i=1}^{n} \frac{A_i}{(1+WACC)^i}}{\sum_{i=1}^{n} \frac{\left(E_t + E_t^{end}\right)_i}{(1+WACC)^i}} \tag{5.28}$$

$$A_i = OPEX_i + E_c \cdot PUN_i \tag{5.29}$$

Where:

- n is the lifetime of the plant;
- $WACC$ is the Weighted Average Cost of Capital;
- A_i represents the cost to run the plant during the year i.

In other words, this parameter allows to predict the price at which energy must be sold to cover the investment, sharing during the plant lifetime, all the cost accounted year by year, over the energy produced by the plant and feed into the grid expanding air through the turbine.

Except for investment costs, that are accounted for in the so called zero year, that is before the first year of operation of the plant, all the other costs such as OPEX and energy price to run the compressor, are on a yearly basis.

In particular, the cost of energy to operate the compressor deserves attention. In fact, as can be seen from the Equation (5.29), the price considered for that energy is the PUN at the hour in which the compressor is working. In other words, even if the UW-CAES plant is coupled with an off-shore wind farm, in this thesis just the convenience of the CAES system is analysed. Then the wind farm can operate independently from the CAES system, selling electricity to it instead of to the grid only when the energy price PUN is too low, but at the same price. This is the case of an underwater compressed air energy storage system that is built after the construction of a wind farm, and then that does not influence its economic return (Figure 5.1). Or just the case of an independent UW-CAES system that operates without any interaction with a wind farm, and hence that buys energy to run the compressor directly from the national electric grid (Figure 5.2).

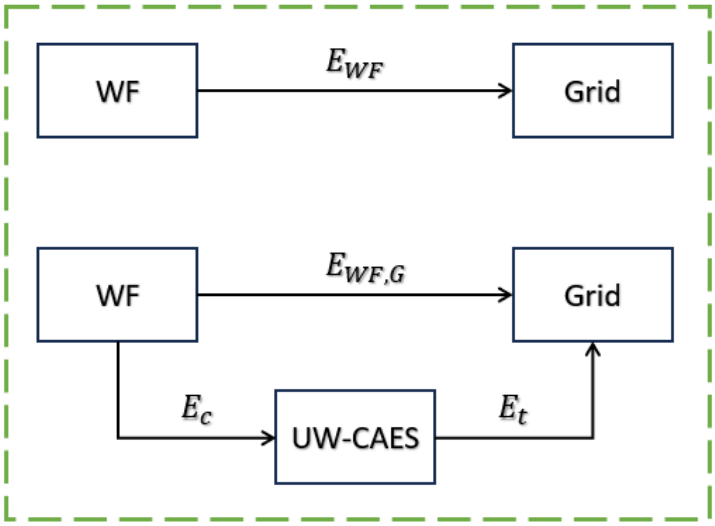

Figure 5.1: Case 1 - UW-CAES system coupled with an off-shore wind farm.

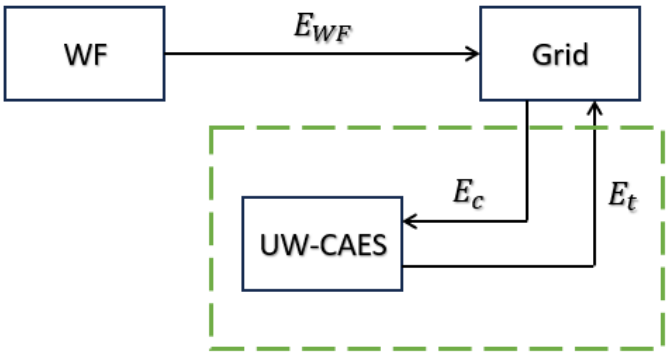

Figure 5.2: Case 2 - Stand-alone UW-CAES system.

The main difference between these two cases is easily visible from the schemes reported in Figure 5.1 and Figure 5.2, where energy flows change basing on the interaction among different parts. But from an economic perspective, if the compressor of the CAES system runs buying electricity at the same price PUN, the two cases coincide.

In fact, in the economic evaluation of Case 1 is necessary to compare the costs and revenues given by the stand-alone wind farm with those given by the coupled system. But the wind farm construction does not depend by the presence of the CAES system, thus its CAPEX and OPEX must not be considered. Hence, looking at yearly costs there are only OPEX of CAES plant that need to be added in the coupled system, and revenues come from the energy feed into the grid both by wind farm ($E_{WF,R}$) and turbine (E_t). Instead, in the case without UW-CAES the revenues come from the energy E_{WF}, that represent all the energy produced by the WF.

If now the stand-alone UW-CAES system is considered, Case 2, other than investment and operating costs, there are the annual expenses related to energy supply for compressor operation (E_c) and revenues related to energy produced by the turbine.

Analysing the revenues given by the two different cases, it is possible to understand that from an economic point of view they are exactly the same:

$$R_1 = E_t \cdot PUN - (E_{WF} - E_{WF,R}) \cdot PUN \tag{5.30}$$

$$R_2 = E_t \cdot PUN - E_c \cdot PUN \tag{5.31}$$

Since PUN changes hour by hour, all these parameters to evaluate revenues in both cases, are vectors containing the energy values and prices allocated to each component hourly. Then prices at which energy is sold by the turbine is different from those at which energy is bought to operate the compressor, and they can both be different from prices at which WF sells its energy. But in Case 1, hour by hour the difference of energy fed into the grid in the stand-alone WF case and coupled system ($E_{WF} - E_{WF,R}$), is exactly the energy provided to the compressor E_c, exchanged at the same price at which the compressor pays for it in Case 2. This proves that for both cases 1 and 2, the economic feasibility can be carried out with the same equations.

For simplicity, Equation (5.31) will be used as reference for the calculation of revenues, calling them only R.

Another parameter that can be taken into account, other than LCOS, is the Net Present Value (NPV). It is the difference between the present value of cash inflows and the present value of cash outflows over a period of time. To derive the present value of the cash flows, a particular rate to discount them is necessary. This rate is derived considering the return of investment with similar risk or cost of borrowing, for the investment, and in this work the $WACC$ is used. Hence, NPV takes into consideration the time value of money. [24]

For a long-term project with multiple cash flow, the following equation allows to calculate the NPV:

$$NPV = -CAPEX + \sum_{i=1}^{n} \frac{(R-O)_i}{(1+WACC)^i} + \frac{V_n}{(1+WACC)^n} \tag{5.32}$$

Where R are the revenues and O are the OPEX, both in €/year, and the last term of the equation represents the actualized cash flow given by the residual value of the plant at the end of its lifetime (V_n). Since there are no such plants in the world, in this analysis its residual value is neglected.

If the value is positive then the project is worthwhile, otherwise the investment will result in a net loss and then some incentives are necessary to make it profitable. In this last case of a negative NPV, the required price at which energy must be sold for having a pay-back-time (PBT) equal to the lifetime of the plant, is equal to the already mentioned LCOS. Then, the difference between LCOS and PUN at which energy produced by the turbine is sold, represents the necessary incentive.

Another important index for the economic analysis is the Internal Rate of Return (IRR), that represents the actualization rate that makes the NPV equal to zero, then can be calculated from Equation (5.32), substituting the weighted average cost of capital with the unknown IRR:

$$-CAPEX + (R-O) \cdot \sum_{i=1}^{n} \frac{1}{(1+IRR)^i} = 0$$

But since the net cash flows do not change year by year, the difference between revenue and OPEX can be taken out of the summation, and the term inside it can be rearranged as follow:

$$-CAPEX + (R-O) \cdot \frac{(IRR+1)^n - 1}{IRR \cdot (IRR+1)^n} = 0 \tag{5.33}$$

The investment is profitable when IRR is higher than WACC, since it represents the intrinsic annual return of an investment project.

6 Results of the Studied Plants

The model illustrated in the previous chapters has been applied to real proposed plants of off-shore wind farms in Italy, with different characteristics in terms of distance from the coast and sea depth, to assess how they can influence both design and operation of an UW-CAES plant and its economic feasibility. They have been proposed by different companies in the last years, considering the wind availability in the Italian seas. Then, following the analysis presented by [4], in which 8 plants have been discussed between those shown in Figure 6.1, the plants of San Pietro, Catanzaro and Trapani have been chosen for this study since they have a useful depth for UW-CAES exploitation and different distances from the coast. In particular, the plant of San Pietro is analysed in more detail as case study. The study of these UW-CAES systems has been conducted taking into account the PUN trend of 2019, 2020 and 2022. The first one is taken as base case, since it well represents the energy market in Italy before Covid pandemic, that has influenced 2020 instead. The 2022 PUN is completely different due to war in Europe and can be considered as an example of extreme case of market in which prices change a lot during the year.

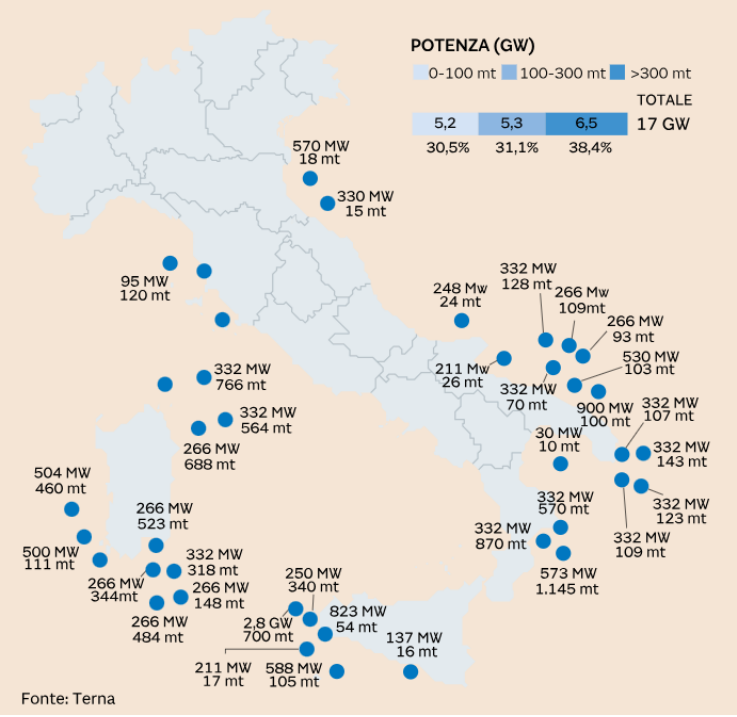

Figure 6.1: Proposed projects of off-shore wind farms in Italy until 2021. [25]

The characteristics of the selected plants are listed in the Table 6.1. The distances from the coast were deduced from an analysis of bathymetry map in the previous work because they are not available from the map of proposed plants.

Table 6.1: Characteristics of the chosen off-shore wind farm.

Plant	Power [MW]	Coast distance [km]	Depth [m]
San Pietro	200	30	500
Catanzaro	332	15	870
Trapani	2800	53	700

The compressor nominal power is taken a quarter of that of the corresponding wind farm, except for Trapani plant because of its huge size, considering 100 MW for this last case. The system of equations discussed for the design of the plant (Chapter 3) allows to find out the air mass flow rate worked by the compressor, that gives the one flowing through the turbine by means of a TDF taken equal to 1. Hence, the air flowing in CtS and HfS are the same in nominal condition, and since the turbine always works in design mode, it is possible to guarantee the best working condition for the HXs during HfS phase.

For the dimensioning of the pipeline, the seabed slope in all cases is considered equal to 4° to calculate its total length, instead the inner diameter of the pipe is assumed to be 0.5 m for San Pietro and Catanzaro plants, and 0.8 m for Trapani plant due to the high air mass flow rate processed in design condition, and to keep pressure drops low along the pipeline due to the high distance from the coast.

All the simulation are conducted with an air storage capacity of 24 hours ($h_{max,T}$), that means that the number of underwater air tanks is carried out considering that they must be able to store enough air to run the turbine for a whole day if necessary.

6.1. Case study: San Pietro plant

The PUN and wind availability have no impact on the design of the different component of the CAES plant, but on the operation of the plant do. For this reason, the results of the design are firstly presented, and later will be discussed the influence of the different PUN trends taken in consideration, showing also the economic results given by the plant operation.

6.1.1. Plant Design

Starting from the constrains given by the site location and with a compressor nominal power equal to 50 MW, the air mass flow rate resulting from the working condition of the UW-CAES plant in design mode is equal to 68.96 kg/s, that allows to extract from the turbine a power of 34 MW in HfS mode.

The compressor characteristics are shown in Table 6.2:

Table 6.2: Results of compressor train in design conditions.

Parameter	Value	Unit
P_c	50	MW
$\dot{m}_{air}$	68.96	kg/s
p_C^{out}	61.45	bar
COT	625	°C
$\beta_{C,tot}$	61.26	-
β_{C1}	1.65	-
β_{C2}	37.57	-

The pressure at the outlet of the compressor train is higher than the underwater pressure at the seabed, equal to 51.3 bar, because it has to overcome all the pressure drops between its exit and the air tanks. The main pressure loss occurs along the pipeline, which in this case is just over 30 km long, leading to a reduction of 8.34 bar. The second part of the compressor train, after the intercooler, need to compensate the pressure drop across this heat exchanger. For this reason, its compressor ratio is slightly higher than the one required to reach $\beta_{C,tot}$.

The intercooler functioning can be observed in Figure 6.2. At the exit of the first compressor the air flow has a temperature around 67 °C. In order to reduce the work of the compressor, it needs to be cooled down. With an intercooler using sea water with an initial temperature of 14 °C, assuming a ΔT_{pp} of 10 °C, it is possible to bring the air temperature at the inlet of the second compressor to 24 °C. To do that, a water mass flow rate of 35.43 kg/s is necessary to not exceed the water temperature of 35 °C due to legislation limits. The sized IC is able to exchange a power equal to 3.1 MW in nominal condition, with a global heat transfer UA parameter of 164.6 kW/K. This parameter is fundamental for the evaluation of the operation of the IC in off-design by means of Equation (4.30), since once it is built, heat exchange surfaces remain unchanged.

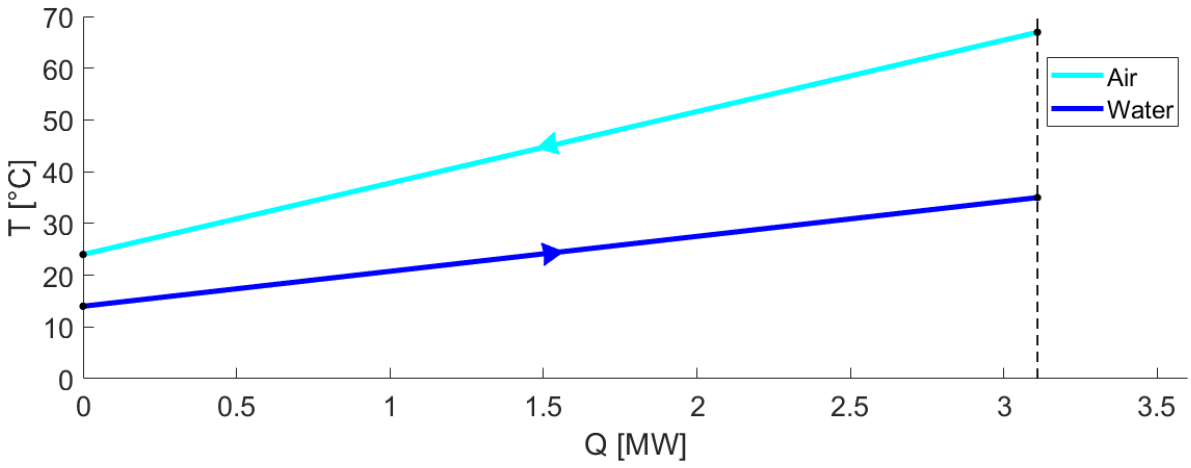

Figure 6.2: Intercooler T-Q diagram in nominal condition.

Following the CtS phase, at the outlet of the compressor train the air flow reaches the TES, which brings the air from a COT of 625 °C down to 55 °C, thanks to three HXs in series using solar salt, thermal oil and sea water in that order, storing the heat to be used during HfS phase. All the results for each heat exchanger in the TES are listed in the Table 6.3:

Table 6.3: Results of TES in design conditions for CtS phase.

Parameter	Solar Salt	Thermal Oil	Sea Water
Q_{HX} $[MW]$	23.4	15.3	3.7
$\dot{m}_{tf}$ $[kg/s]$	48.5	29.2	17.7
T_{in} $[°C]$	290	80	30
T_{out} $[°C]$	600	290	80
UA_{air} $[kW/K]$	937.4	611.7	147.7

During the CtS phase, also the air properties in Table 6.4 are calculated. They are necessary to assess the UA parameters for each HXs during HfS phase in design condition and CtS phase in off-design, by means of Equation (3.37) and Equation (4.33) respectively.

Table 6.4: Air properties across TES in design condition for CtS phase.

HX	μ $[Pa \cdot s]$	k $[W/m \cdot K]$	Pr $[-]$
Air-Salt	$3.6 \cdot 10^{-5}$	0.055	0.718
Air-Oil	$2.7 \cdot 10^{-5}$	0.040	0.711
Air-Water	$2.2 \cdot 10^{-5}$	0.032	0.728

For the HfS phase instead, the TES balance gives the results reported in Table 6.5, warming up the air from sea water temperature up to the TIT, thanks to the heat stored in the thermal tanks. Obviously, in this case the air flows through the HXs in opposite direction, passing from the Air-Water heat exchangers to the Air-Salt one. This heating process allows to reach a final temperature of the air at the inlet of the turbine equal to 576.11 °C.

Table 6.5: Results of TES in design conditions for HfS phase.

Parameter	Sea Water	Thermal Oil	Solar Salt
Q_{HX} $[MW]$	3.6	15.2	22.6
$\dot{m}_{tf}$ $[kg/s]$	17.2	28.9	46.8
T_{in} $[°C]$	80	290	600
T_{out} $[°C]$	30	80	290
UA_{air} $[kW/K]$	143.1	591.2	906.9

It is evident that the results of TES are very similar for the two presented phases, because in design conditions the air mass flow rate flowing through the plant is the same. The same can be said for Figure 6.3 and Figure 6.4 those represent the heat

exchange processes across TES during both phases. In fact, during air cooling phase a total thermal power of 42.4 MW is exchanged, and during air heating phase 41.4 MW.

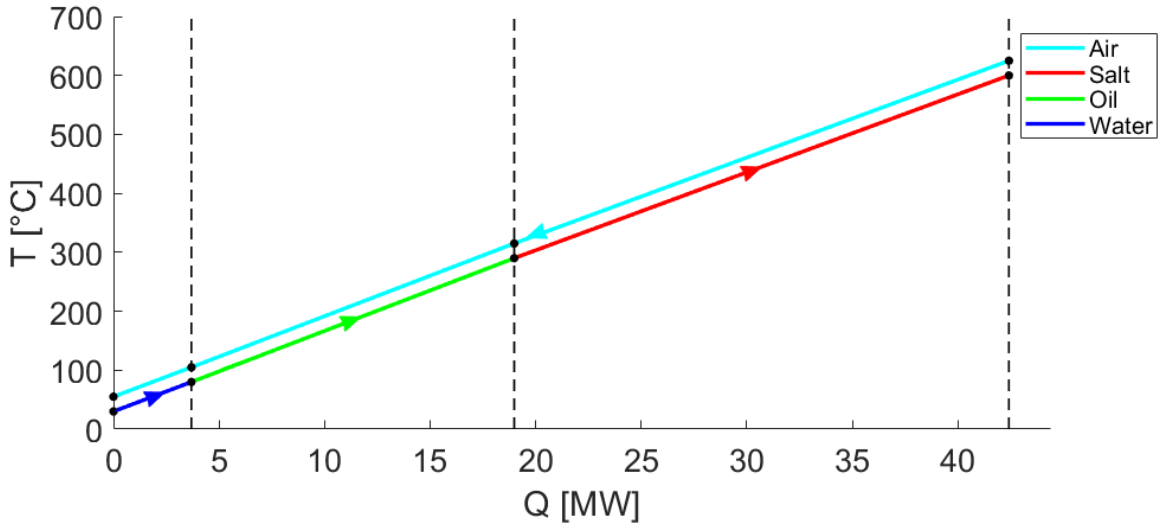

Figure 6.3: Air cooling to storage (CtS) process through TES.

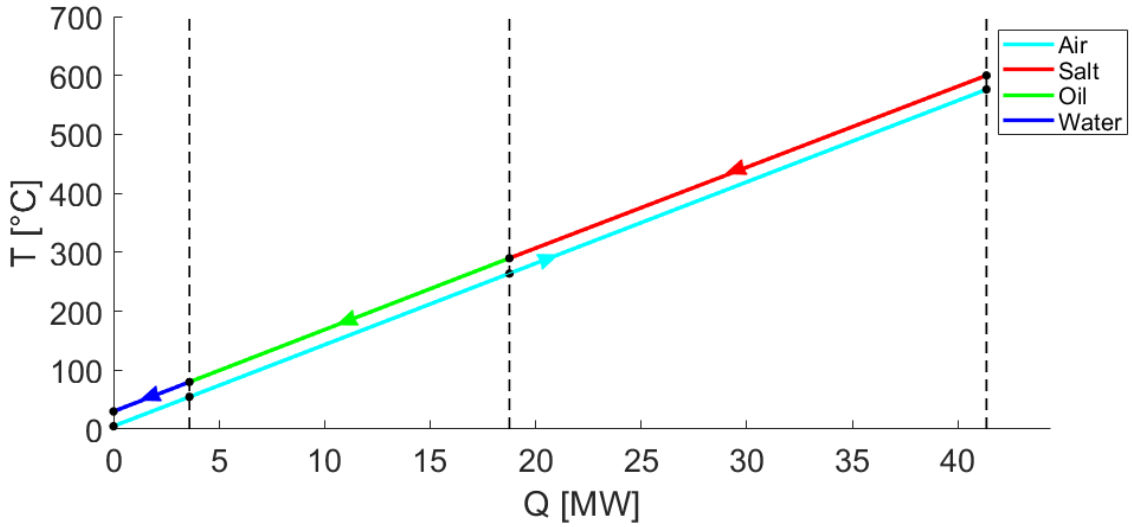

Figure 6.4: Air heating from storage (HfS) process through TES.

During HfS phase, the stored air from underwater tanks at seabed pressure, flows along the pipeline to TES, to be heated up as already showed and to expand through the turbine. Since the mean density of air through the pipeline is lower than during CtS phase because the pressures are lower, the pressure loss is higher for Equation (3.32), leading to a Δp_{pipe} of 8.82 bar. After passing through the 3 heat exchangers, the air flow arrives at the turbine inlet with a pressure of 41.2 bar, ready to expand up to ambient pressure, taking care that its temperature at the turbine outlet is higher than 5 °C to avoid freezing problem. The results regarding the turbine dimensioning are shown in Table 6.6:

Table 6.6: Results of turbine in design conditions.

Parameter	Value	Unit
P_t	34	MW
$\dot{m}_{air}$	68.96	kg/s
TIT	576.11	°C
TIP	41.2	bar
TOT	88.83	°C
β_T	40.67	-

The total reduction of 10 bar of pressure between air tanks and turbine intake, influences its power output, leading to a P_t that is 3.35% lower than an ideal case without pressure drops along the circuit.

The different points of the cycle in nominal condition are presented in the Figure 6.5, that shows the thermodynamical cycle on the diagram of temperature in function of specific entropy. The two phases of compression and expansion are plotted sequentially just to evidence the entire path the air takes, but in the real case they are temporally separated, as the plant stores or produces energy according to its convenience hour by hour.

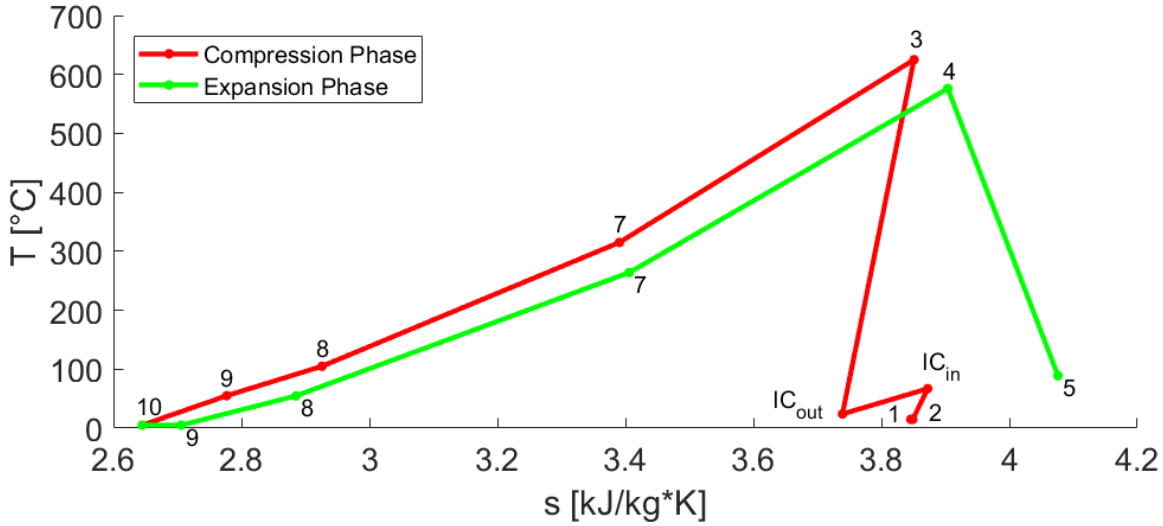

Figure 6.5: Thermodynamic diagram of the air cycle on T-s diagram.

The markers represent the different points in the UW-CAES plant, following the schemes reported for both phases in Figure 2.1 and Figure 2.2 respectively. It is evident the pressure drops across the pipeline between points 9 and 10, that during CtS phase is also accompanied by a decrease in temperature to reach the sea water one starting from the temperature at the outlet of the air-water heat exchanger.

Now that the main results of turbomachinery and TES have been presented, it is possible to introduce those of the underwater components, which make this CAES an UW system.

The pipeline thickens is sized to resist to the difference between operating pressure and external hydrostatic pressure, that is maximum at its intake. The concrete coating instead, depends on the buoyancy forces the pipeline must face and it is also sized to improve the pipe stability on the seabed. Starting from an inner diameter of 0.5 m, the results shown in Table 6.7 are obtained:

Table 6.7: Results of pipeline and concreate coating thickness.

Parameter	Value	Unit
t	0.007	m
D_o	0.514	m
t_c	0.087	m
D_{co}	0.688	m

Regarding the air storage tanks instead, with a required air storage capacity $h_{max,T}$ of 24 hours, the number of necessary energy bags and concreate caissons is 3 and 19 respectively.

6.1.2. Plant Operation

With all the components composing the system that have been sized, it is possible to investigate how the plant works during a year. One of the main constrains is the output power profile of the wind farm during the year. It obviously changes depending on the availability of wind in the site under analysis. To obtain profiles that are consistent with the original one, to be used for simulations over several years, an algorithm developed in previous work on CAES coupled with a renewable source has been used in this thesis. It is a MatLab code based on the first-order Markov chain approach and its principle of operation is widely discussed in [22]. The elaboration of this method is based on real wind data obtained for an area of south-west Sardinia, therefore consistent with the San Pietro plant. Thanks to the MatLab code it was possible to generate 14 plausible production profiles, but here for simplicity is discussed only the first one, illustrated in Figure 6.6.

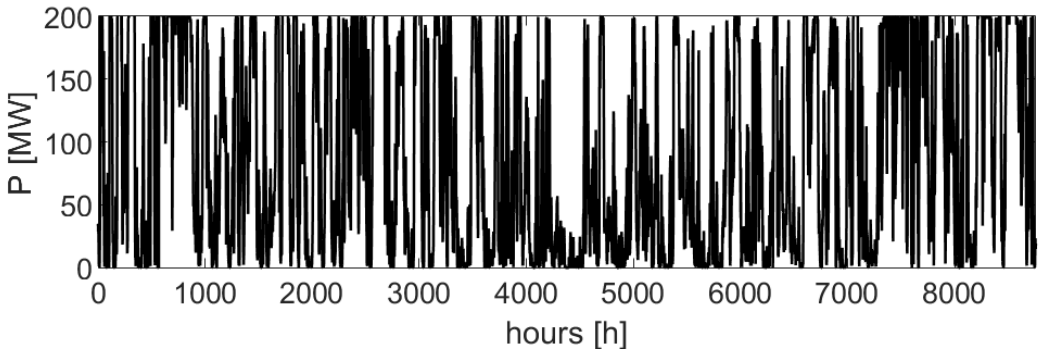

Figure 6.6: Wind farm power output profile.

Then, the other main constrain is the PUN, and in the following Figure 6.7 the investigated years are shown:

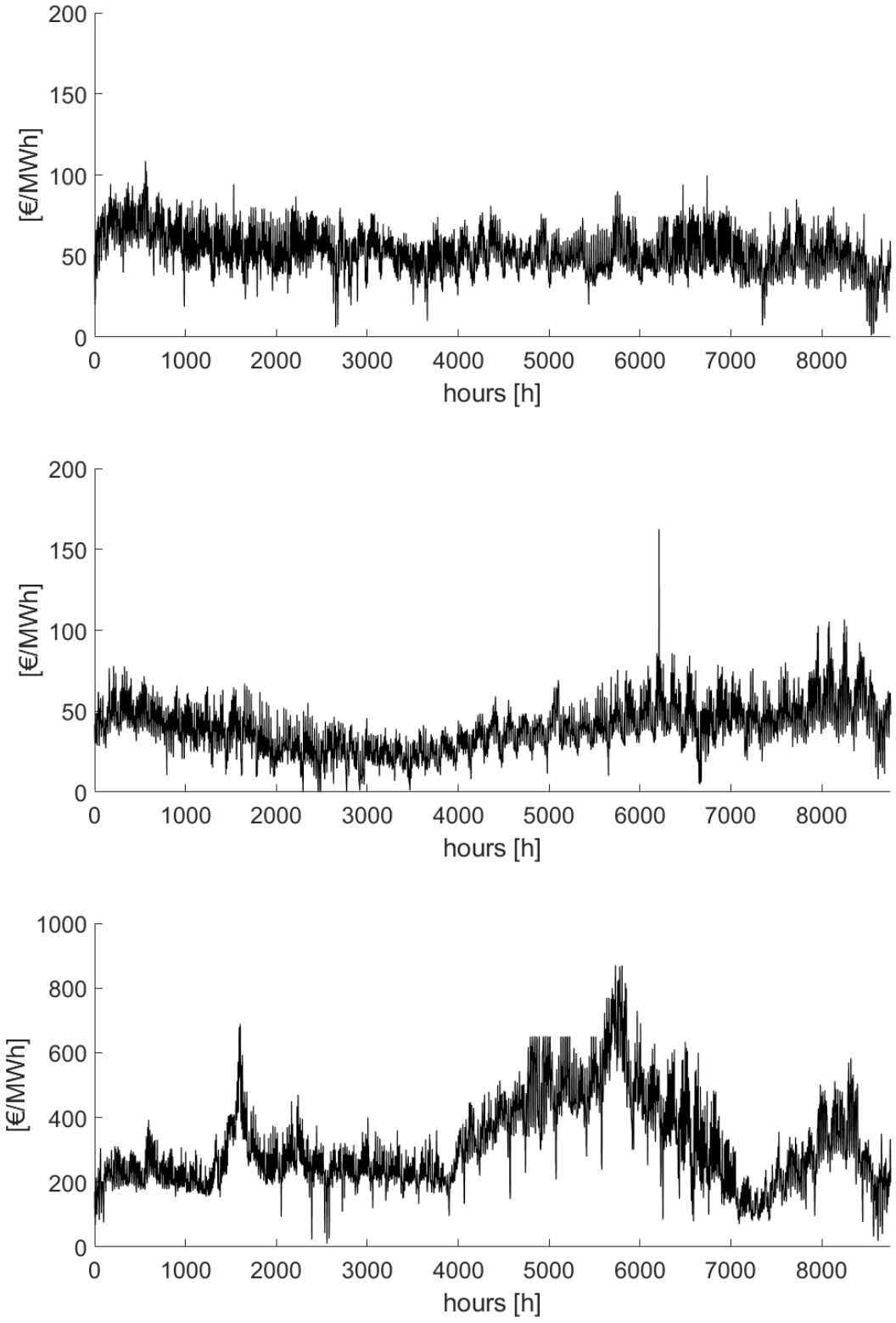

Figure 6.7: From top to bottom: PUN 2019; PUN 2020; PUN 2022.

It is important to note that the PUN 2022 has a wider range of variation, which is between 0 and almost 900 €/MWh, unlike the first two that rarely exceed 100 €/MWh. As explained in Chapter 4, the thresholds for the activation of compressor or turbine

are assessed considering a certain margin around the moving average electricity price, evaluated over a period comparable with the air storage size. Then, since in this work 24 hours are taken as size of the air storage and a margin of ±10% is considered, these thresholds are evaluated considering a period of 24 hours around the hour under consideration. In this way, high variations of prices on short period affect the plant starts up, leading to a reduction of hours of plant operation in 2022 respect to other years in which the fluctuations are limited to smaller range of price. However, at the same time this makes possible to increase the hours of operation of the plant from 40.6% in 2019 to 368.5% in 2022, respect to a case in which this evaluation is made on average annual price. Results about equivalent hours of turbomachinery, number of start-ups, electric energy flows and round-trip efficiency for San Pietro plant during the three years under consideration, are reported in Table 6.8.

Table 6.8: San Pietro plant results of operation.

Parameter	2019	2020	2022
$\boldsymbol{h_{eq,c}}$ $[\boldsymbol{h}]$	1768	1972	1498
$\boldsymbol{h_{eq,t}}$ $[\boldsymbol{h}]$	1756	1961	1491
$\boldsymbol{\#\, on_c}$ $[-]$	496	496	445
$\boldsymbol{\#\, on_t}$ $[-]$	553	561	504
$\boldsymbol{E_c}$ $[\boldsymbol{GWh}]$	88.4	98.6	74.9
$\boldsymbol{E_t}$ $[\boldsymbol{GWh}]$	59.4	66.3	50.4
$\boldsymbol{RTE}$ [%]	67.66	67.65	67.66

The operation of the plant of San Pietro coupled with the off-shore wind farm, obviously leads to a reduction of energy fed into the electric grid respect to the case of the stand-alone WF, from 816.9 GWh to 787.9 GWh in 2019. This happens due to the fact that the UW-CAES system has a certain RTE lower than 100% for the presence of loss of energy across the plant, especially given by the pressure drops across the pipeline.

Regarding the compressor, that can work out of design condition based on the power output of the wind farm, is interesting to note that it absorbs a mean power of about 45 MW during the three years under consideration, that is 90% of its nominal power. This means that it mostly runs at full load, allowing to maintain high efficiency of compressor train and it is a consequence of its small power respect to the San Pietro wind farm one.

An example of the operation of the plant in 2019 can be seen in Figure 6.8, where on top is shown the activation of compressor and turbine, with positive power values for compressor and negative for turbine, together whit the air mass accumulation during the year that follows the turbomachines operation. It is important to monitor its trend since is one of the most important constrains: if the air tanks are full is not possible to run the compressor by storing more air, and if they are empty is not possible to run the turbine.

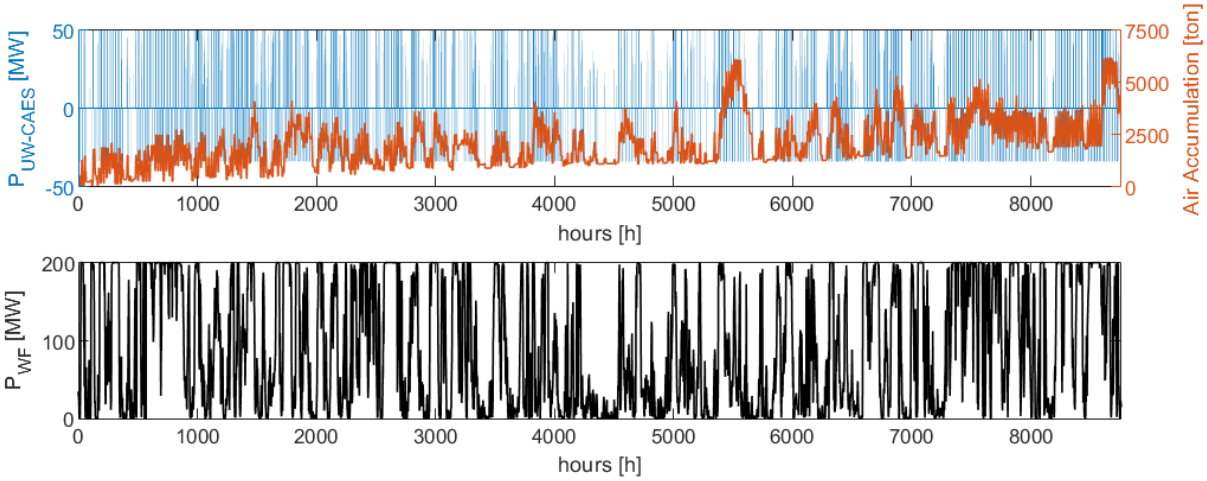

Figure 6.8: San Pietro plant operation in 2019 based on the moving average PUN logic.

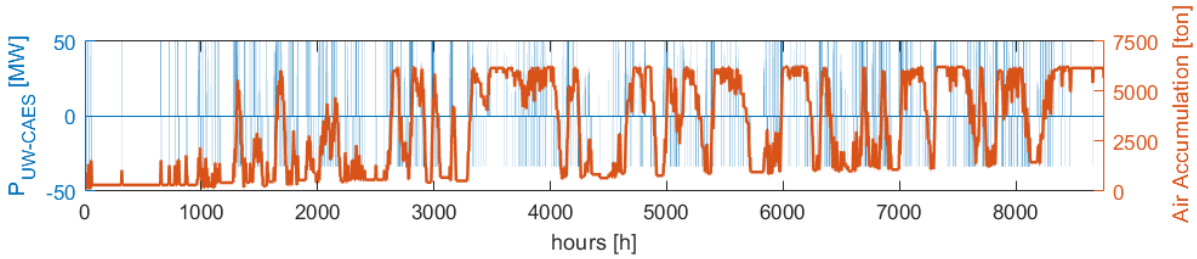

Figure 6.9: San Pietro plant operation in 2019 based on the average annual PUN logic.

Figure 6.9 allows to underline the big difference made by the logic used to evaluate compressor or turbine start-up, based on the moving average of the PUN, compared to the other logic based on the annual average. It is evident that the number of turbomachines activations is much lower, leading to less equivalent hours.

The operation of the plant is also important for the dimensioning of the thermal fluid tanks. In fact, the MatLab code calculates the number of required tanks for each thermal fluid knowing that they have a height and inner dimeter of 20 meters. Then, monitoring the mass accumulation of TFs during the year, it is possible to determine their number. For example, in Table 6.9 are listed the results of San Pietro plant during 2019 with the maximum quantities of TFs accumulated and the height reached inside the tanks. It is possible to see that for all the different thermal fluids, only 1 tank is needed for the hot side and 1 for the cold side, as the maximum height is reached by seawater but is less than the height of the used tank. For the same plant in 2020 and 2022, similar results are obtained.

Table 6.9: Necessary thermal fluids quantities and maximum tanks filling in 2019.

TF	$m\ [ton]$	$V\ [m^3]$	$H\ [m]$
Solar Salt	3409.4	1999.4	6.4
Thermal Oil	2128.5	3129.3	10
Sea Water	5712.6	5795.5	18.5

The trends of accumulation and utilisation of the three TFs are shown in Figure 6.10, together with those of the stored thermal energy.

The continuous accumulation of sea water is not a problem, because it could be cooled down and released into the sea. Unfortunately, it is not possible to transfer the stored energy in the hot sea water tank to another thermal fluid, as done with salt and oil, because water temperatures are lower than those of other fluids. Then in the case of release into the sea, a dissipative process occurs, but it is necessary if is not possible to use its thermal energy.

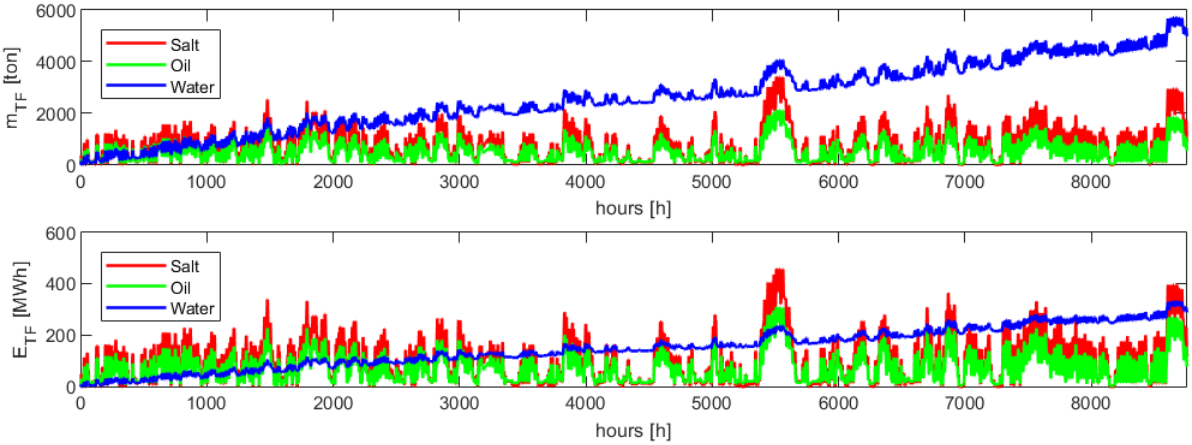

Figure 6.10: Trend of mass and energy accumulations of thermal fluids in 2019.

The effect of the heat exchanger added to transfer energy from salt to oil is visible from the trends of these two fluids. In fact, they are similar both in terms of mass and energy. To better understand the importance of this HX, the Figure 6.11 shows the same trends as shown in Figure 6.10 but without the use of the salt-oil HX.

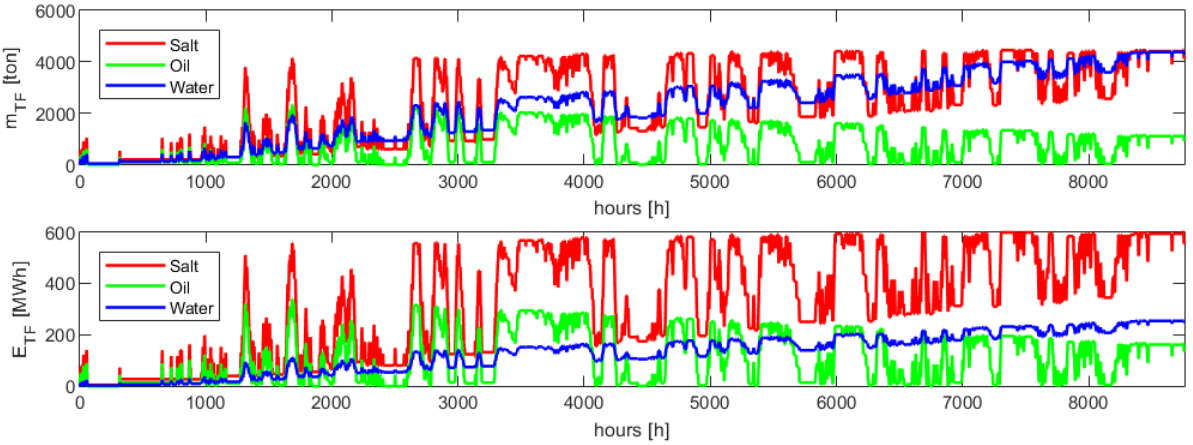

Figure 6.11: Trend of mass and energy accumulations of thermal fluids in 2019 without the salt-oil HX.

The introduction of this HX allows to recover some hours of plant operation, avoiding shutting it down for lack of hot thermal oil needed to heat up the air before expansion through the turbine. At the same time, however, it shifts the problem of lack of hot TF

from the oil to the salt, as can be seen from the detail of the mass accumulation of TFs in Figure 6.12, which shows that sometimes during 2019 almost all the energy stored in the salt is transferred to the thermal oil, leading to a lack of hot solar salt. Thus, the introduction of this HX improves the operation of the plant, but other constrains need to be evaluated to limit salt consumption.

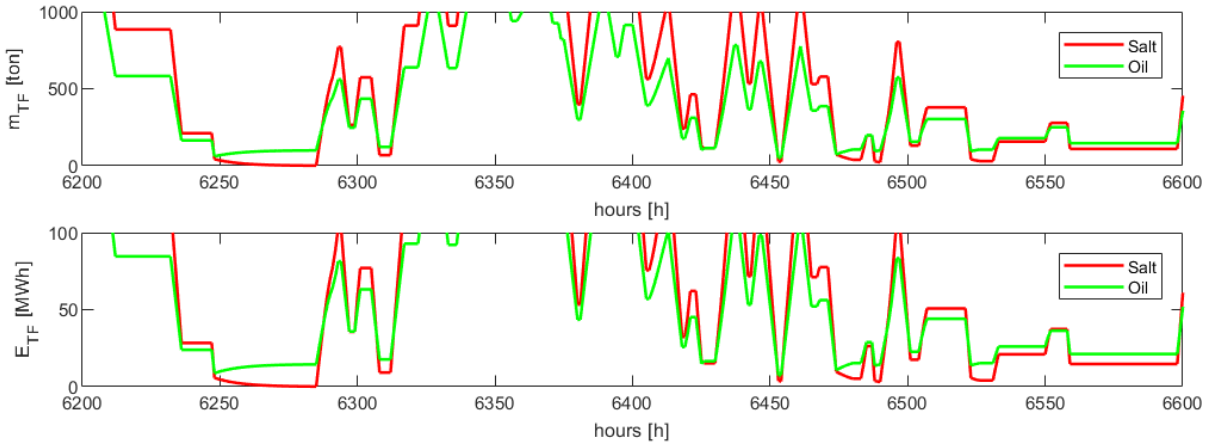

Figure 6.12: Detail of mass and energy storage trends to highlight salt-oil HX operation.

To conclude this analysis, the way in which air and TFs tanks are exploited during a year is shown in Figure 6.13, to understand whether it is worth building that number of tanks or the option to reduce them can be considered if the plant operation is not greatly affected.

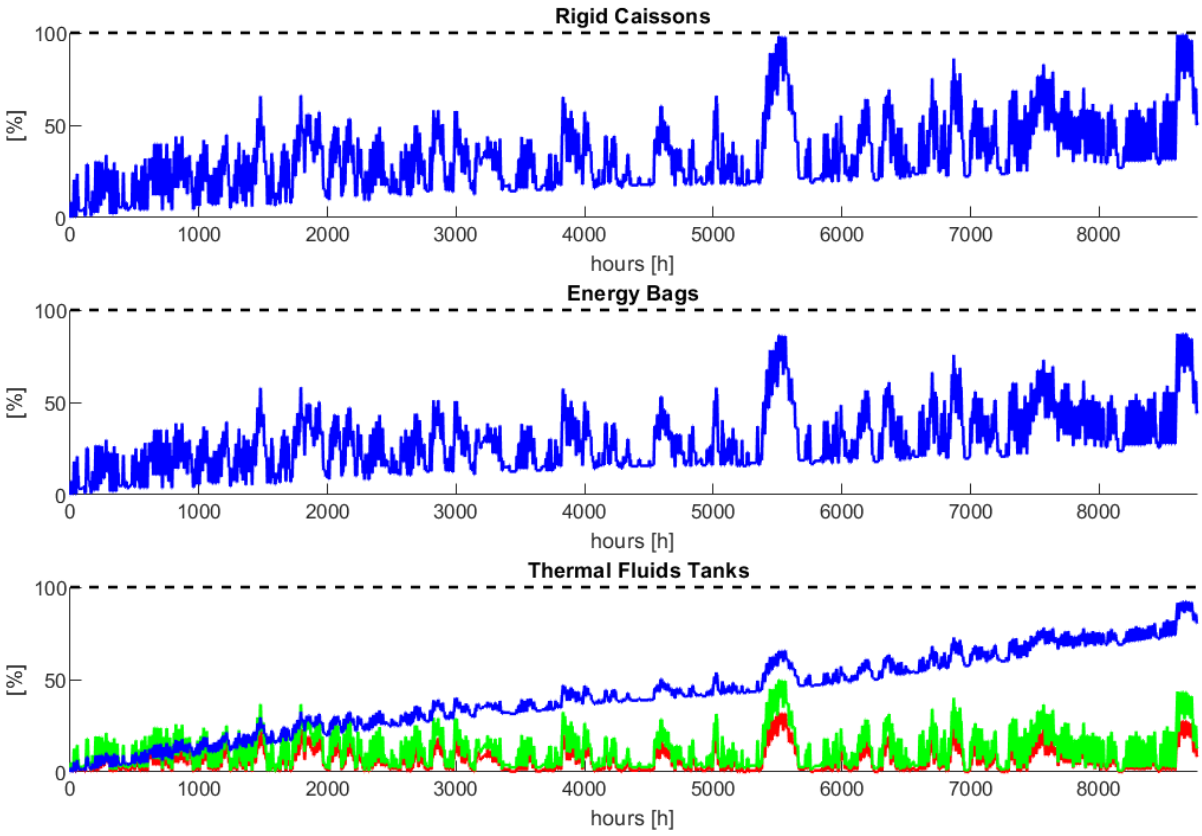

Figure 6.13: From top to bottom, filling percentage: air in rigid caissons; air in energy bags; sea water (blue), thermal oil (green), solar salt (red) in TFs tanks.

In both cases of underwater tanks analysed, rigid caissons and energy bags, their number is fully exploited for a negligible period. The same can be said regarding the TFs tanks to store thermal energy, suggesting that smaller tanks can be used at least for solar salt and thermal oil.

6.1.3. Economic Results

The CAPEX and OPEX of the plant mainly depend on the size of the components, that is established with the design. Hence, they are the same for the 3 studied years, except for air tanks and TES, because they depend respectively by the stored energy in underwater tanks and the quantity of necessary TFs, which slightly change with the considered year. The main difference is given by the type of selected underwater tanks, which also affects the construction costs. In the following Table 6.10 the investment costs of the plant and the operation costs are listed, showing the difference between the two possible options for air storage:

Table 6.10: Results of CAPEX and OPEX for San Pietro plant.

UW-storage	CAPEX [M€]	OPEX [M€/y]
Rigid Caisson	1129.2	34.8
Energy Bag	567.3	17.6

The results show a net difference between the two options, that is given by the high investment cost for the 19 rigid caissons, other than their maintenance that is calculated as a percentage of their CAPEX. The share of costs to be attributed to each component are shown in Figure 6.14 and Figure 6.15.

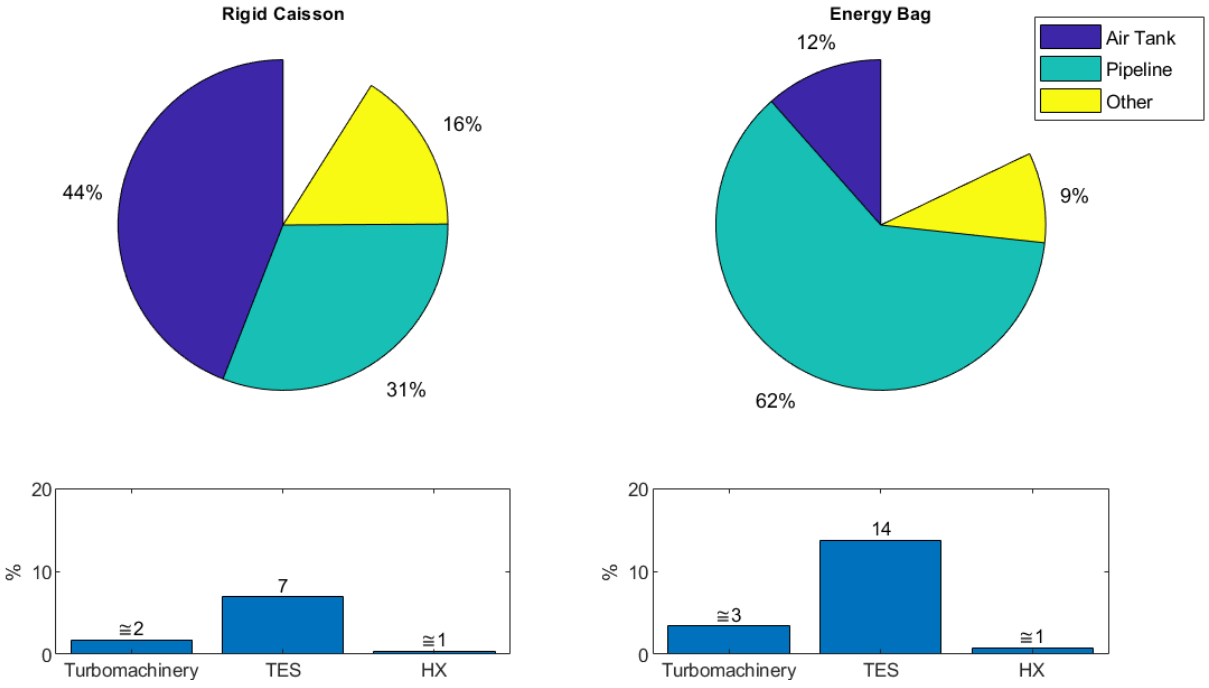

Figure 6.14: CAPEX share for San Pietro plant basing on possible UW-storage technologies.

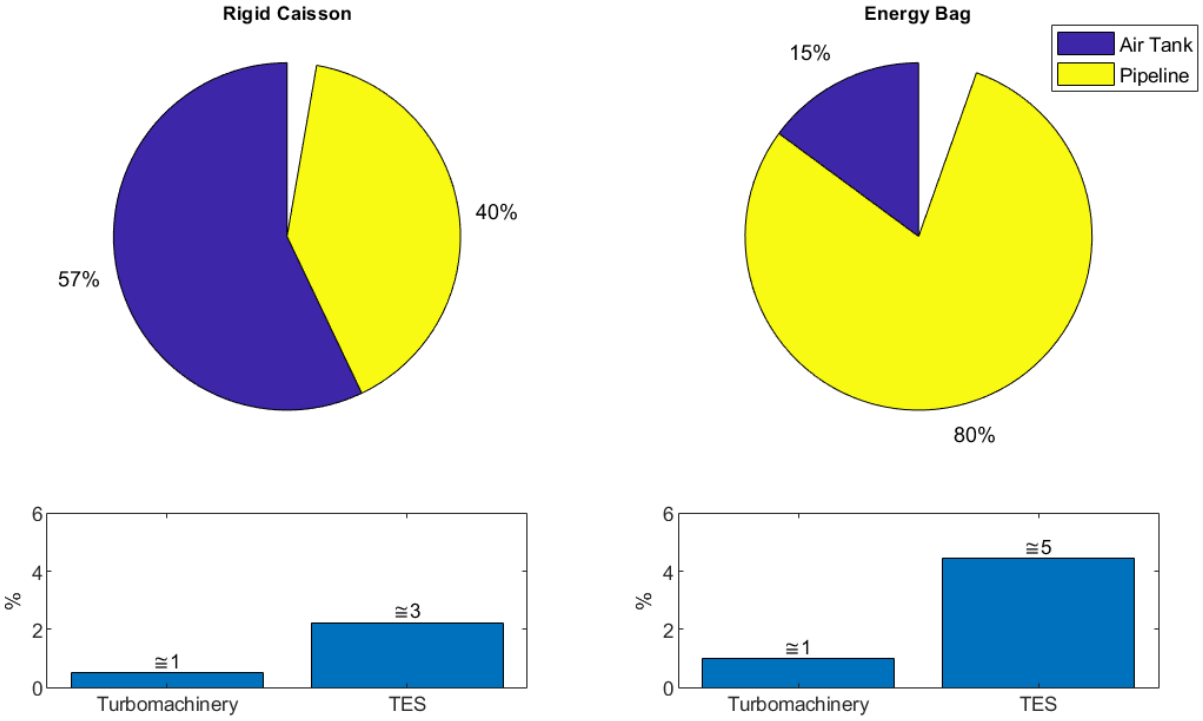

Figure 6.15: OPEX share for San Pietro plant basing on possible UW-storage technologies.

Given these costs and knowing the energy flows of compressor and turbine from the annual plant operation, it is possible to carry out the LCOS of the UW-CAES system

by means of Equation (5.28) with a WACC assumed equal to 7%, in which the net difference in term of costs of the two possible air storage systems is reflected. From Table 6.11 it is possible to note that it also differs by the years because it is influenced by both the PUN trend and the energy flows.

Table 6.11: Results of LCOS for San Pietro plant.

LCOS [€/MWh]	2019	2020	2022
Rigid Caisson	2263.5	2019.9	2935
Energy Bag	1168.3	1039	1645

Even in the case of plant with energy bags as underwater tanks, that has lower costs, the LCOS is much higher than the typical PUN at which electric energy is exchanged on the market. Hence, to make the investment profitable it is necessary to think about some incentives, to cover the difference between its value and price at which energy is sold by the UW-CAES system when air expands through the turbine. The same conclusion could be reached by looking at the revenues of the plant over a year, that are much lower than the OPEX, leading to negative cash flow every year of the plant lifetime. In fact, the OPEX are in the order of millions of euros, instead revenues in the order of thousands of euros. For this reason, values of NPV are not reported because they are negative. To bring the NPV to zero at the end of the plant's lifetime, the energy fed into the grid must be sold at the same price of LCOS. In the following Table 6.12 are reported the values of the revenues, the mean prices at which the CAES plant sell the energy produced by the turbine following the PUN trends, and then the necessary incentives to cover the investment for both case of air storage systems:

Table 6.12: Other economic results to investigate the convenience of San Pietro plant.

Parameter	2019	2020	2022
$\boldsymbol{Revenues}$ $[\boldsymbol{k€}]$	182.7	344.8	419.5
$\boldsymbol{PUN_t^{avg}}$ $[€/\boldsymbol{MWh}]$	63.4	48.7	345.7
$\boldsymbol{Incent_{RC}}$ $[€/\boldsymbol{MWh}]$	2200.1	1971.1	2589.3
$\boldsymbol{Incent_{EB}}$ $[€/\boldsymbol{MWh}]$	1104.9	990.2	1299.5

6.2. Other Plants

The plant of Catanzaro differs from San Pietro mainly in the distance from the coast, which is just half of the case already analysed, and in the depth of the site. The Trapani plant, instead, differs from the other two by the size of the wind farm and the distance from the coast, which is much greater. Therefore, the results of the design, operation and economic feasibility will be briefly presented highlighting the main differences.

The results given by the compression trains design starting from the nominal power of the compressors and the location specifics, are shown in the following Table 6.13:

Table 6.13: Results of compressor trains in design conditions.

Parameter	Catanzaro	Trapani
P_c $[MW]$	83	100
$\dot{m}_{air}$ $[kg/s]$	105.6	132.6
p_C^{out} $[bar]$	97.3	77.2
$\beta_{C,tot}$ $[-]$	96.98	77
β_{C1} $[-]$	2.62	2.07
β_{C2} $[-]$	37.42	37.50

Underwater pressures at the seabed are 88.5 bar and 71.4 bar respectively. The compressor outlet pressures are higher to overcome the pressure drops, especially through pipelines, where they reach 5.9 bar and 3.6 bar during the compression phase. For the HfS phase instead, they are 6.3 bar and 3.7 bar respectively, allowing for the characteristics listed in the Table 6.14 for turbine design:

Table 6.14: Results of turbines in design conditions.

Parameter	Catanzaro	Trapani
P_t $[MW]$	57	70
TIT $[°C]$	576.3	576.1
TIP $[bar]$	79.7	65.6
TOT $[°C]$	41.6	54.6
β_T $[-]$	78.68	64.8

It is important to remember that the inner dimeter of the pipe for the plant of Catanzaro is the same as for San Pietro plant, that is 0.5 m, but for the Trapani plant it is 0.8 m because otherwise it was not possible to reach a solution by means of *fsolve* function on MatLab, which for smaller inner diameter does not converge due to the high distance from the coast, resulting in high pressure drops. The larger diameter makes it possible to reduce pressure losses even if the pipe length is significant, allowing convergence to be achieved. This produces, together with the loading conditions inside and outside the pipeline, the results for the thickness of the pipe and concreate coating shown in the Table 6.15.

Table 6.15: Results of pipeline and concreate coating thickness.

Parameter	Catanzaro	Trapani
t $[m]$	0.011	0.014
D_o $[m]$	0.522	0.828
t_c $[m]$	0.087	0.12
D_{co} $[m]$	0.696	1.068

In order to run the turbine for 24 hours, the number of required energy bags is the same as for the plant of San Pietro, but the number of rigid caissons changes. It is 17 and 22 for Catanzaro and Trapani, because the greater sea depth allows more air to be

stored in the same volume, thanks to the higher pressure and therefore higher air density, but at the same time the higher nominal power of the turbine requires more air, resulting in a greater number of rigid caissons for the Trapani plant. The number of energy bags does not change because they are much larger than the rigid caissons, enabling a wider range of air mass to be covered with the same number of bags.

Regarding the heat exchangers of the TES and the IC, the results given by the design in terms of power exchanged and mass flow rate of thermal fluids are reported in Table 6.16 for the CtS phase and in Table 6.17 for the HfS phase.

Table 6.16: Results of thermal powers and TFs flows exchanged during CtS phases.

Parameter	Catanzaro	Trapani
$\boldsymbol{Q_{IC}}$ $[\boldsymbol{MW}]$	10.8	9.7
$\boldsymbol{\dot{m}_{IC,water}}$ $[\boldsymbol{kg/s}]$	123.8	110.2
$\boldsymbol{Q_{HX,salt}}$ $[\boldsymbol{MW}]$	36.1	45.2
$\boldsymbol{Q_{HX,oil}}$ $[\boldsymbol{MW}]$	23.8	29.6
$\boldsymbol{Q_{HX,water}}$ $[\boldsymbol{MW}]$	5.8	7.2
$\boldsymbol{\dot{m}_{HX,salt}}$ $[\boldsymbol{kg/s}]$	74.7	93.4
$\boldsymbol{\dot{m}_{HX,oil}}$ $[\boldsymbol{kg/s}]$	45.4	56.6
$\boldsymbol{\dot{m}_{HX,water}}$ $[\boldsymbol{kg/s}]$	27.9	34.5

Table 6.17: Results of thermal powers and TFs flows exchanged during HfS phases.

Parameter	Catanzaro	Trapani
$\boldsymbol{Q_{HX,salt}}$ $[\boldsymbol{MW}]$	34.6	43.5
$\boldsymbol{Q_{HX,oil}}$ $[\boldsymbol{MW}]$	23.1	29.1
$\boldsymbol{Q_{HX,water}}$ $[\boldsymbol{MW}]$	5.6	6.9
$\boldsymbol{\dot{m}_{HX,salt}}$ $[\boldsymbol{kg/s}]$	71.6	89.9
$\boldsymbol{\dot{m}_{HX,oil}}$ $[\boldsymbol{kg/s}]$	44.2	55.6
$\boldsymbol{\dot{m}_{HX,water}}$ $[\boldsymbol{kg/s}]$	26.8	33.4

The operation of the plant is mainly influenced by the trends of PUN and power output of the wind farm, so the performance of these two plants in terms of equivalent hours does not change much compared to the San Pietro plant. The RTEs of Catanzaro are slightly higher, around 68.4%, thanks to the lower pressure drops through the pipeline due to the shorter distance from the coast, while for Trapani they are around 69.5% because, although the length of the pipeline is 53 km, its larger diameter makes it possible to reduce pressure drops, which only have an impact of 1.01% on the turbine output.

Obviously, the quantities of energy exchanged are different because the size of the turbomachines change, but what mainly distinguishes these plants from the former is the costs. In fact, as seen for the case study, most of the CAPEX and OPEX are

represented by the underwater components: pipeline and underwater tanks. In these cases, the number of underwater air tanks does not change considerably. The length of the pipeline, on the other hand, has a great influence, as it varies from 15 km in Catanzaro to 53 km in Trapani.

Table 6.18: Results of CAPEX and OPEX for plants of Catanzaro and Trapani.

Parameter	Rigid Caisson	Energy Bag
$CAPEX_{Catanzaro}$ [M€]	1238.6	478.3
$OPEX_{Catanzaro}$ [M€/y]	35.7	12.3
$CAPEX_{Trapani}$ [M€]	2652.8	1353.4
$OPEX_{Trapani}$ [M€/y]	85.7	45.7

Table 6.18 shows the investment costs and operation and maintenance costs for both plants, where the air tanks in Catanzaro plant accounts respectively 55% and 21% of CAPEX for rigid caisson and energy bag solutions, instead the pipeline accounts for 178 M€. For Trapani plant, the pipeline represents 960 M€ of capital expenditure, and the air tanks 43% and 11% of the CAPEX respectively.

Following the results obtained for the San Pietro plant, the year 2020 can be taken into account to compare the cost-effectiveness of these two plants in the best case, as it leads to lower LCOS values.

Table 6.19: Results of LCOS for plants of Catanzaro and Trapani in 2020.

LCOS [€/MWh]	Rigid Caisson	Energy Bag
Catanzaro	1316.5	520.9
Trapani	1927.3	1016.1

Even for these two plants, annual revenues are lower than operating expenses. Thus, although the Catanzaro plant has LCOS that are about half those of San Pietro, as can be seen from Table 6.19, they are still too high compared to the PUN prices, which leads to the investment not being worthwhile without the introduction of some incentives. Furthermore they are also higher than other large-scale energy solutions, such as pumped hydro energy storage and different batteries technologies for energy storage [26] [27].

7 Sensitivity Analysis

In this work, a sensitivity analysis was carried out to assess how the results obtained in the previous chapter are affected by variations in the size of certain plant components, site specifications, dimensioning factors such as continuous turbine operating hours or certain constraints.

A technical and an economic sensitivity can be distinguished. The former will be presented only for the case study, the latter will be discussed for the three analysed plants to better understand what can contribute to make them more convenient and attractive for investment.

Lastly, other special analyses are carried out by making strong assumptions such as neglecting the OPEX of the pipeline and underwater tanks, or neglecting the presence of the pipeline, or even using electricity price trends from other countries.

7.1. Technical Sensitivity Analysis

The analysis of the behaviour of the San Pietro plant in design conditions has been done varying:

- Depth of the site;
- Distance from the coast of the site;
- Pipeline inner diameter.

In other words, starting from the San Pietro plant, which consists of a compressor with a nominal power of 50 MW, connected by a 0.5 m internal diameter pipe to an air storage system located 30 km from the coast and at a sea depth of 500 m, the three mentioned parameters are varied by taking the same compressor power. In this way, it is possible to study how the design of the system changes in terms of component sizes, mass flow rates involved and heat flows.

It is intuitable that the location depth is one of the parameters that most influences an UW-CAES plant. Indeed, from the sensitivity analysis performed on it, the results of the design change quite a bit. As the sea depth increases, the pressure on the seabed rises, leading to higher compression ratio that the compressor must satisfy. Consequently, since the enthalpy variation on the compressor increase but its power remains the same, a lower mass flow rate of air results. The reduction in air flow within the pipeline brings to lower pressure drops both during compression and expansion

phases. Even if a reduction of air mass flow rate occurs, the increase in expansion ration improves the performance of the turbine in a first moment, leading to higher nominal power output and thus higher RTE in design conditions. The best performances for a plant with the characteristics of San Pietro are reached for a sea depth around 700 meters. These considerations are shown in Figure 7.1.

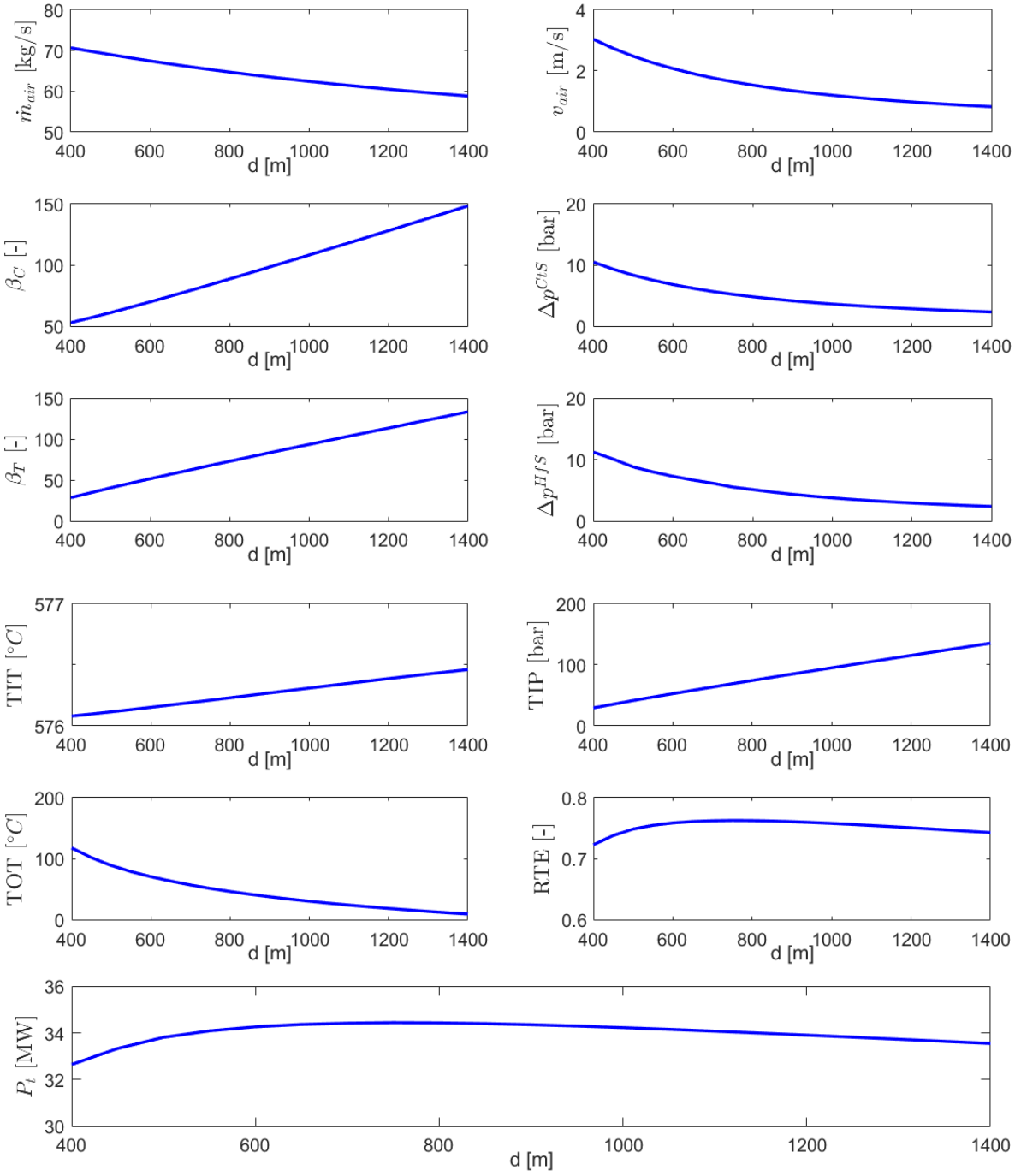

Figure 7.1: Sensitivity analysis on how location depth affects compressor and turbine characteristics.

The heat exchange is influenced by the lower mass flow rate, resulting in trends in agreement with those of the air flow rate. Therefore, lower heat stored and lower air flow lead to a TIT that does not change considerably, but since the expansion rate increase then the TOT decrease starting from the same temperature at the turbine inlet.

Contrary to what might be expected, the distance from the coast does not significantly affect compressor and turbine design.

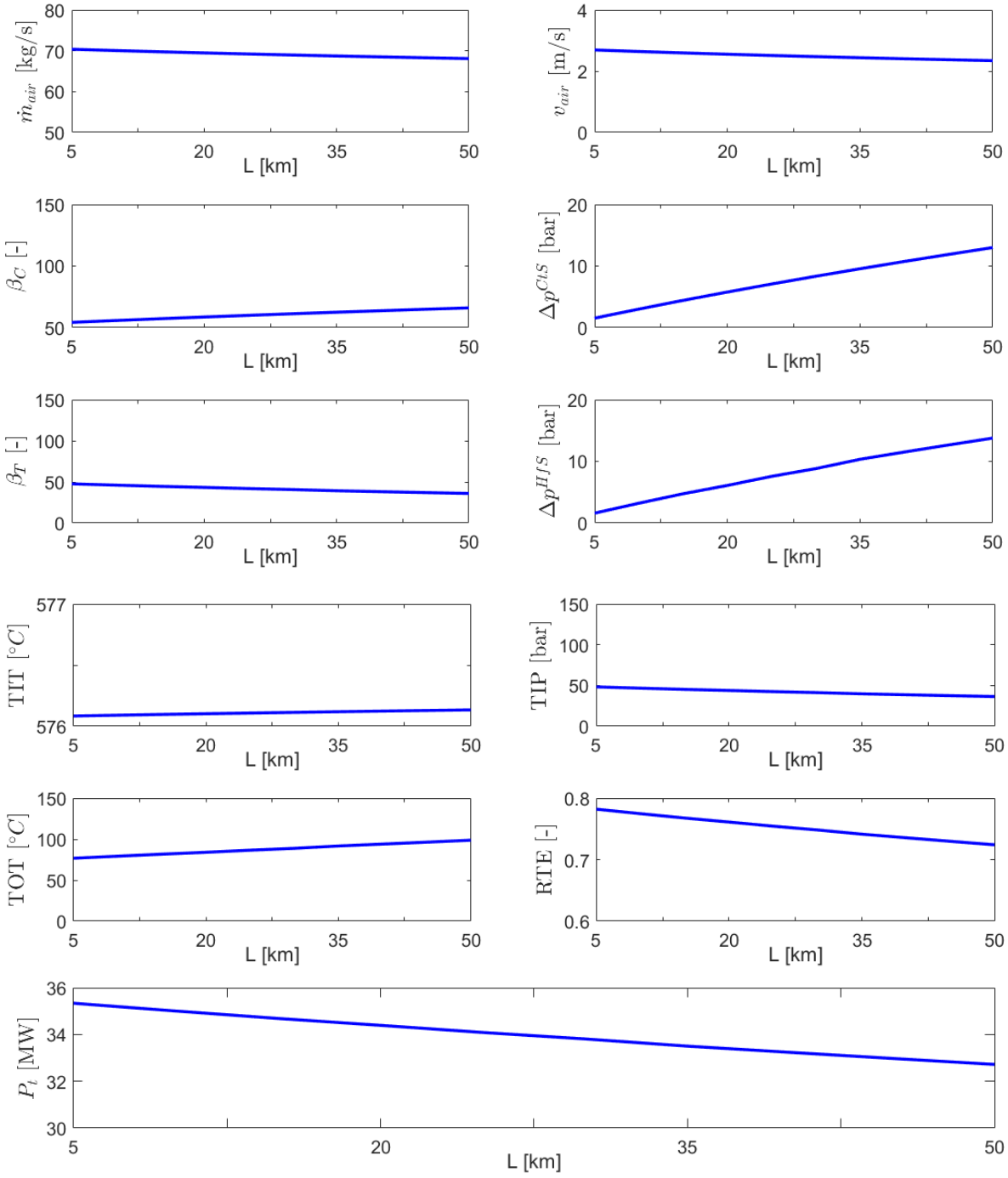

Figure 7.2: Sensitivity analysis on how distance from the coast affects compressor and turbine characteristics.

As the Figure 7.2 above shows, the only changes involved are pressure drops, which increase linearly with distance from the coast, but which slightly affect the compression and expansion ratio. Since the pressure drops are proportional to the square of the volumetric flow rate, they cause a small change in the air mass flow rate. But these near-constant values, together with the lower pressure drops for low distances, allow the system to achieve excellent performance with an RTE of almost 80% under design conditions, calculated as the ratio between turbine and compressor works in design mode. This sensitivity demonstrates that it is possible to improve the efficiency of a UW-CAES system by reducing the length of pipe connecting turbomachines and air storage.

Concerning the variation of the pipe diameter, values below 0.4 m were not considered because MatLab's *fsolve* function does not converge to a result on the plant design equation system with the default number of iterations set. From Figure 7.3, it can be seen that the diameter of the pipe influences the pressure drop, as reducing the pipe cross-section increases the fluid velocity, leading to higher pressure drops. This is reflected in a low RTE for small diameter pipes. But on the other hand, increasing the size does not significantly improve system performance, with the RTE tending to 80% for diameters above 0.8 m. This happens because a larger pipe section brings pressure losses close to zero, making it impossible to increase the air mass flow rate, and thus RTE and P_t. The only effect a larger pipe can give is an increase in the associated investment costs, which as already seen in the previous chapter are one of the major CAPEX voices.

In order to verify that the friction factor can be calculated with Equation (3.5) to solve the system that gives the design of the plant, the Reynolds number and the ratio ϵ/D are evaluated for all sensitivities to check that they respect the limits that the equation requires. In Figure 7.4 they are plotted in the case of the pipeline diameter variation, which is the case that most influence these parameters, highlighting the limits to be respected.

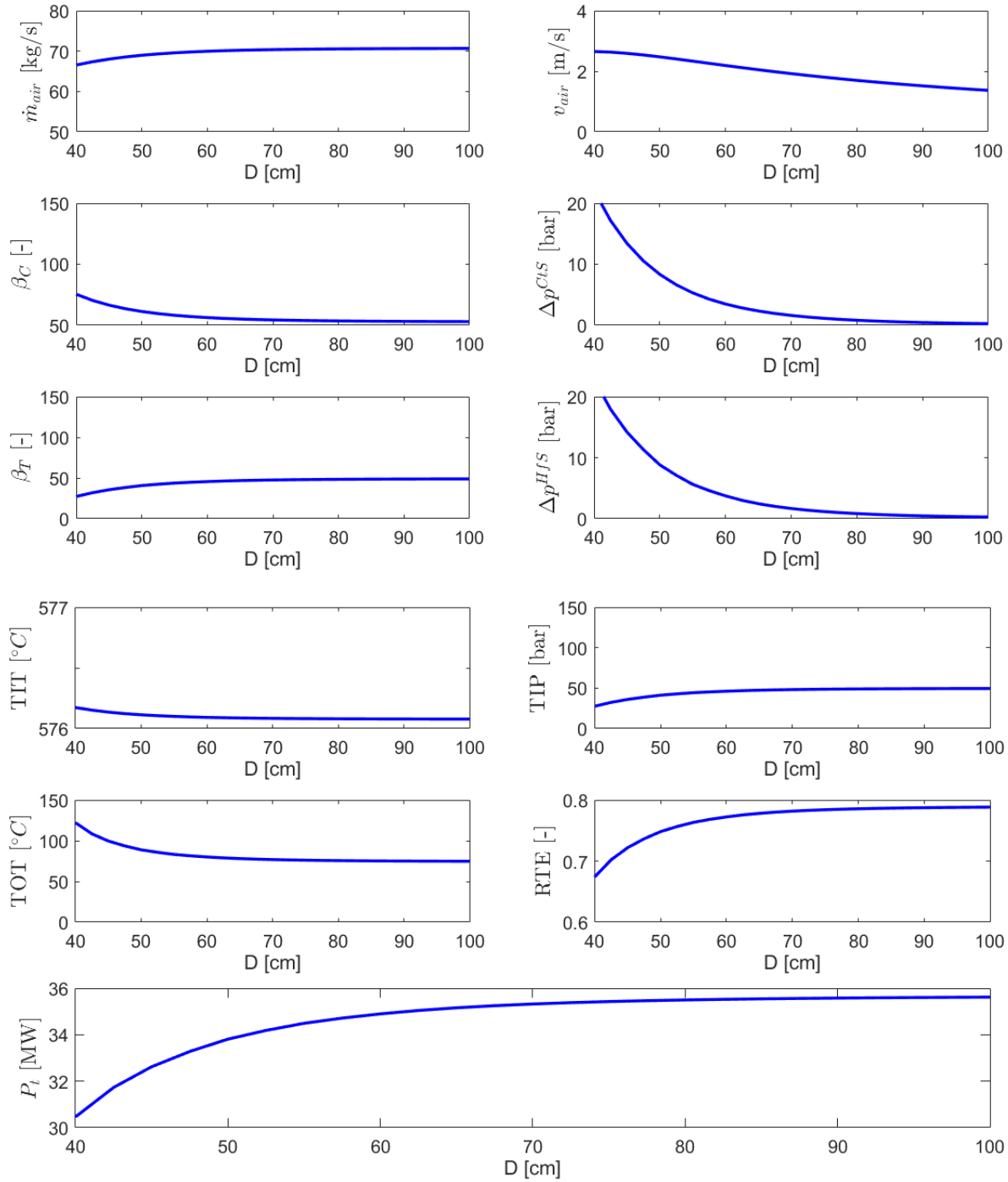

Figure 7.3: Sensitivity analysis on how pipeline diameter affects compressor and turbine characteristics.

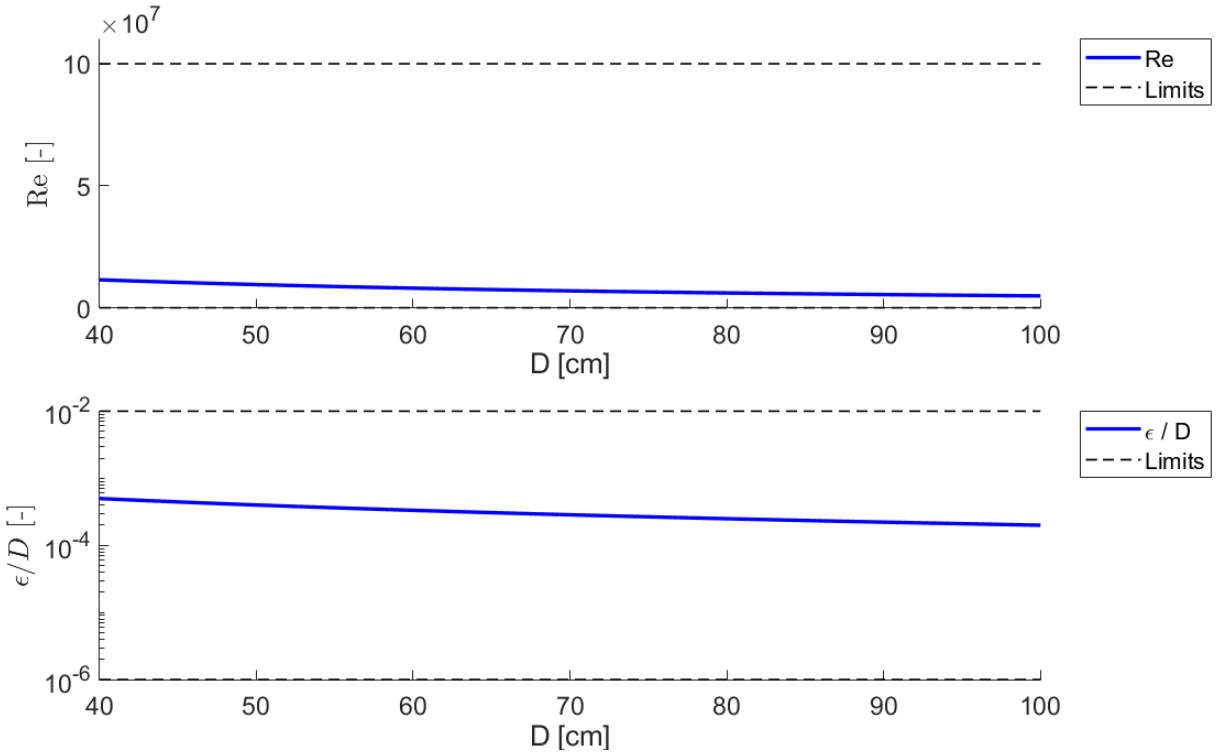

Figure 7.4: Limits check for the applicability of the friction factor equation.

As already mentioned in the sensitivity analysis on the location depth, air mass flow rates of thermal fluids and thermal flows that are exchanged in the HXs of TES follows the trends of the air mass flow rate for all the presented analysis. With regard to the IC, instead, the mass flow rate of seawater required to cool the air temperature does not only depend on the air mass flow rate, but above all on the compression ratio, because a higher β_C means a higher air temperature at the outlet of the first compressor, resulting in a higher water flow rate required. The variation in sea depth is a perfect example for understanding this behaviour, as the increase in compression ratio as depth increases is accompanied by a decrease in air flow, but the necessary sea water flow rises (Figure 7.5).

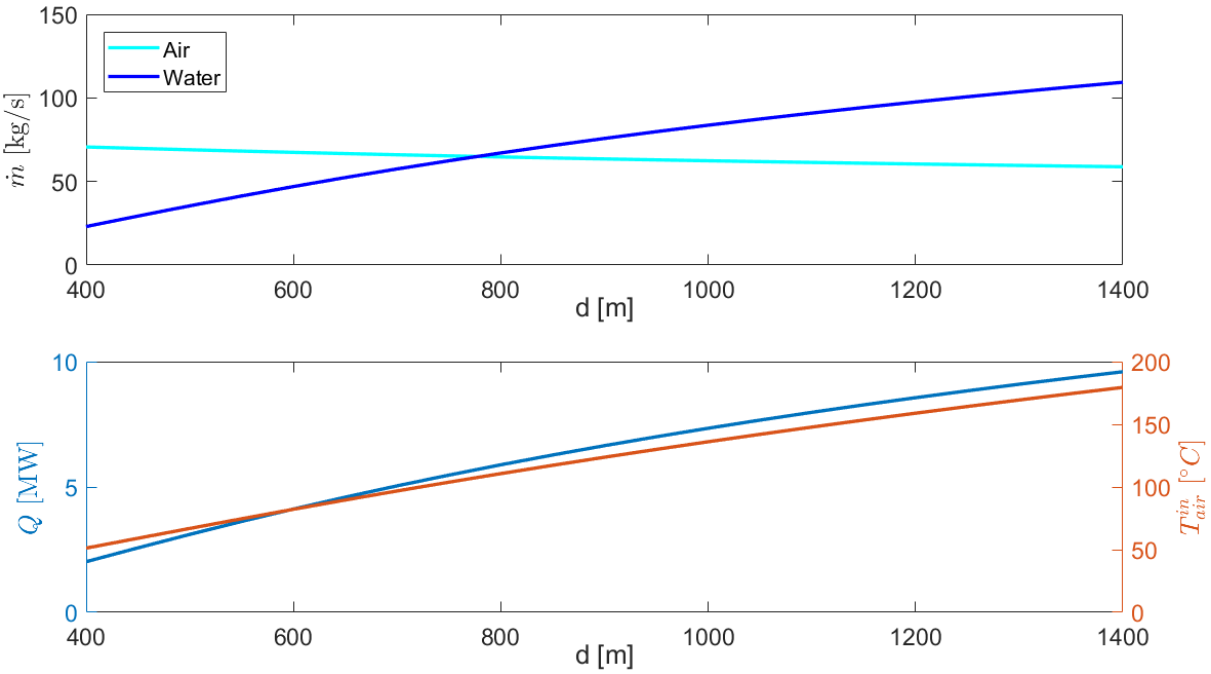

Figure 7.5: Influence of sea depth variation on intercooler functioning in design conditions.

7.2. Economic Sensitivity Analysis

In the following, the economic sensitivity analysis for the San Pietro plant in 2019 is presented to highlight the trend of the main results, and then some examples of analysis on other plants are discussed.

Before starting with the sensitivity on the studied plants and their operation, an analysis is made on the influence of the number of operating hours of the plant during a year. This is done because it is directly related to the LCOS, as it affects the energy exchanged by the turbomachines, and can help to understand how to make the investment more profitable, in other words how to reduce the value of the LCOS. Therefore, given the design of the plant, the amount of energy absorbed by the compressor is calculated by varying its h_{eq}, and with the RTE the energy produced and fed into the grid by the turbine is estimated. Then, the LCOS variation for both the air storage solutions is carried out as shown in Figure 7.6. This allows to understand with a first analysis the effect of the equivalent hours of operation of the plant and, consequently, of the amount of stored energy, on the economic feasibility of an UW-CAES system, without taking care of size of air storage, TFs availability and other constrains.

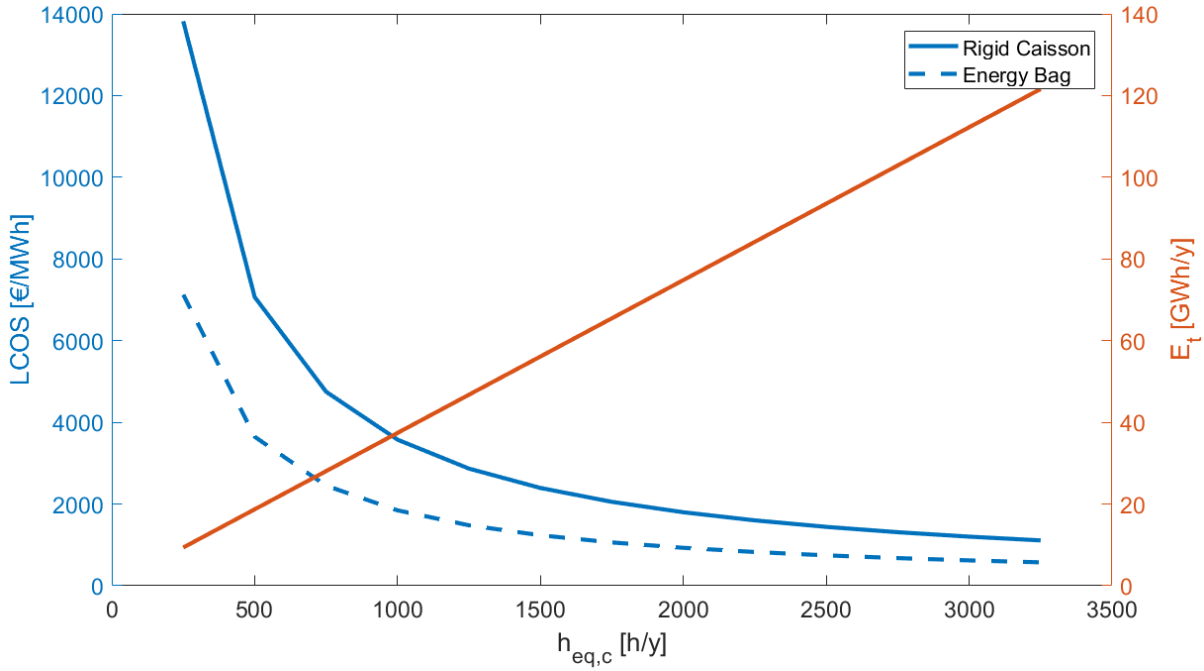

Figure 7.6: Influence of compressor equivalent hours on LCOS.

These trends obtained for the plant of San Pietro are valid for any plant and underline the importance of finding a logic to run the plant as much as possible.

At this point, knowing the importance of the h_{eq} on the economic evaluation of the plants, a sensitivity analysis was carried out considering the main parameters that affect their operation, varying the following:

- size of compressor in terms of nominal power;
- PUN limits;
- size of underwater air storage system.

Firstly, as the key role of the h_{eq} has been clarified, the way it is influenced by the listed parameters is detailed and the results are shown in Figure 7.8.

Compressor size changes the plant design, leading to different turbine size, heat exchangers characteristics, air and thermal fluids mass flow rates, and air storage size, which will change in terms of number of tanks, but not in terms of number of hours of continuous turbine operation that it makes possible. Therefore, all the costs of investment and O&M will increase as the compressor power increases, except for the pipeline that is not affected by these changes. At the same time, the higher power required by the compressor to operate, with the same power output from the wind farm, leads to a small reduction in the working hours of the plant. The case study presents a P_c of 50 MW, which is varied between 20 and 80 MW in this analysis.

The PUN limits variation was made by changing between ±0% and ±50% the thresholds around the average periodic cost of electricity that determine the activation of compressor or turbine, as shown with an example in Figure 7.7. The increase in these margins leads to a reduction in the average cost of the electricity that must be

purchased to operate the compressor and an increase in the average price of the electricity at which the energy produced by the turbine is sold. At the same time, however, the constraints that must be met for the plant to start operating are tightened, significantly reducing the hours of operation. In fact, the figure show that in the case limit of ±50%, both compressor and turbine almost never work, because the PUN is almost always higher or lower than the thresholds respectively.

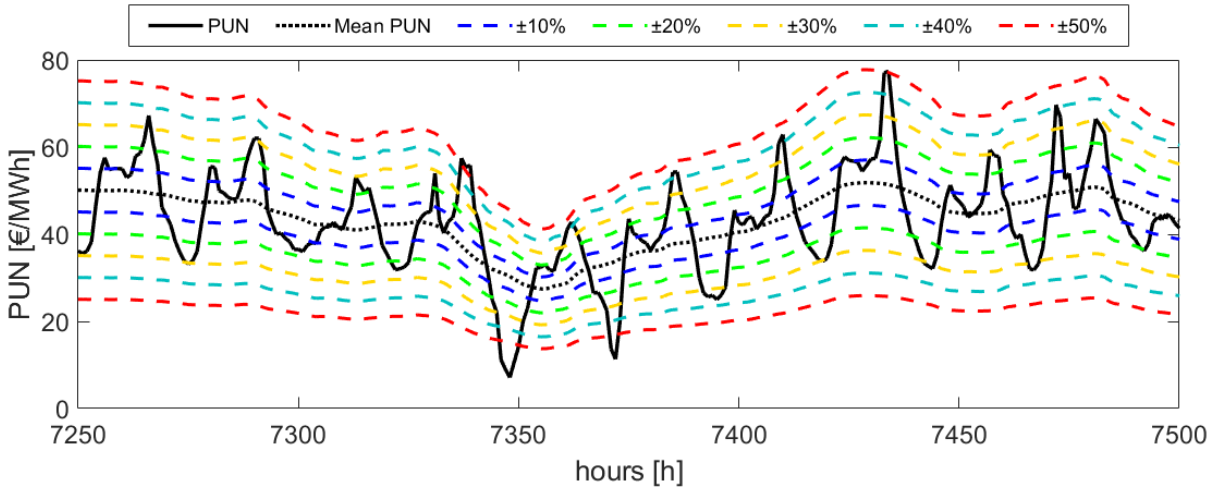

Figure 7.7: Example of PUN 2019 limits for compressor and turbine activation.

The size of the underwater air storage system instead, as with the PUN limits, does not affect the plant design, except for the number of underwater tanks that allows more hours of continuous operation of the turbine. Obviously, by increasing its size, the compressor can work longer as the volume of air storage is greater, and the probability of the compressor having to stop due to lack of space to store air is reduced, also bringing greater flexibility to the turbine. In this work, a storage size between 12 and 168 hours was evaluated to analyse how plant operation changes from half-day to weekly storage.

The results suggest that the best way to increase the number of equivalent hours is to reduce the width of the threshold around the average periodic PUN. In fact, taking it to zero, in other words running the compressor for PUN lower than this mean value and the turbine for PUN higher, it is possible to reach 2983 equivalent hours of operation of compressor and 2972 of turbine, instead of the approximately 1760 hours obtained in the case study using ±10% as limits. The other parameters, on the other hand, do not affect the h_{eq} consistently, but in general it can be stated that a reduction in compressor size and a larger underwater storage system allow for a better utilisation of air storage, respectively increasing the system's operating hours by up to 16% and 12.5% compared to the base case.

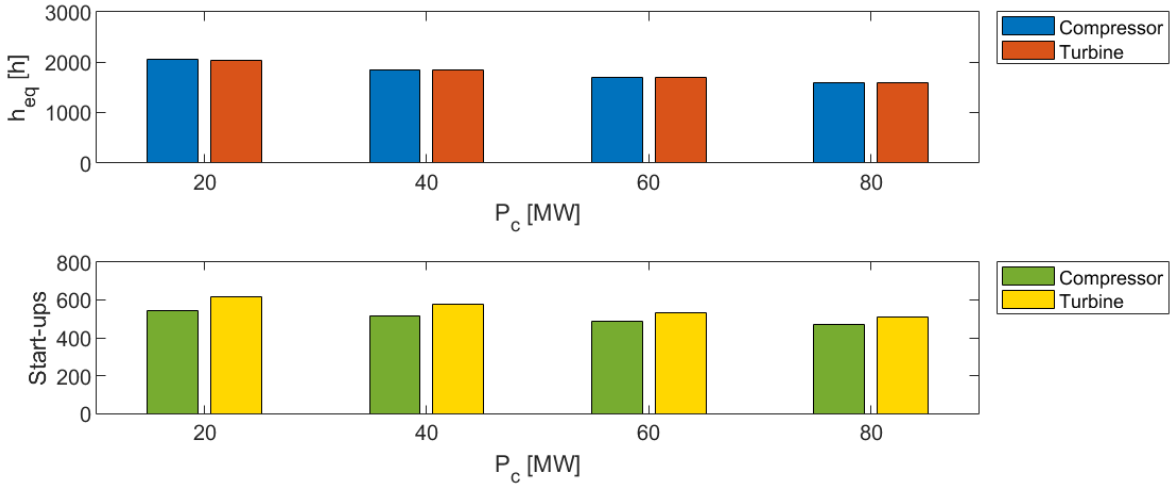

(a) Compressor power variation.

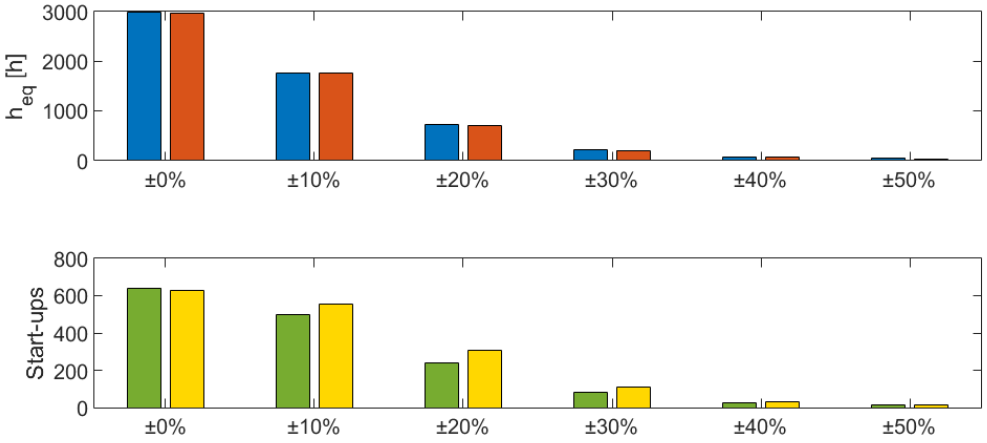

(b) Margine variation of PUN limits.

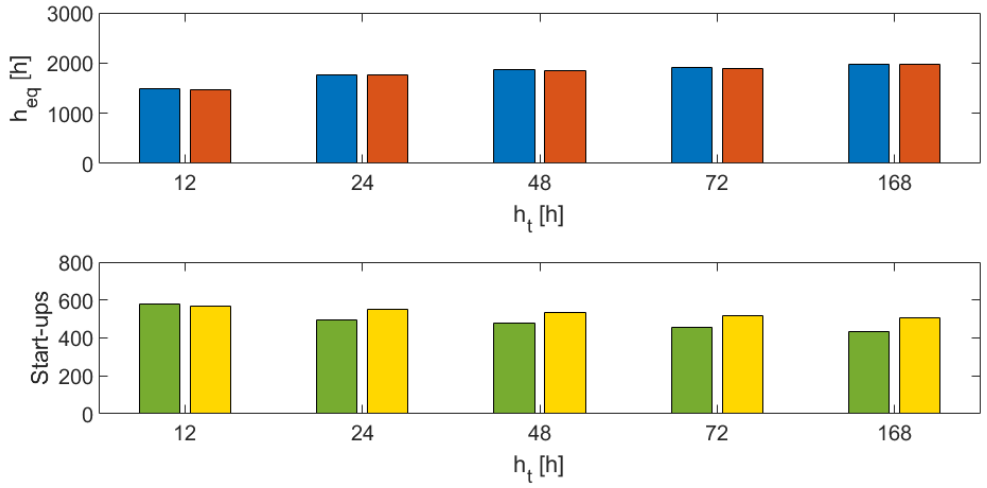

(c) Air storage size variation.

Figure 7.8: Results on equivalent hours and number of start-ups of turbomachines.

Knowing the link between the equivalent hours of operation of the plant and the exchanged energy with the electric grid, that influences the LCOS, its analysis is carried out and presented in Figure 7.9.

As mentioned above, as compressor power increases, an increase of CAPEX and consequently OPEX occurs, with a small reduction in compressor and turbine operating hours. This suggests an increase in LCOS, but at the same time, the energy exchanged by the plant rises due to the larger size of turbomachines. Therefore, the levelized cost of storage decrease for solution with energy bags as underwater tanks. Since the increase in energy absorbed by the compressor is not proportional to that produced by the turbine, there is a decrease in the RTE of the plant and a slower decrease in the LCOS as P_c increases. The same does not happen for the solution with rigid caissons because their costs, as already said in Chapter 6, have a greater influence on CAPEX than energy bags.

Regarding the variation of PUN limits, the sharp decrease in the plant's operating hours leads to a reduction of the energy absorbed and produced by the UW-CAES system, with a consequent increase in the LCOS. The round-trip efficiency is almost constant instead, because the decrease in energy flow between compressor and turbine is proportional.

Finally, it is interesting to analyse the influence of the turbine's continuous operating hours on the LCOS. In fact, this is the only case in which the equivalent hours of both compressor and turbine slightly increase. Moreover, the energy flows, even if not linearly, rise proportionally for both turbomachines leading to a constant RTE. But the increase in the number of air tanks leads to LCOS trend that is in agreement with costs trends, as shown in Figure 7.10.

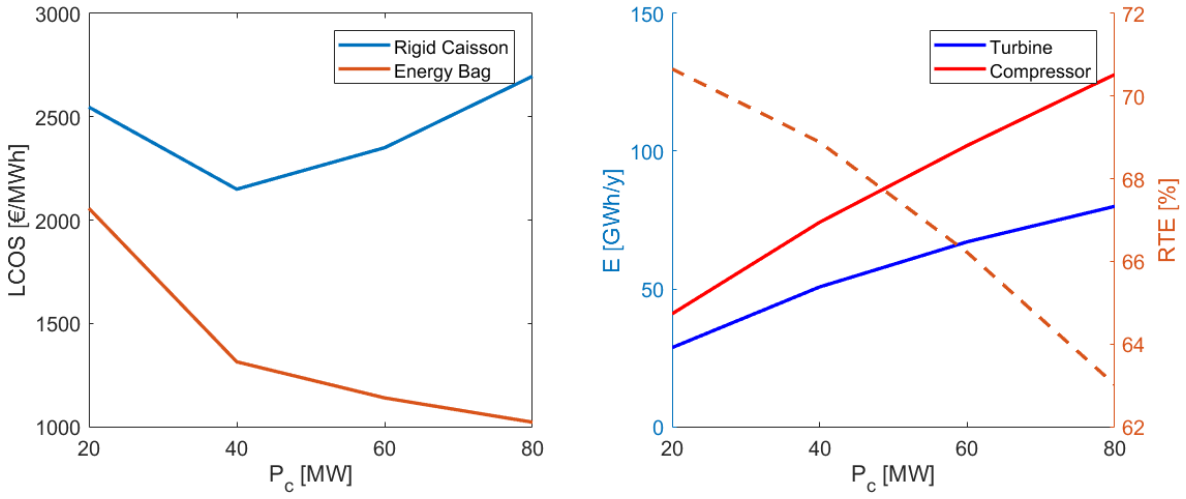

(a) Compressor power variation.

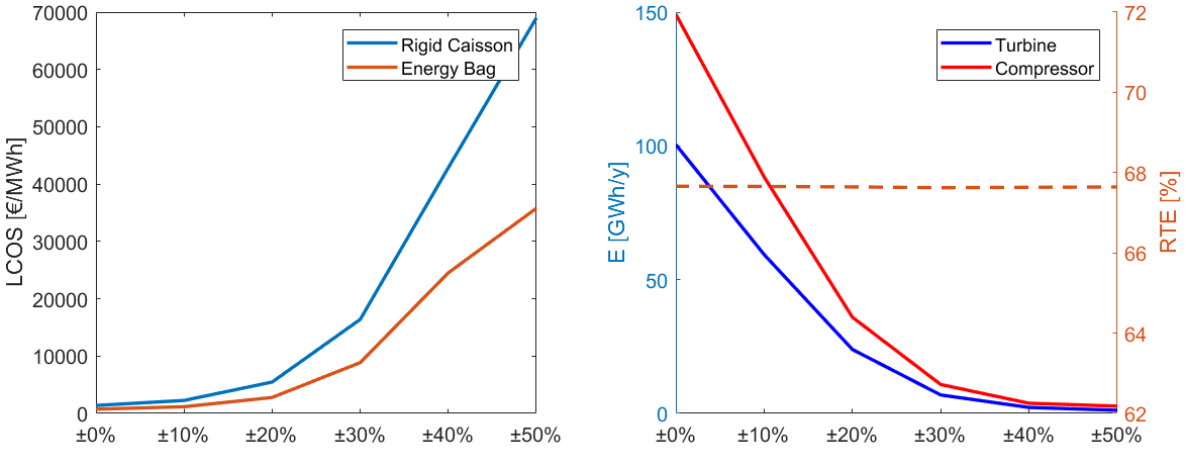

(b) Margine variation of PUN limits.

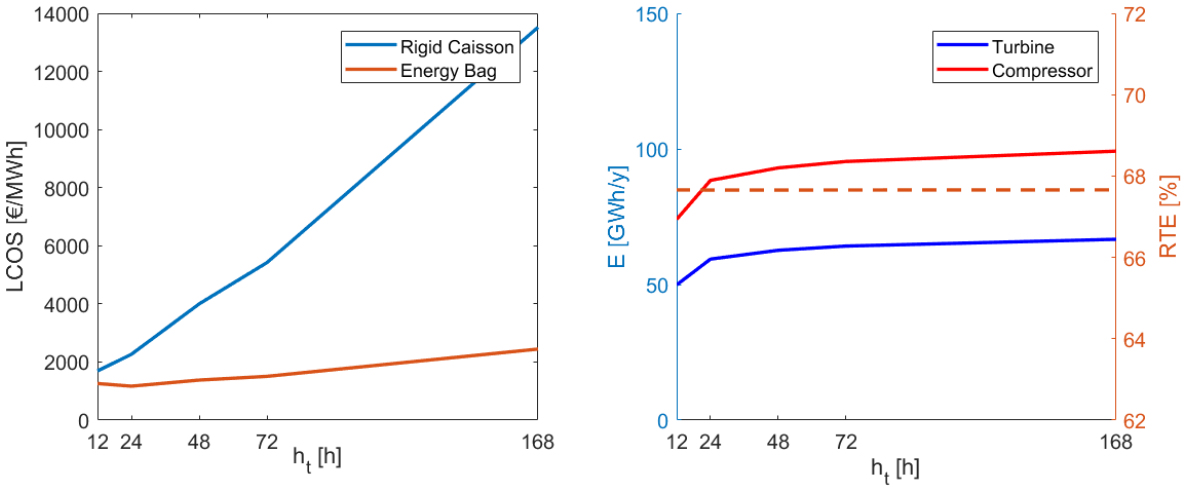

(c) Air storage size variation.

Figure 7.9: Results on LCOS, RTE and energy flows of turbomachines.

These trends of CAPEX and OPEX are a consequence of the already mentioned increase of air tanks number, that is considerable. Furthermore, their impact on investment and operative costs are shown in Figure 7.11.

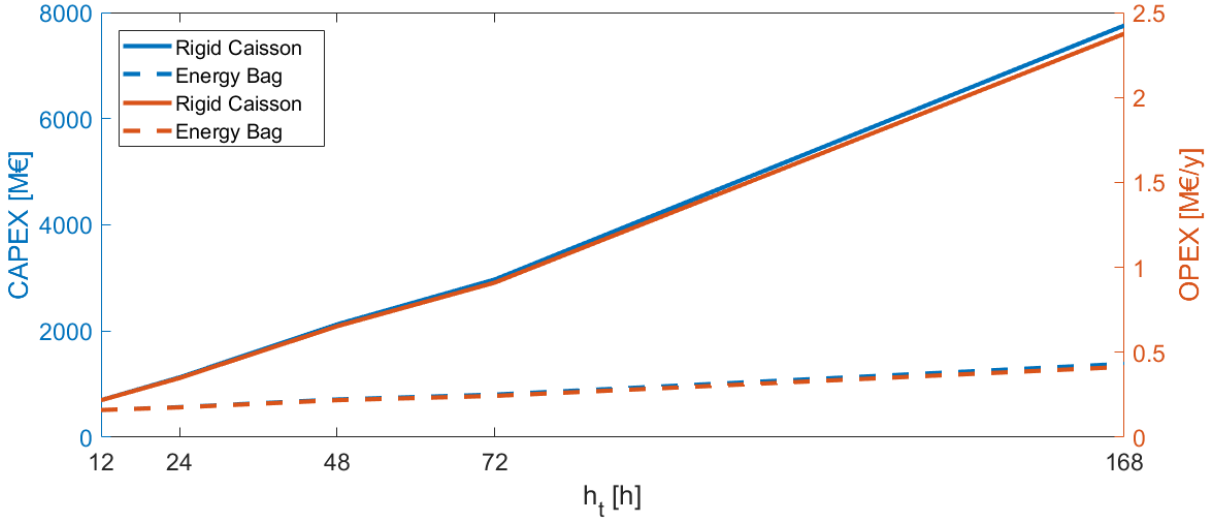

Figure 7.10: Trends of CAPEX and OPEX with air storage size variation.

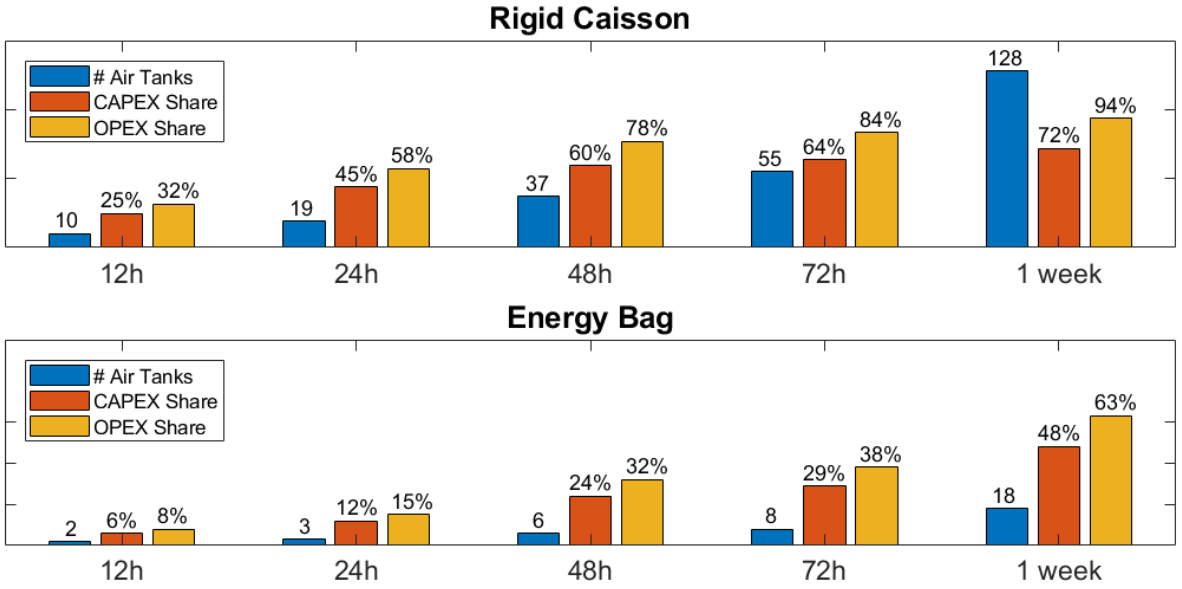

Figure 7.11: Number of required air tanks and their influence on CAPEX and OPEX. From top to bottom: rigid caissons and energy bags solutions.

The results show that the hours of continuous turbine operation have a negative impact in terms of LCOS, due to the high costs related to underwater air tanks, and that the base case of daily storage with 24 hours of autonomy is the best case for the solution with energy bags. But what mainly influences the cost of the energy produced are the threshold margins to determine PUN limits. Since increasing these margins leads to the plant being turned off most of the time during the year, the LCOS rises. But by reducing the limit to zero, an LCOS of 737.6 €/MWh can be achieved for the energy bags solution, respect to 1168.3 €/MWh of the case study. Otherwise, a bigger

compressor can help to reduce the LCOS, for example up to 1022 €/MWh with an 80 MW compressor.

For the other years considered, 2020 and 2022, the same trends are obtained as those already shown for the plant of San Pietro in 2019. Following what has already been said, the maximum values of h_{eq} are reached in 2020 with 3025 hours for the compressor and 3013 for the turbine, bringing the PUN limits to zero. This leads to the best case for LCOS as well, that is 711.3 €/MWh in the case of UW-CAES plant using energy bags as underwater storage system.

Regarding the other two plants, Catanzaro and Trapani, again the same trends are obtained for all the three years under consideration. The three parameters on which the sensitivity is based, are varied in the same range except for the compressor power, as each plant has a different compressor size. In the case of Catanzaro, it varied between 30 and 120 MW, with the base case of 83 MW. Instead, for the plant of Trapani it varied in a range between 30 and 150 MW, starting from a base case of 100 MW.

As already mentioned in Chapter 6, the most convenient solution is reached for Catanzaro plant in 2020 with energy bags as underwater air tanks, during which an LCOS of 356 €/MWh is obtained bringing to zero the PUN limits range. This is possible tanks to the lower investment cost for the Catanzaro plant respect to the other two, and with equivalent hours of 3075 and 3065 reached for compressor and turbine respectively.

Instead, the plant of Trapani, due to the high distance from the coast and thus the high costs related to its pipeline, results in an LCOS of 689.6 €/MWh in the best case, starting from 1016.1 €/MWh.

7.3. Other cases

One of the biggest problems that results from the operation of these plants and their economic analysis, are the quotes of CAPEX and OPEX of pipeline and air tanks. In particular their operation and maintenance costs are orders of magnitude higher than revenues, making impossible an economic return of the investment. In this direction, two cases have been analysed referring to the San Pietro plant in 2019: firstly, the influence of their OPEX on the LCOS, then the impact of the pipeline CAPEX.

The OPEX for the San Pietro plant are 34.8 M€/y and 17.6 M€/y for rigid caissons and energy bags solution respectively. But considering the operative costs equal to zero for air tanks and pipeline they became 962.1 k€/y. Unfortunately, these costs are still higher than the revenue per year given by the CAES system in 2019, that are 182.7 k€/y, leading to a LCOS of 1633 €/MWh with rigid caissons and 883 €/MWh with energy bags. Thus, even if the uncertainty on the OPEX of these two important components of the system, that together account for more than 95% of the total value (Figure 6.15),

their neglection does not make the investment convenient, even with a decrease in LCOS of 27.8% and 24.4% respectively (see Table 6.11).

The other analysis instead is done neglecting the pipeline length and thus its cost, that come from the idea to use an off-shore platform in which all the components of the plant on the land are located: turbomachines, heat exchangers and TES. In fact, in this case shown in Figure 2.6(b), the pipeline is necessary just to connect the turbomachines on platform with the underwater air tanks. Since the pipeline investment cost is 350 million of euros for the San Pietro plant, this brings to a sensibly reduction in CAPEX and OPEX respect to the case study (Table 6.10), resulting in values listed in Table 7.1:

Table 7.1: Results of CAPEX, OPEX and LCOS for San Pietro plant in 2019, neglecting pipeline cost.

UW-storage	CAPEX [M€]	OPEX [M€/y]	LCOS [€/MWh]
Rigid Caisson	782.1	20.9	1456
Energy Bag	217.7	3.6	411

Even if a reduction of 64.8% of LCOS occurs in the case of energy bags as air storage system, the value results still too high compared with electricity prices. Furthermore, in the case of an UW-CAES systems with all the components close to the off-shore wind farm, costs to purchase a platform with all the operation and maintenance costs related must be taken into account. Rather, this analysis shows how the distance from the coast significantly influences the costs of the plant, confirming what had already been seen with the Catanzaro plant, which was cheaper due to its greater proximity to the coast.

To complete the analysis, one other electricity price trend has been considered. Always referring to 2019 to compare the results with the Italian PUN, the prices of Germany are taken in consideration. This choice is given by the presence in the German electricity prices of negative values, due to an excess of energy production and thus of availability on the market, and a lower average price during the year. The difference between distribution of Italian PUN and German prices in 2019 in the gross electricity market can be seen in Figure 7.12, where the black dotted line represents a price equal to zero €/MWh. The German prices are lower than zero for a total of 211 hours during that year, hours during which the compression phase could be advantageous since the UW-CAES plant would be paid to absorb energy from the grid, or else the off-shore wind farm would pay to fed energy into the grid. Thus, the compression phase during that hours of negative energy price would be a remunerative phase, contrary to what normally happens, making the storage system more convenient. Furthermore, price fluctuations are generally smaller in the German market, as can be seen in Figure 7.13.

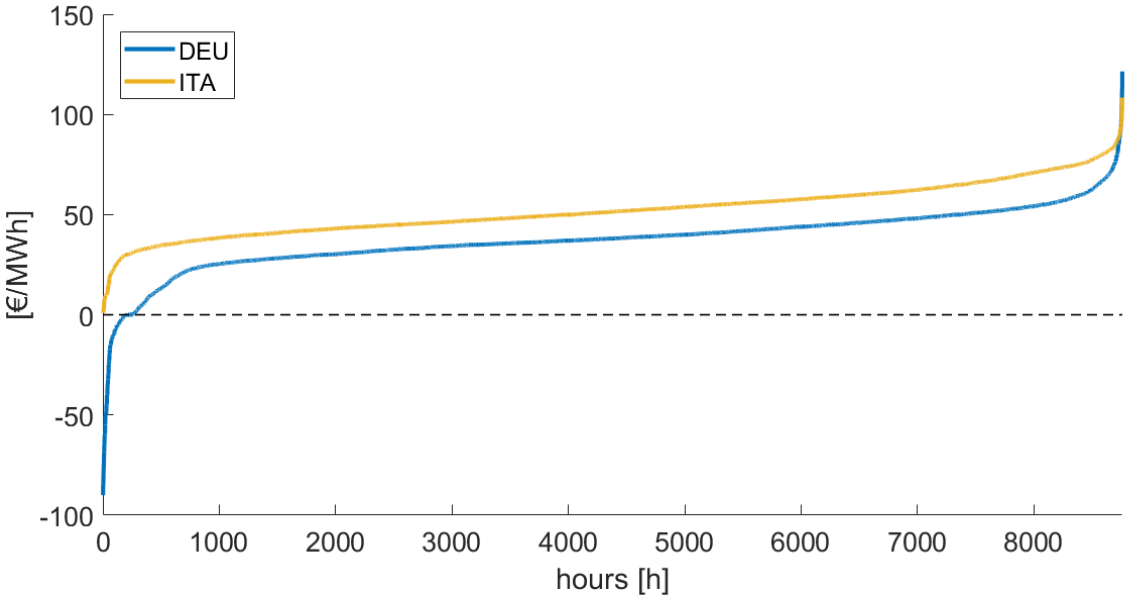

Figure 7.12: Distribution of Italian PUN and electric energy prices in Germany in 2019.

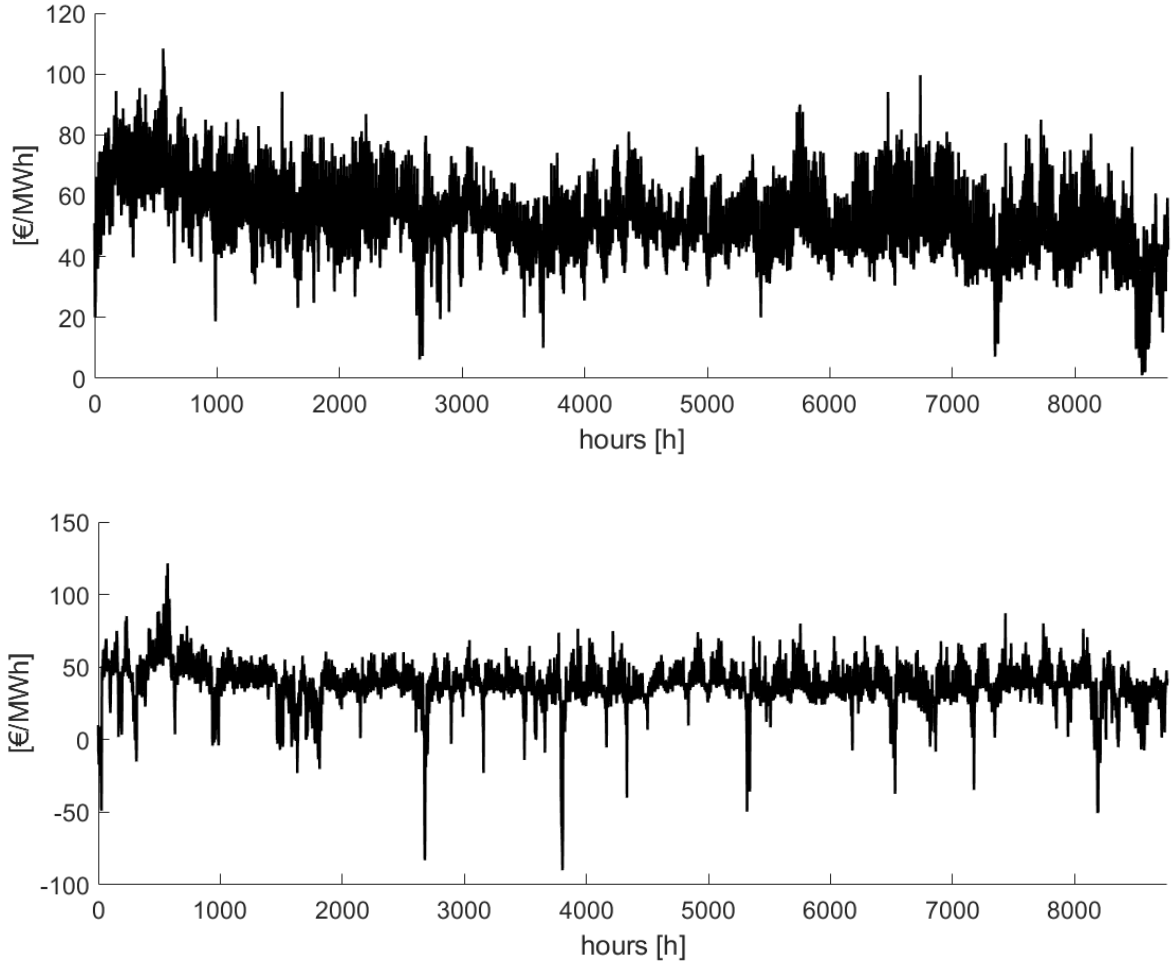

Figure 7.13: Trend of Italian PUN and German electricity prices in 2019: Italy on top, Germany on bottom.

From the simulation of the San Pietro plant following the German market in 2019, the results reported in Table 7.2 are obtained. From a comparison with the results obtained for the same plant using the Italian PUN, it is possible to see an improvement in performance of the plant given by the German market, not only for the increase in equivalent hours of turbomachines operation and consequently energy flows, but also for the reduction of their numbers of start-ups, meaning that turbomachines would work more continuously. This is a consequence of the smaller fluctuation of prices in the German market.

Table 7.2: Results of San Pietro plant performance in 2019: Italian and German electricity market.

Parameter	ITA	DEU
$h_{eq,c}$ [h]	1768	1965
$h_{eq,t}$ [h]	1756	1957
# on_c [−]	496	475
# on_t [−]	553	513
E_c [GWh]	88.4	98.2
E_t [GWh]	59.4	66.2
RTE [%]	67.66	67.66

Considering that the same plant is used for this analysis as in the case study, thus the same CAPEX and OPEX reported in Table 6.10 are obtained, reduction of the LCOS occurs, with a particular improvement in the revenues given by the plant operation during the year (Table 7.3). In fact, the plant works in compression mode for 147 hours during negative energy prices, resulting in a remuneration of 110.2 k€.

However, this improvement in plant operation condition still brings to high LCOS to consider the investment convenient. But the analysis suggests that the possibility in negative prices of electric energy can allows to a better exploitation of storage systems such as an UW-CAES.

Table 7.3:Economic results of San Pietro plant in 2019: Italian and German electricity market.

Parameter	ITA	DEU
$Revenues$ [k€]	182.7	517.1
PUN_t^{avg} [€/MWh]	63.4	47.7
$LCOS_{RC}$ [€/MWh]	2263.5	2018.3
$LCOS_{EB}$ [€/MWh]	1168.3	1037.2

8 Conclusion and future developments

The thesis work discussed in the previous chapters aimed to evaluate the techno-economic feasibility of a specific energy storage system: an Adiabatic Underwater Compressed Air Energy Storage (CAES) system. After describing the structure of the written model that simulates the plant's operation using MatLab, the results obtained for selected plants were presented. These plants were chosen based on proposals for offshore wind farms in the Italian seas.

It is evident that the cost of the energy stored by the plant is very high. Specifically, the Levelized Cost of Storage (LCOS) in all analysed cases is considerably higher than the prices of electricity in the Italian market. This is true even when considering the PUN (Prezzo Unico Nazionale) for 2022, which presents significantly higher values than usual due to global economic instability caused by the ongoing war in Ukraine. Certainly, the trend in energy prices influences the cost of energy produced by the CAES. It has been observed that lower average annual prices lead to a lower Levelized Cost of Storage (LCOS). This is evident in the results obtained for the three considered years 2019, 2020, and 2022, with lower values reported for 2020, the year in which the PUN has the lowest average value among the three.

However, it is essential to note that other constraints imposed in the model defining the plant's operation have a significant impact. An example is the logic chosen for defining the activation of the compressor or turbine. If the PUN is assessed on an hourly basis compared to the annual average, the plant operates for only a few hours a year, resulting in very high LCOS. Instead, opting for a logic based on the moving average of the PUN over a certain time interval, significantly increases the operating hours, thereby reducing the LCOS value. In addition, the width of the margin around the mean value of the PUN used also influences the results. By reducing this margin to zero, in other words by activating the compressor and turbine for values both below and above the moving average PUN, the operating hours of the turbomachines increase. Certainly, a more detailed operational logic for the plant could be implemented in future works, incorporating increasingly complex strategies. For example, based on the moving average of the PUN, activation of the compressor or turbine could be considered only if the conditions met in the evaluation hour persist for a certain number of consecutive hours. This approach is designed to minimize the number of start-ups for the turbomachines and maintain a more continuous operation. Alternatively, operation for a minimum number of hours could be imposed once the turbomachine is activated. Furthermore, a different logic to operate the salt-oil heat

exchanger can be investigated to limit the consumption of thermal energy stored in solar salt.

But what has been seen that has a significant impact on the costs of energy produced by this storage system is also a defining characteristic: pipeline and air storage systems. The analysis of different plants in Trapani, Catanzaro, and San Pietro reveals that the depth of the site and distance from the coast and, consequently, the length of the pipeline have a strong impact, both in technical terms due to pressure losses from friction between the airflow and the pipeline walls, and in economic terms, as it is one of the components with the highest investment and O&M costs. In fact, the analysis carried out considering the costs of pipelines equal to zero, as if the on-shore plant was situated on an off-shore platform, has demonstrated a meaningful decrease of LCOS for the San Pietro plant in 2019. Therefore, based on this specific consideration, it can be said that the choice of location is fundamental. Finding locations where the seabed is deep near the coast can make CAES a more attractive solution by reducing pipeline-related costs. Alternatively, a fully off-shore plant configuration could be considered, using a platform like for oil extraction or a large decommissioned ship anchored directly at the air storage site (Figure 2.6(b)). This would result in a significantly shorter pipeline. This is a plant solution that could be deepened in future research, taking into account the purchase and management costs of such an off-shore platform, and evaluating its cost-effectiveness compared to an on-shore plant or determining the distance from the coast beyond which it becomes more advantageous.

Regarding the other fundamental element, the air storage system, two types were evaluated: rigid caissons and energy bags. However, a significant cost difference was observed due to the smaller size of rigid caissons, which require a much higher number of tanks. The solution with energy bags appears to be more cost-effective, but further investigations are needed, such as sizing the ballast required to keep them anchored to the seafloor. Alternatively, the option of the plant layout shown in the Figure 2.6(c) could be considered, with rigid caissons serving as ballast for wind turbines in the off-shore wind farm. Evaluating whether the adoption of this combination can make their use more convenient, considering that it would reduce the costs related to ballast that should be used for wind turbines.

Hence, there are several elements that can contribute to reduce the plant cost and the LCOS value, leading to the best-case scenario among those analysed at €356/MWh. This result was achieved by considering the year with the lowest energy costs among the three, 2020, for the Catanzaro plant, which is the closest to the coast with approximately 15 km of required pipeline and using energy bags as air tanks. This combination of factors, along with an air storage size of 24 hours and a margin of ±0% on the moving average of PUN, allows for more than 3000 equivalent hours of compressor and turbine operation. The results obtained in this specific case are comparable with LCOS of different batteries technologies for energy storage, but

higher than other solution such as pumped hydro energy storage systems that are widely used [26] [27].

Another possibility for next works could be, for example, the analysis of hybrid systems, in which hydrogen is produced by means of electrolysers using electric energy provided by the off-shore wind farm. This hydrogen could then be burned to heat up the air stream after the TES, achieving higher turbine inlet temperatures and thus allowing to obtain a greater enthalpy variation across the turbine, and thus more power.

In conclusion, further developments and studies on the layout and optimization logic of the UW-CAES system are needed to try to make this energy storage solution more convenient and comparable with other solutions already used, considering the role it can play once it is integrated into the electricity grid, improving the management of energy production from non-programmable renewable sources.

Bibliography

[1] 'Renewable energy highlights', IRENA, 2023. [Online]. Available: https://mc-cd8320d4-36a1-40ac-83cc-3389-cdn-endpoint.azureedge.net/-/media/Files/IRENA/Agency/Publication/2023/Jul/Renewable_energy_highlights_July_2023.pdf?rev=61160fc74ada4f0daa670f5003820602&hash=2AAF8D76203C02D849633E37F6F06243

[2] 'Rapporto Statistico GSE - FER 2021', 2023. [Online]. Available: https://www.gse.it/documenti_site/Documenti%20GSE/Rapporti%20statistici/Rapporto%20Statistico%20GSE%20-%20FER%202021.pdf

[3] J. Moore and B. Shabani, 'A Critical Study of Stationary Energy Storage Polices in Australia in an International Context: The Role of Hydrogen and Battery Technologies', *Energies*, vol. 9, p. 674, 2016, doi: 10.3390/en9090674.

[4] C. Galli, 'Techno-Economic Assessment of Underwater Compressed Air Energy Storage coupled with Offshore Floating Wind Farms', Politecnico di Milano - Tesi di Laurea Magistrale - Ingegneria Energetica, 2022.

[5] C. R. Matos, P. P. Silva, and J. F. Carneiro, 'Overview of compressed air energy storage projects and regulatory framework for energy storage', *Journal of Energy Storage*, vol. 55, 2022, doi: 10.1016/j.est.2022.105862.

[6] J. D. Hunt *et al.*, 'Compressed air seesaw energy storage: A solution for long-term electricity storage', *Journal of Energy Storage*, vol. 60, p. 106638, 2023, doi: 10.1016/j.est.2023.106638.

[7] A. J. Pimm, S. D. Garvey, and M. De Jong, 'Design and testing of Energy Bags for underwater compressed air energy storage', *Energy*, vol. 66, pp. 496–508, 2014, doi: 10.1016/j.energy.2013.12.010.

[8] A. Aghahosseini and C. Breyer, 'Assessment of geological resource potential for compressed air energy storage in global electricity supply', *Energy Conversion and Management*, vol. 169, pp. 161–173, 2018, doi: 10.1016/j.enconman.2018.05.058.

[9] S. Houssainy, M. Janbozorgi, P. Ip, and P. Kavehpour, 'Thermodynamic analysis of a high temperature hybrid compressed air energy storage (HTH-CAES) system', *Renewable Energy*, vol. 115, pp. 1043–1054, 2018, doi: 10.1016/j.renene.2017.09.038.

[10] M. Astolfi, G. Guandalini, M. Belloli, A. Hirn, P. Silva, and S. Campanari, 'Preliminary Design and Performance Assessment of an Underwater Compressed

Air Energy Storage System for Wind Power Balancing', *Journal of Engineering for Gas Turbines and Power*, vol. 142, no. 091001, Aug. 2020, doi: 10.1115/1.4047375.

[11] M. Belloli and A. Hirn, 'Underwater Compressed Air Energy Storage (CAES): system design optimization, economics and simulation', Politecnico di Milano - Tesi di Laurea Magistrale - Ingegneria Energetica, Ingegneria Meccanica, 2018.

[12] *DECRETO LEGISLATIVO 3 aprile 2006, n. 152*. [Online]. Available: https://www.isprambiente.gov.it/it/garante_aia_ilva/normativa/normativa-ambientale/Dlgs_152_06_TestoUnicoAmbientale.pdf

[13] A. Bonk and T. Bauer, 'Solar Salt - Thermal Property Analysis : Extended Version', Deutsches Zentrum für Luft- und Raumfahrt (DLR), 2022. doi: 10.57676/3REA-P782.

[14] 'THERMINOL SP - Heat Transfer Fluids By SOLUTIA'. [Online]. Available: http://twt.mpei.ac.ru/TTHB/HEDH/HTF-SP.PDF

[15] arvengtraining, 'Basics of Shell & Tube Heat Exchangers', Arveng Training & Engineering. [Online]. Available: https://arvengtraining.com/en/basics-of-shell-tube-heat-exchangers/

[16] S. Di Michele and N. Frascella, 'Numerical Simulation and Economic Analysis of Adiabatic Underwater CAES for the Enhancement of an Offshore Wind Farm', Politecnico di Milano - Tesi di Laurea Magistrale - Ingegneria Energetica, 2017.

[17] F. P. Incropera, D. P. Dewitt, T. L. Bergman, and A. S. Lavine, Eds., *Fundamentals of heat and mass transfer*, 6th ed. Hoboken, NJ: John Wiley, 2007.

[18] G. A. Antaki, *Piping and Pipeline Engineering: Design, Construction. Maintainance, Integrity and Repair*, 0 ed. 2003. doi: 10.1201/9780203911150.

[19] 'Determine Thickness of Concrete for Concrete Coated Pipeline', DrillingFormulas.Com. [Online]. Available: https://www.drillingformulas.com/determine-thickness-of-concrete-for-concrete-coated-pipeline/

[20] 'Cost Indices – Towering Skills', Towering Skills. [Online]. Available: https://toweringskills.com/financial-analysis/cost-indices/

[21] G. F. Carbone, 'Simulazione di funzionamento e dimensionamento preliminare di sistemi CAES sottomarini (UW-CAES) connessi a centrali eoliche offshore', Politecnico di Milano - Tesi di Laurea Magistrale - Ingegneria Energetica, 2016.

[22] L. Mammoliti, 'Techno-economic optimization and comparison of P2G and UW-CAES systems coupled to a floating wind farm', Politecnico di Milano - Tesi di Laurea Magistrale - Ingegneria Energetica, 2020.

[23] V. Jülch, 'Comparison of electricity storage options using levelized cost of storage (LCOS) method', *Applied Energy*, vol. 183, pp. 1594–1606, 2016, doi: 10.1016/j.apenergy.2016.08.165.

[24] 'NPV (Net Present Value) – Formula, Meaning and Calculator', cleartax. [Online]. Available: https://cleartax.in/s/npv-net-present-value

[25] J. Giliberto, 'Rinnovabili, in arrivo 39 centrali eoliche nel mare davanti alle nostre spiagge. Ecco dove', Il Sole 24 ORE. [Online]. Available: https://www.ilsole24ore.com/art/rinnovabili-arrivo-39-centrali-eoliche-mare-alle-nostre-spiagge-ecco-dove-AEnv5hu?refresh_ce=1

[26] L. Li *et al.*, 'Comparative techno-economic analysis of large-scale renewable energy storage technologies', *Energy and AI*, vol. 14, 2023, doi: 10.1016/j.egyai.2023.100282.

[27] A. Ghilardi, A. Baccioli, G. F. Frate, M. Volpe, and L. Ferrari, 'Integration of ocean thermal energy conversion and pumped thermal energy storage: system design, off-design and LCOS evaluation', *Applied Thermal Engineering*, vol. 236, 2023, doi: 10.1016/j.applthermaleng.2023.121551.

List of Figures

List of Tables

List of acronyms

A-CAES	Adiabatic Compressed Air Energy Storage
CAES	Compressed Air Energy Storage
CAPEX	Capital Expenditure
CEPCI	Chemical Engineering Plant Cost Index
COT	Compressor Outlet Temperature
D-CAES	Diabatic Compressed Air Energy Storage
GDP	Gross Domestic Product
GSE	Gestore dei Servizi Energetici
HX	Heat Exchanger
IC	Intercooler
IOT	Intercooler Outlet Temperature
IRR	Internal Rate of Return
IS	International unit System
LCOS	Levelized Cost of Storage
NPRES	Non-Programmable Renewable Energy Sources
NPV	Net Present Value
O&M	Operational and Maintenance
OPEX	Operational Expenditure
PBT	Pay-Back Time
PSH	Pumped Storage Hydropower
PUN	Prezzo Unico Nazionale
PV	Photovoltaic
RTE	Round Trip Efficiency
TDF	Turbine Dimension Factor
TES	Thermal Energy Storage
TF	Thermal Fluid
TIP	Turbine Inlet Pressure
TIT	Turbine Inlet Temperature

TOT	Turbine Outlet Temperature
UPS	Uninterruptible Power Supply
UW	Underwater
UW-CAES	Underwater Compressed Air Energy Storage
WACC	Weighted Average Cost of Capital
WF	Wind Farm

List of symbols

Variable	Description	SI unit
T	temperature	K
p	pressure	Pa
cp	specific heat capacity	J/kg·K
η	efficiency	-
ρ	density	kg/m^3
k	thermal conductivity	W/m·K
μ	viscosity	Pa·s
Pr	Prandtl number	-
ϵ	wall roughness	m
g	gravity constant	m/s^2
d	sea depth	m
$\dot{m}$	mass flow rate	kg/s
h	enthalpy	J/kg
s	entropy	J/kg·K
f	friction factor	-
D	diameter	m
Re	Reynolds number	-
L	length	m
P_c	compressor power	W
v	fluid velocity	m/s
β_C	compression ratio	-
Q	thermal power	W
U	global heat transfer coefficient	W/m^2·K
A	area	m^2
Nu	Nusselt number	-
h	convective heat transfer coefficient	W/m^2·K
P_t	turbine power	W
t	thickness	m
D_o	outer diameter	m
S	allowable stress	Pa
S_y	minimum yield stress	Pa
F	design factor	-

E_0	weld joint factor	-
σ	stress	Pa
y	temperature coefficient	-
W	specific weight	kg/m
SG	concreate specific gravity	-
F_b	buoyancy force	N
V	volume	m^3
m	mass	kg
E	energy	J
$\dot{V}$	volumetric flow rate	m^3/s
h_{eq}	equivalent hours	h
C	cost	€
r	pressure ratio	-
γ	c_p/c_v ratio	-
U	stored energy at seabed depth	J
u	specific energy at seabed depth	J/m^3
A_i	operation costs	€/y
R	revenues	€/y
O	OPEX	€/y
$h_{max,T}$	hours of continuous turbine operation	h
β_T	expansion ratio	-
$\#on$	number of start-ups	-
H	height of thermal fluid tanks	m

Acknowledgments

Ringrazio di cuore Danae per il contributo dato durante tutto il percorso universitario, per i momenti di svago giocando a calcio, le nuotate al mare e le passeggiate in spiaggia. Inoltre, vorrei ringraziare anche Milo, che negli ultimi anni e in particolare durante il periodo della tesi, è sempre riuscito a supportarmi e non si è mai tirato indietro quando avevo bisogno di sfogarmi.